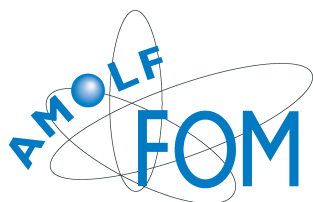


Analysis of Chaperone Complexes by
Fourier Transform Ion Cyclotron
Resonance Mass Spectrometry



The work described in this thesis was performed at the FOM Institute for Atomic and Molecular Physics, Kruislaan 407, 1098 SJ Amsterdam, The Netherlands.

ISBN: 978-90-77209-21-9

Analysis of Chaperone Complexes by Fourier Transform Ion Cyclotron Resonance Mass Spectrometry

2008© Rimco Geels (rgeels@hotmail.com)

Cover: Jelmer ten Hoeve, FunFolio.nl

A digital version of this thesis can be downloaded from: <http://www.amolf.nl>.

Analysis of Chaperone Complexes by Fourier Transform Ion Cyclotron Resonance Mass Spectrometry

Analyse van chaperone complexen met behulp van Fourier transformatie
ion cyclotron resonantie massaspectrometrie

(met een samenvatting in het Nederlands)

Proefschrift

ter verkrijging van de graad van doctor aan de Universiteit Utrecht op
gezag van de rector magnificus, prof. dr. J.C. Stoof, ingevolge het besluit
van het college voor promoties in het openbaar te verdedigen op vrijdag 28
maart 2008 des middags te 4.15 uur

door

RIMCO BERNARDUS JOHANNES GEELS
geboren op 31 juli 1977, te Alphen aan den Rijn

Promotoren: Prof. dr. R. M. A. Heeren
Prof. dr. A. J. R. Heck
Prof. dr. S. M. van der Vies

This work is part of research project FOM-01FB12-1 of the "Stichting voor Fundamenteel Onderzoek der Materie (FOM)", which is financially supported by the "Nederlandse organisatie voor Wetenschappelijk Onderzoek (NWO)".

Contents

1	Introduction	11
1.1	Noncovalent protein complexes	11
1.1.1	Tertiary and quaternary association of proteins . . .	11
1.1.2	Protein complexation and function	12
1.1.3	Chaperonins	12
1.1.4	Protein folding landscape	16
1.1.5	GroES and gp31	18
1.2	Studying noncovalent protein complexes using mass spec- trometry	20
1.3	Scope of the thesis	21
2	Mass spectrometry of noncovalent protein complexes	23
2.1	Electrospray ionization	23
2.2	Mass spectrometers	26
2.2.1	Time of flight mass spectrometry	26
2.2.2	Fourier transform ion cyclotron resonance mass spec- trometry	29
2.2.3	FT-ICR-MS theory	29
2.2.4	FT-ICR-MS experimental setup	34
2.2.5	Tandem mass spectrometry with the FT-ICR-MS . .	36
	Nozzle-skimmer dissociation	37
	Collision activated dissociation	38
	Sustained off-resonance collision activated dissociation	38
	Infrared multiphoton dissociation	39
	Electron capture dissociation	40
2.2.6	Protein fragmentation	41
2.3	Temperature controlled ESI	42
2.3.1	Technical data thermoprobe	42
2.4	Gas-phase vs. solution-phase	44
2.4.1	Implications for this research	47

3	ECD as structural probe for noncovalent gas-phase protein assemblies	49
3.1	Introduction	50
3.2	Experiment	50
3.3	Results and discussion	51
3.3.1	ECD leads to dissociation of noncovalent bonds for specific charge states of gp31 heptamers	51
3.3.2	Pentamer species of gp31 originate via dimer ejection from the heptamer	54
3.3.3	ECD products have not had backbone cleavage	54
3.3.4	Multiple electron capture before dissociation	55
3.3.5	Comparison of ECD with SORI-CAD reveals different dissociation mechanics	56
3.3.6	Gas-phase structure determines ECD pathway	58
3.4	Conclusion	58
3.5	Acknowledgement	59
4	Comparative gas-phase activation of two similar noncovalent heptameric protein complexes: gp31 and GroES	61
4.1	Introduction	62
4.2	Experiment	63
4.3	Results and discussion	64
4.3.1	Thermodynamic stabilities of GroES and gp31 are comparable	66
4.3.2	The different activation mechanisms result in comparable breakdown diagrams	67
4.3.3	Dissociation pathways for GroES and gp31 exhibit differences	70
	Charge state of ejected monomer depends on activation technique, parent charge and parent species	70
	Charge state of the ejected monomer relates to the extent of unfolding	72
	Activation of complexes results in overall charge loss	73
	Loss of charge happens during or after dissociation of the complex	75
	Charge stripping is a kinetic effect	78
	Difference gp31 and GroES	78
4.4	Conclusion	79
4.5	Acknowledgement	80
5	Solution-phase and gas-phase thermal activation of the co-chaperonins GroES and gp31 probed by mass spectrometry	81

5.1	Introduction	82
5.2	Experiment	85
5.3	Results and discussion	86
5.3.1	Solution-phase thermal dissociation monitored by mass spectrometry	86
5.3.2	Thermal denaturation probed with fluorescence spec- troscopy	90
5.3.3	Probing the folding state of the species using mass spectrometry	92
5.3.4	Gas-phase thermal activation using mass spectrometry	93
5.4	Conclusion	97
5.5	Acknowledgement	97
	Bibliography	99
	Summary	119
	Samenvatting	123
	Nawoord	129
	Curriculum Vitae	133
	List of Publications	135

Introduction

1.1 Noncovalent protein complexes

1.1.1 Tertiary and quaternary association of proteins

Proteins are synthesized as chains of amino acids, chemically bonded together by amide bonds, creating so-called polypeptides.¹ These chains are like strings of beads without any specific overall three dimensional structure. This is called the primary structure of a protein. After synthesis the protein is far from being in its biologically active state and has to go through a number of steps to reach its biologically active form. First, the secondary structure has to be formed, i.e. α -helices and β -sheets. The information needed to create the secondary structure is contained within the primary structure of the protein. The primary structure largely determines the final active overall conformation.^{2,3} This does not mean that the creation of secondary structure will always be biologically correct. The environment in which the protein resides will influence the formation of the secondary structure. The hydrogen-bridges formed within the protein that create the three dimensional structure have to compete with hydrogen bonding to environment molecules, like water.

After the secondary structure is obtained, the tertiary structure has to be formed. The manner in which the α -helices and β -sheets curl up into a specific conformation depends on the hydrophobicity of the environment. An aqueous surrounding will cause hydrophilic parts to assemble on the outside of the protein and forces hydrophobic parts of the protein to its interior. Formation of internal sulfide bridges also contributes to the final tertiary structure of the protein and stabilizes it. Together the secondary and tertiary structures constitute the "folding" of the protein. The protein now has a three dimensional structure that can interact with other proteins and substrates. The biological functioning of the protein is dependent on its three dimensional folding state. For some proteins the tertiary structure represents their final native conformation. For a lot of proteins it is not. Proteins can, for instance, associate with other proteins to form large

complexes. Association of proteins into complexes is termed quaternary structure.¹

The activity of a protein depends predominantly on its tertiary and quaternary structure, but also on the location and structure of specific residues. After obtaining its final conformation, proteins can undergo so-called post-translational modifications. In this process specific residues are chemically altered by adding (or removing) specific end groups. Examples of these modifications are: phosphorylation, de-amidation, oxidation and methylation.⁴⁻¹⁰ These modifications can be permanent or transient in nature, depending on the requirement. The function of a protein is governed by all the factors listed above. The (folding-) state of a protein is very dynamic and changes more or less continuously during reactions and a changing environment, back and forth between different functional and non-functional states.

Since the conformation of a protein is the major determinant of its function much research is directed towards understanding and manipulating the protein structure. Part of the molecular biology research is focused especially on the quaternary association of proteins, the relation between complexation and function.

1.1.2 Protein complexation and function

Protein complexes are created in a variety of ways and can be covalently or noncovalently bonded, depending on the chemical properties of the inter subunit amino acids. Noncovalent bonds are for instance created by hydrogen bonding or ionic interactions, while covalent linkages involve the formation of external sulfide bridges. Protein complexes can be formed from 1) two or more different proteins, 2) two or more of the same proteins, 3) a protein with a non-protein, like DNA or lipid binding. Complexation with a non-protein often occurs transiently during a specific activity of the protein.

Protein complexes can be categorized on the basis of their occurrence, i.e. (semi-)permanent or transient. Transient protein complexes are often formed at specific times during which a particular biological activity is needed, for instance during signal transduction or transcription. The functions of protein complexes are numerous and large structures can sometimes create an artificial environment in which a substrate protein can be folded, the family of chaperonins, or degraded, the proteasome.

1.1.3 Chaperonins

Chaperonins exist in all organisms and appear in a wide variety of forms. Chaperonins assist other cellular proteins with folding.^{11,12} They form the last step in the transfer of information from DNA to biological activity. As

mentioned above, all the information that is required to attain the native structure resides within the amino acid sequence, so in principle nascent polypeptide chains should be able to obtain their biologically native state by themselves. However, in practise it is not trivial for proteins to attain their native state and there are many possibilities of misfolding. Misfolded proteins are the cause of many diseases, like Alzheimer's, Parkinson's, Creutzfeldt-Jacob syndrome and BSE.¹³⁻¹⁶ In addition, if proper folding of proteins would be determined by entropy and statistics alone, this would lead to very long folding times, incompatible with life.¹⁷ This is where the family of chaperonins comes into play, i.e. to prevent or restore misfolded intermediates and shorten the folding trajectory. The chaperonins are one family of the larger group of molecular chaperones, which are required in a large variety of cellular processes such as protein synthesis, translocation, signal transduction and degradation.¹⁸ They function in a variety of ways.

First, chaperonins can prevent and restore nonnative aggregation of proteins. When polypeptides are being synthesized they have a high affinity for folding, but sometimes cannot fold properly, in particular when the aminoterminal end of the polypeptide has to interact with the carboxy terminus that is not yet synthesized. Also, newly-synthesized polypeptide chains are prone to aggregation as a result of exposed hydrophobic residues, which tend to interact with other cellular components. So newly synthesized polypeptides have to be protected from aggregation. Intermediate folding structures of proteins also have the tendency to aggregate with other proteins. Upon aggregation these proteins cannot properly fold into their active state. Chaperonins help in these cases.^{19,20} Chaperonins prevent aggregation through a mechanism of isolation and confinement.

Second, chaperonins can accelerate the folding for certain slow-folding proteins. Even without the risk of misfolding or aggregation, it can still be that the amount of protein obtaining its native fold is small. This occurs when the path to native conformation is long, for instance when there are many folding intermediates, or when there is a high energy barrier to folding. Chaperonins have been shown to accelerate folding of these kinds of proteins dramatically by reducing or accelerating the rate-limiting steps.^{20,21}

Third, chaperonins can have an annealing function. Many misfolded proteins cannot naturally refold into their proper native state, but are assisted by the chaperonins. Binding to a chaperonin facilitates partial unfolding of these misfolded proteins to allow subsequently proper folding, so the protein will not end up in a misfolded state.²²

Fourth, chaperonins can create a closed environment for still unfolded polypeptides to fold into their native state. This is the so-called "Anfinsen" model describing the functioning of chaperonins. The chaperonin contributes both passively and actively to the folding process. Passively by creating the closed environment for the protein to fold and actively

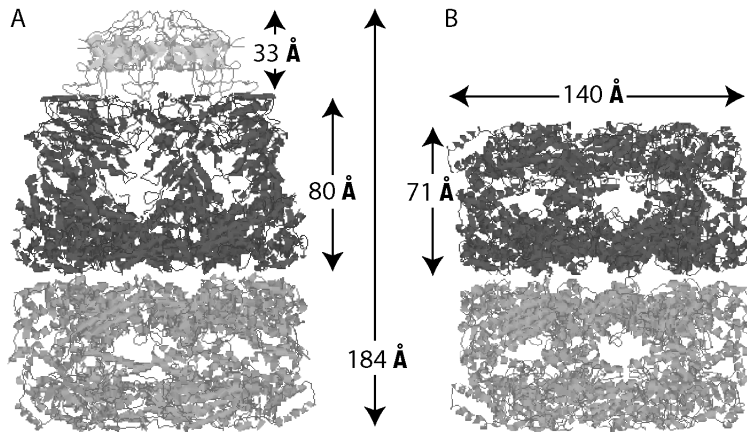


Figure 1.1: crystal structures of the tetradecameric GroEL with (a) and without (b) the GroES cap. Crystal structure data are taken from the protein data bank (PDB accession codes: 1AON and 1J4Z).

by changing its interior wall from hydrophobic to hydrophilic, inducing detachment of the substrate into the cavity and forcing hydrophobic parts of the substrate into the substrate's interior. The protein can either fold in a single folding cycle or through multiple folding cycles, i.e. iterative folding.^{21,23-25}

Fifth, it has been shown that chaperonins can also assist folding of proteins that are too large to fit into the "Anfinsen cage". In this case only a part of the protein interacts with the chaperonin to fold.²⁶

Some of the members of the chaperonin family are known as the heat-shock proteins.²⁷ Heat-shock proteins are proteins of which expression is induced after applying heat stress conditions. Increasing the temperature can cause proteins to denature, which results in an extra demand of proteins that facilitate (re)folding and prevent aggregation, like the chaperonins. The range of proteins that require assistance for their folding is large. Most molecular chaperones are promiscuous in their choice of substrate proteins.

One of the best-studied chaperonins is the chaperonin from *Escherichia coli*, which is absolutely required for the folding of 3-5% of all the *E. coli* proteins.^{21,28} This chaperonin is necessary for survival of *E. coli*, showing the importance of these complexes for protein folding.^{29,30} The *E. coli* chaperonin consists of two type of proteins: GroEL and GroES.^{18,23} The crystal structure is shown in Figure 1.1. The main body of the chaperonin is made up of two hollow, non-covalently bound heptameric protein rings stacked back to back together, GroEL. Each subunit has a mass of 57kDa, totaling 800kDa for the entire tetradecameric GroEL complex. Each ring

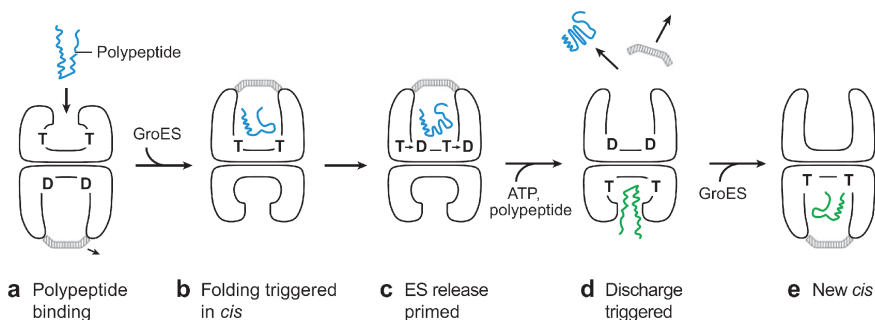


Figure 1.2: Schematic representation of the GroE folding cycle. T denotes ATP, D denotes ADP. (a) Nonnative substrates bind to the *trans* ring of EL, whether ATP is bound to the ring before or after substrate binding remains to be shown. (b) The ring with substrate and ATP bound now binds ES. Binding of ES is associated with conformational changes in this *cis* ring, releasing the substrate in the cavity and triggering the folding of the substrate. (c) ATP hydrolysis in the *cis* ring weakens the affinity for ES. (d) Binding of ATP in the *trans* ring causes ES to dissociate releasing the substrate from the cavity. (e) ES binds on the other side creating a new *cis* folding complex, essentially equal to (b) by a 180° rotation. Adapted from: Grantcharova³⁷

has seven-fold symmetry and contains an open cavity which can be closed by the GroES co-chaperonin. GroES consist of seven identical non-covalently bound subunits, organized in a circular fashion, giving rise to seven fold symmetry. Each subunit of GroES has a mass of ~ 10 kDa. One GroES heptamer can bind on one side of the tetradecameric GroEL in the presence of Mg-ATP or Mg-ADP. The overall dimensions of the chaperonin are depicted in Figure 1.1.^{31–33} When closed, the volume of the folding cavity is $\sim 175,000 \text{ \AA}^3$ and it can accommodate substrate proteins of up to ~ 60 kDa.³⁴ Each GroEL subunit consists of three domains. An equatorial domain, participating in the contacts with the opposite GroEL ring and containing the nucleotide (ADP and ATP) binding site.³⁵ An intermediate region; this region exhibits most conformational changes upon binding of nucleotides and GroES. Lastly, the apical domain, which contains the interaction sites for the substrate proteins as well as for the co-chaperonin GroES.^{12,23,27,36}

The basic interaction sequence of the chaperonin with its substrates is shown in Figure 1.2.

A substrate attaches itself to the empty *trans* ring of GroEL. Subsequent cooperative binding of 7 ATP molecules changes the ring, creating high affinity for GroES on the ATP-bound side. Upon binding of GroES the substrate is displaced from the wall of the GroEL ring and is released

into the interior of the cavity, where it folds.³⁸ After hydrolysis of the ATP molecules the *cis* ring (where the substrate and GroES are bound) is weakened.³⁹ Binding of substrate and ATP to the *trans* ring induces release of GroES and the (partly-)folded substrate from the *cis* ring. Although only one substrate should bind at one time also the bare double GroEL donut with two bound substrates has been measured, separate from the folding cycle.⁴⁰ After release from the complex, the substrate is either completely folded, or it is in an intermediate state and still has affinity for GroEL. Then it can rebind and go through multiple rounds of folding before it is completely natively folded.²⁵ The same procedure now repeats itself in the opposite ring. The complete folding cycle takes about 15 seconds.²³ This remarkable function has made this chaperonin system one of the most widely studied systems in molecular biology. How then is the final native conformation of a protein determined?

1.1.4 Protein folding landscape

Energetically the folding of a polypeptide can be seen from an energy landscape point of view. The landscape is determined by the free energy of any given conformation,⁴¹ which depends on the enthalpy of binding and the entropy of the conformation. If (part of) the protein folds, its position on the energy landscape will change, to reflect the new (lower) free energy. Globally, a change towards the native conformation will lower the free energy of the protein. The energy landscape can be seen as a folding-funnel indicating the folding-pathway to the native state.⁴²⁻⁴⁴ The energy of the native conformation will be at the bottom of this funnel; see Figure 1.3.

The funnel is perceived to be relatively steep, to represent the obvious stability of natively folded proteins. Small conformational changes or temperature fluctuations will not cause the protein to lose its conformation immediately. The folding funnel is, for most proteins, not smooth. It has many energy barriers and local free energy minima. Although for many proteins their native conformation is naturally reached, a lot of proteins also get "stuck" in so-called kinetic traps: local free energy minima with an energy barrier that, under normal circumstances, is impossible to overcome. The energy landscape is not only an inherent property of the protein, but is to a great extent influenced by the aqueous cellular environment, often a necessity for the protein to be able to reach its active state. Also, interactions of proteins with substrates or other proteins can drastically alter the energy landscape. Artificial changes in the environment are often used to induce conformational changes, such as chemical denaturing or increased temperature. What would be the effect of completely removing the environment on the energy landscape? (See paragraph 2.4)

Considering the energy landscape of proteins that need chaperonins to fold, the chaperonin has multiple functions; as mentioned in section 1.1.3.

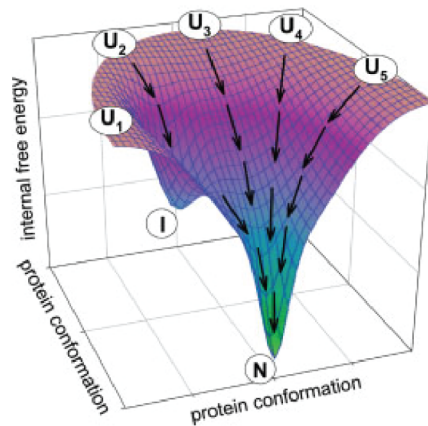


Figure 1.3: Schematic representation of the free energy landscape of a protein. Unfolded proteins start of at any position on the edge of the folding funnel (U1..U5). At the bottom of the folding funnel, the native state is represented (N). The arrows indicate examples of the folding pathway the individual proteins may follow towards the native state. Along the folding pathway, proteins can get transiently trapped in a local minimum, thereby attaining an intermediate folding state (I), before continuing down the funnel. *Adapted from: Konermann⁴⁵*

These proteins do not have a smooth energy landscape. Their landscape exhibits local free energy minima that will kinetically trap the proteins in an intermediate "mis"folded state. Binding of the "mis"folded protein to a chaperonin will remove the protein from its position in the trap back to a position on the folding landscape from where it can continue to fold, hopefully without ending up in another misfolded state. This is depicted in Figure 1.4b. The chaperonin has the ability to influence the folding landscape of a protein by making it more smooth, thereby preventing the possibility of ending up in a local free energy minimum that is not the native state. This is depicted in Figure 1.4c. The lowest energy conformation is still determined by the primary structure of the polypeptide and not influenced by the chaperonin. The chaperonin only provides a means to get there.

Since the final lowest energy minimum is determined by the primary structure of a protein, it is difficult to imagine that two proteins that do

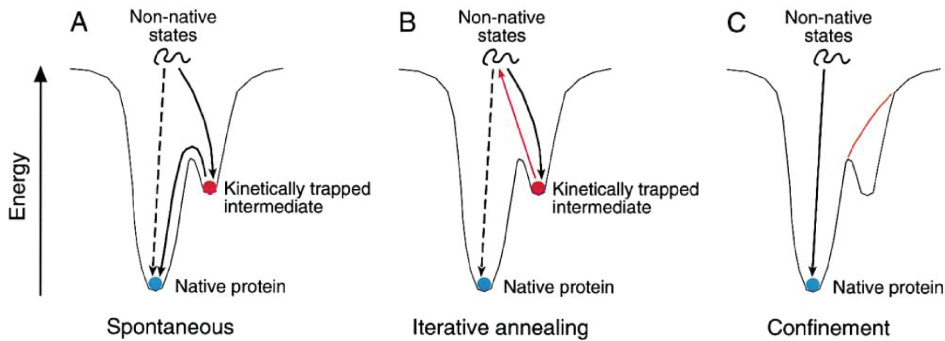


Figure 1.4: During spontaneous folding it is possible for a protein to get kinetically trapped (left graph). Chaperonins can solve this problem by unfolding the misfolded protein thereby moving it back to the top of the folding funnel (iterative annealing, middle graph), or the chaperonins can smooth the potential energy surface, preventing the unfolded protein from being trapped (confinement, right graph). Adapted from: Hartl²⁷

not have a high primary sequence identity will have a comparable lowest free energy structure. There are however examples of proteins where this is indeed the case. GroES and gp31 are an example of this. The next paragraph deals with these two protein assemblies.

1.1.5 GroES and gp31

The GroEL-GroES chaperonin complex can fold a great variety of cellular proteins. Bacteriophages like λ and T4 utilise the *E. coli* host chaperonins for the folding of their own proteins.⁴⁶ There is however a very interesting exception to this. When *E. coli* becomes infected by bacteriophage T4 (see Figure 1.5), DNA replication and protein synthesis of the host is taken over and is utilized for producing new progeny phages. When infected with T4, the translation and expression machinery of *E. coli* is taken over and used to create reproductions of the parent T4. The amount of bacteriophages inside the bacterium will increase until about 200, after which the bacterial cell lyses, releasing all the progeny phages into the environment. The whole cycle takes approximately 30 minutes.⁴⁷⁻⁴⁹

The major bacteriophage proteins that make up the capsid are gp23 and gp24. Of these two proteins, gp23 needs chaperonin assistance to fold properly into its native state. However, despite the fact that the GroEL-GroES chaperonin can fold a vast array of proteins, it cannot fold gp23. The capsid protein has a molecular weight of ~ 56 kDa, which is on the upper limit of what this complex can fold. It thus seems that gp23

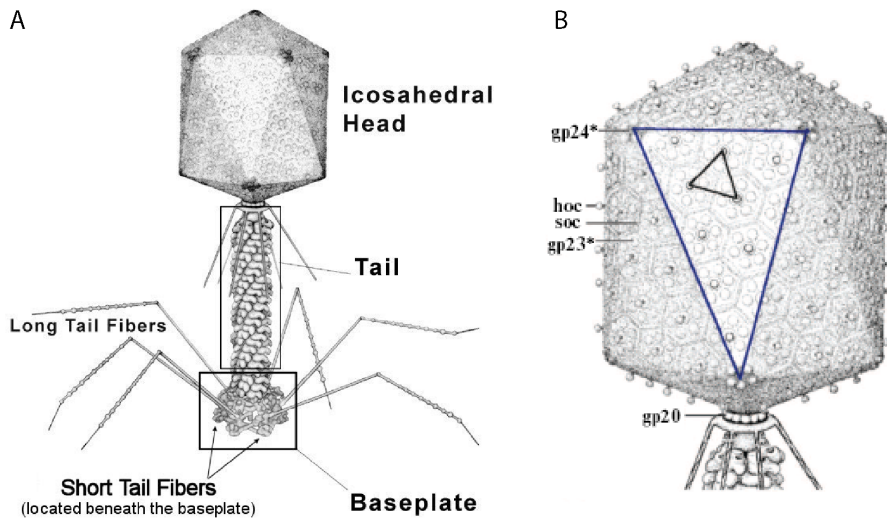


Figure 1.5: View of bacteriophage T4. It consists of an icosahedral head, with major capsid proteins gp23 and gp24. The head is connected to a tail which is again attached to a base plate. There are six short and six long fibers that T4 used to attach itself to *E. coli* for infection. *Credit A: The figure has been adapted by Petr Leiman (Purdue University) from a drawing by Fred Eiserling (UCLA). B: Adapted from: Mesyanzhinov⁵⁰*

may be too big to fold inside the GroEL-GroES complex. T4 has created a solution to this problem. It substitutes GroES with its own phage-encoded protein gp31, thus exchanging the lid of the folding cage for a different one. Gp31 works well together with GroEL and the GroEL-gp31 chaperonin complex does fold gp23. With the properly folded gp23, the bacteriophage can construct its capsid and multiply.⁵¹⁻⁵⁴

The difference in function between the GroEL-GroES and GroEL-gp31 complexes have been studied extensively^{31,55-59}. The GroES and gp31 co-chaperonins have a very similar quaternary structure, see Figure 1.6. Both are non-covalently bound homo-heptameric complexes arranged in a circular fashion. Gp31 (84kDa) is somewhat larger than GroES (72kDa). The crystal structures of the two proteins are very similar although they only have 14% amino acid sequence identity.⁵⁷ Besides their difference in mass, there are some other differences. From the crystal structure it

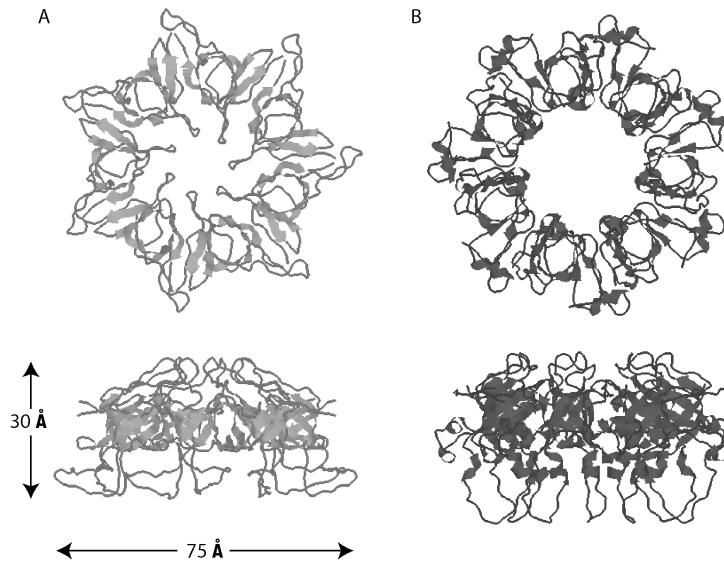


Figure 1.6: crystal structures of the heptameric GroES (a) and the heptameric gp31 (b). Crystal structure data are taken from the protein data bank (PDB accession codes: 1AON and 1G31).

can be seen that gp31 has a more open roof structure. Also, gp31 has a large mobile loop for interaction with GroEL. Various investigations now tend to point out that the GroEL-gp31 complex has a somewhat larger interior cavity than GroEL-GroES. This enlargement might be enough for (intermediate folded) gp23 to fit into the folding cavity.⁵⁶

The investigations into the differences between these two proteins continue and also in this thesis these two will be the subject of research. Gas-phase thermodynamic properties of the complexes will be investigated to create new methodologies for analyses of large non-covalently bound complexes and to reveal differences in behavior between the complexes. For the analysis mass spectrometry is used.

1.2 Studying noncovalent protein complexes using mass spectrometry

To understand the functioning of complex systems such as living cells, we need to understand the building blocks first. By taking proteins from cells and putting them in an artificial environment, *in vitro*, the complexity of the problem is reduced. The complexity can be reduced further by

completely eliminating the environment from the equation and putting the individual proteins in the gas phase for analysis. Although the *in vivo* functioning of a protein depends to a large extent on its environment, studying proteins separate from this environment will greatly enhance our knowledge of their behavior.

Mass spectrometry is an excellent technique to study proteins in the gas phase. Masses can be measured with unprecedented accuracy and a variety of gas phase reactions can be used to analyze protein structure. With the development of electrospray ionization, it has become possible to evaporate entire noncovalent complexes into the gas phase, while retaining the labile hydrogen bonds.⁶⁰ And although the mass resolution for large proteins (complexes) is not as great as for smaller proteins, it is possible to easily ascertain the stoichiometry of protein complexes. Any small changes in the complex are observed as changes in the mass of the complex. Heterogeneity of samples is often difficult to see in *in vivo* techniques, but shows up directly using mass spectrometry. In the next chapter the various techniques of mass spectrometry will be dealt with in detail.

1.3 Scope of the thesis

Mass spectrometry offers a wide variety of possibilities to analyze proteins separate from their environment and in interaction with their environment. Mass spectrometry is thus of great use to the field of structural biology. The established mass spectrometry methods are extensive and their amount is ever increasing. New methods grow increasingly more sophisticated and require increasingly more knowledge from the experimentalists. Moreover, the field is moving to the study of increasingly more complex (protein) systems. Where mass spectrometry was first used to study only relatively small proteins and complexes now complete biological systems are evaporated into the gas-phase and analyzed.

The study of such complexes requires new methodologies to be constructed and evaluated. What can we learn from these complexes by studying them in the gas-phase with mass spectrometric methods? How do we interpret the (complex) results obtained with these new techniques, to make them useful for broad application? What are the effects of the removal of solvent on the behavior of the complexes? What physical parameters and mechanisms determine protein behavior in the gas-phase? These questions will be addressed with the use of the two model proteins GroES and gp31. These two proteins are part of chaperonin complexes. Gaining insight into the physical parameters determining their behavior can help answer the bigger question of what physical properties govern the functioning of chaperonin-assisted protein folding.

Chapter two gives an overview of the mass spectrometric techniques used. It deals with the advantages and disadvantages of these techniques. After explaining the techniques the relation of the gas-phase to the solution-phase structure will be explained.

Chapter three shows the effect of electron capture on the stability of the gas-phase complexes. It shows that gas-phase conformation of the noncovalent complex influences its behavior under electron capture.

Chapter four compares the effect of gas-phase collision activation techniques on the two protein complexes. The various activation methods result in different dissociation characteristics, depending on the mechanism of activation. It also reports on differences in gas-phase behavior between the two complexes.

Chapter five shows the effect of thermal activation of the complexes before mass spectrometric analyses. This shows the gas-phase measurement of solution-phase activation and reveals how applicable these thermostability measurements are. This chapter continues with the comparison to gas-phase thermal activation. Major differences in the behavior of the protein complexes are observed and discussed.

Mass spectrometry of noncovalent protein complexes

2.1 Electrospray ionization

Protein analysis with mass spectrometry (MS) requires the transfer of the protein from the solution-phase to the gas-phase and the generation of either positive or negative charged species. Electrospray ionization (ESI) is one of the techniques available to perform this task. It was first described by Dole⁶¹ and was introduced for use with mass spectrometry by Fenn *et al.*⁶⁰ It is a means of atmospheric pressure ionization, whereby a solution containing the analyte is sprayed in the direction of the inlet of the mass spectrometer. The mechanism of electrospray is visualized in Figure 2.1. The protein in its buffer solution is guided towards a narrow spray tip, usually around $10\mu\text{m}$ in diameter. A high voltage is applied to the solution (1 - 4kV), either via direct contact with an electrode, or via a (gold-)coating on the spray tip. The spray tip is usually made from fused silica, meaning it is not electrically conductive by itself. It is possible to do both positive and negative ESI. In this thesis positive ESI is used. The solution, with an excess of positive charges, is ejected from the tip forming a so-called Taylor cone.⁶² From this cone droplets are ejected. These droplets grow increasingly smaller, due to evaporation of solvent molecules and due to fission caused by Coulombic repulsion.

There are two mechanisms proposed by which the desolvation and charging of proteins within the droplets proceeds: the ion evaporation method (IEM) and the charge residue model (CRM). The IEM was the first mechanism to be proposed.⁶⁵ This model states that when the droplets become smaller, the electric field will become strong enough to push off ions into the ambient gas. Evaporated ions can remain somewhat solvated. This model applies mainly to small ions. For the ionization and evaporation of proteins, i.e. considerably large ions, the CRM is more applicable.^{61,66} In the CRM the large droplets first dissociate into smaller ones containing

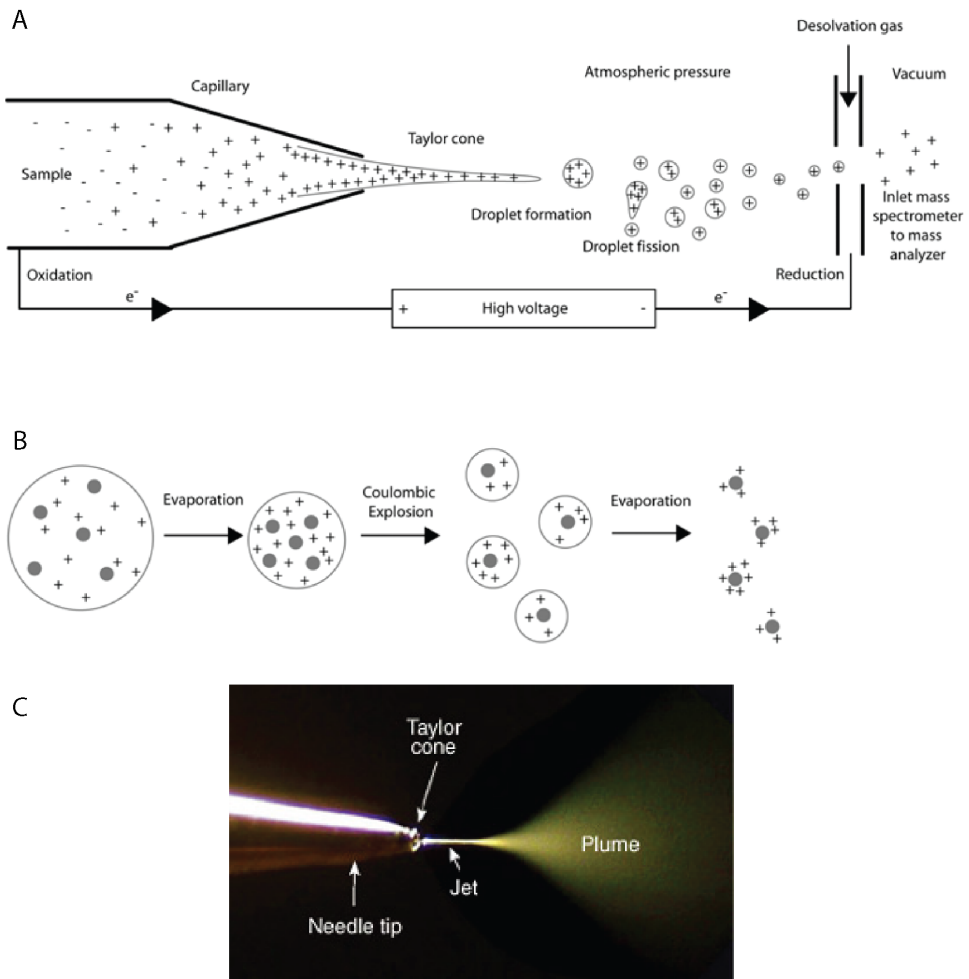


Figure 2.1: (a) Overview of the mechanics of the electrospray ionization technique. The high voltage applied to the spray sample causes positive charge to build up at the spray tip. Due to the charge and the pressure a so-called Taylor cone is formed. From the Taylor the charged droplets well decrease in size and split, until eventually single charged proteins are left. (b) Zoom of the droplet evaporation and fission during electrospray ionization in the Charge Residue Model. (c) photo of an actual Taylor cone. Adapted from: Benesch⁶³ and New Objective⁶⁴

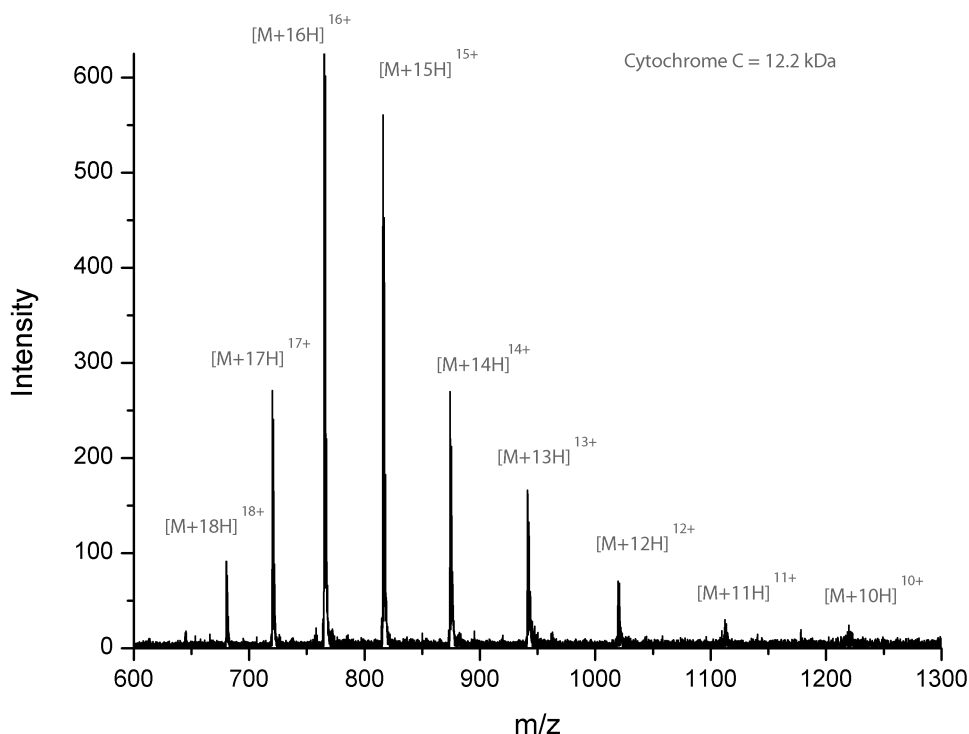


Figure 2.2: Typical mass spectrum of denatured Cytochrome C. The sample is denatured in a buffer of methanol, water and acetic acid (69%/29%/2%). The Gaussian charge state distribution is typical for ESI mass spectra.

only one analyte molecule via a sequence of Rayleigh instabilities, also called Coulomb explosions. The solvent molecules then evaporate off these small droplets, leaving behind the charges that eventually reside with the analyte protein, see Figure 2.1b. There is still much debate on the exact evaporation/ionization mechanism.⁶⁶⁻⁷⁰

Upon entering the mass spectrometer, the ion evaporation and desolvation continues. To aid the desolvation of the ions a heated capillary or heated drying gas is used. The created gas-phase ions are then ready for measurement and/or manipulation. Typically, a mass spectrum of one type of protein will show multiple charge states which is called the charge state distribution, an example is shown in Figure 2.2.

Electrospray ionization made evaporation of nonvolatile compounds possible. It is a very soft ionization techniques that can be tuned to leave noncovalent interactions between the analyte molecules intact. That is called native ESI, in contrast to nonnative ESI, and depends on the solution

conditions used. In the example of Figure 2.2 Cytochrome C was dissolved in a denaturing solution. Typically, proteins are denatured by using 50% organic solvents combined with a small amount of acid lowering the pH. Denaturing solvents allow for easy evaporation. Denatured proteins have a relatively large surface area allowing them to acquire many charges during the ESI process, which makes them easily measurable. However, when trying to measure intact noncovalent proteins complexes, the proteins may not be denatured, otherwise the complex is destroyed. Native ESI is needed to measure these complexes. A water-based solvent combined with ammonium acetate can be used for native ESI. The pH of the sample then remains near physiological at pH 6.8 and the proteins remain in their native state. However, exact solution conditions have to be tuned for efficient ionization and evaporation of the sample. Since native proteins have a smaller surface area they will acquire fewer charges during the ESI process, causing them to appear at higher m/z in the mass spectra.

Besides the differences between native and nonnative ESI, on the whole, ESI generates more highly charged ions compared to other ionization techniques. This makes ESI a suitable technique to utilize for ionization of large noncovalent protein complexes like the GroES and gp31 co-chaperonins. They will not only remain intact, but the high number of charges on the ions puts them in the mass/charge range measurable by mass spectrometry. The downside of conventional electrospray is the relatively large amount of sample consumption. To overcome this also nano-electrospray can be used.⁷¹ The difference for nanospray is that the needles have a smaller diameter ($1\mu\text{m}$) and that it can be used without a backing sample flow, reducing sample consumption. Nowadays, ESI of less than a picomole of protein complex can be readily achieved.

2.2 Mass spectrometers

Once the analyte molecules are evaporated into the gas-phase and ionized they can be mass analyzed in the mass spectrometer (MS). There are various ways of measuring the mass of ionized molecules. In this thesis time-of-flight and ion cyclotron resonance methods are used. Measurement apparatus for these methods are commercially available. The rest of this section discusses the various analytical MS techniques used in this thesis.

2.2.1 Time of flight mass spectrometry

Time-of-Flight (TOF) measurement of ions, is based on the determination of the time it takes for an ion to travel a certain distance. Ions can be accelerated by electric fields to a specific kinetic energy. The velocity of an ion obtained after acceleration depends on the acceleration potential, its charge and its mass. More specific, the velocity of the ion will be

proportional to its mass (m) over charge (z) ratio (m/z ratio). Ions of different m/z subject to the same acceleration potential will thus obtain different velocities. By measuring the time it takes to travers a certain distance the m/z ratio of the ions can be calculated.⁷²

The resolution that can be obtained using TOF systems depends on numerous factors. For instance, the starting kinetic energy distribution of the ion bunch will lead to peak broadening. This effect can be partly overcome by using orthogonal extraction TOF, whereby the ions are accelerated orthogonally for TOF measurement. Using this technique, the initial velocity distribution along the direction of the ion beam does not have an influence on the flight time of the ions. Another improvement is made by using a reflectron halfway through the flight path. By reflecting the ions, energy variations at the start of the measurement are compensated when the ions arrive at the end of the flight path. This improves the time-focussing of the ions on the detector and hence decreases peak width.

An example of a TOF device is shown in Figure 2.3. The inlet of the mass spectrometer is on the left side. This is where gas-phase ions are generated using ESI. The gas-phase ions are extracted orthogonally by the sample cone. This ensures that most of the solvent does not enter the mass spectrometer and thus reduces contamination. Via another 90° turn the ions now enter a transport hexapole (Q0). The sequential chambers in the mass spectrometer are progressively pumped, gradually reducing the background pressure. By applying a DC voltage offset to the hexapole rods and a RF field over the hexapole rods, the ions can be guided forward towards the final mass analyzer stage, with the lowest pressure. The pressure in the analyzer is kept low to minimize collisions with neutrals during mass analysis. Typical pressures are indicated in the figure.

The setup shown in Figure 2.3 has an extra chamber inserted between the transport hexapole and the TOF measurement. This chamber consists of a quadrupole (Q1) and a collision cell (Q2). This extra chamber allows for so-called tandem mass spectrometry measurements. The quadrupole (Q1) can be set for mass-selection. Only ions of a selected m/z window are then allowed to pass through the quadrupole. Ions of other m/z will not have stable flight paths through this quadrupole and hit the quadrupole rods or be ejected outward. This ion selection is the first MS-stage. The selected precursor ions subsequently enter the collision cell. The pressure inside this cell is raised by introducing a noble gas (usually Argon). The analyte ions will (inelastically) collide with the Argon gas and transform part of their kinetic energy into internal energy. The kinetic energy with which the ions enter the cell can be accurately controlled. When the internal energy of the ions reaches the dissociation threshold they will fragment creating all kinds of product ions. This process is called collisional activated dissociation (CAD). Products created in (and after) the collision cell are subsequently mass analyzed. Using this setup it is thus possible to

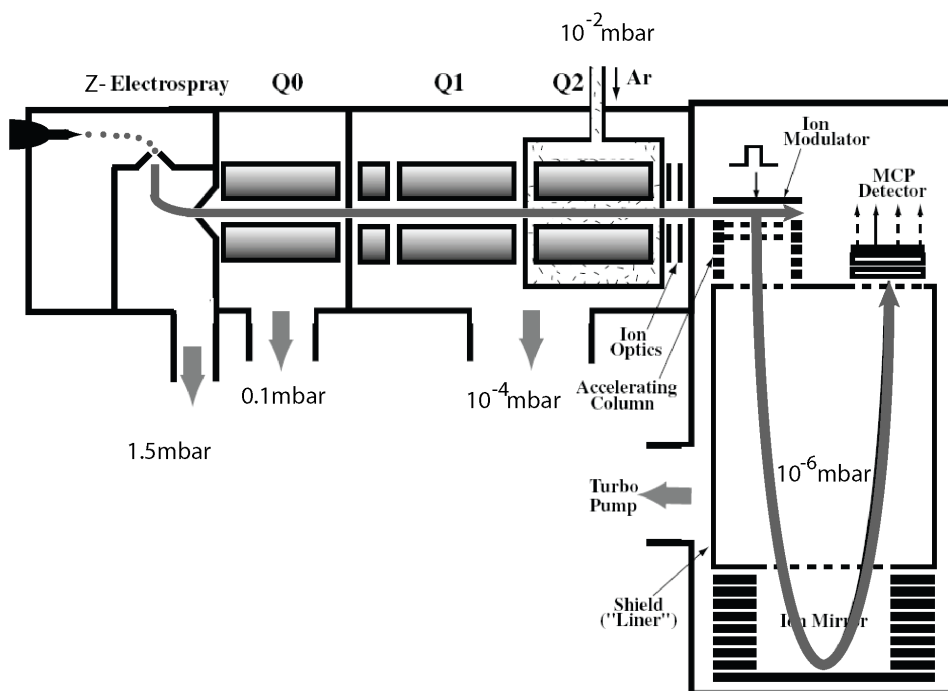


Figure 2.3: Schematic cross-section of a q-TOF instrument. On the left side the ion (ESI) Z-spray source is shown. Via sequential pumping stages, the pressure goes down to $\pm 10^{-6}$ mbar in the flight tube. In case of CAD, the collision cell can be loaded with Argon to a pressure of $\pm 10^{-2}$ mbar. The ion flight path is indicated by the gray line.

qualitatively investigate fragmentation pathways of ions. This machine is called a quadrupole time of flight mass spectrometer (q-TOF).

Normally, the pressure in the source region and the first quadrupole is kept low (± 1.5 mbar and ± 0.1 mbar respectively), to allow the newly formed ions to drift into the mass spectrometer. Analysis of relatively large protein complexes (high m/z), as used in this thesis, requires the pressure in the source region to be raised to ± 5 -9 mbar.⁷³⁻⁷⁵ Since the ions are formed at considerable electrical potentials, they will acquire a high kinetic energy and will need to be slowed down in order to transport them properly through the first stages of the mass spectrometer to the analyzer. Light ions are easily slowed down via collisions with background gas molecules (mostly nitrogen from the ambient air) in the source region. Heavy ions, however, have relatively little energy transfer upon collision with the much lighter nitrogen. Many more collisions are needed to slow these ions down,

requiring a higher pressure in the source region. The pressure in the source region can be controlled via a throttle valve controlling the air flow to the vacuum pump. Besides increasing the pressure, also the quadrupole has to be adjusted, because it is normally not possible to study macromolecular protein complexes. This is due to the limited m/z range of the quadrupoles. By modifying the RF unit of the quadrupole to operate at lower frequency, ions of up to $32,000m/z$ can be analyzed.

A major characteristic of the time-of-flight technique is the short measurement timescale. After evaporation the ions are measured within a few hundred microseconds. This means there is little time for (meta-)stable conformations of the ions, created in the ionization process or in the collision cell, to decay before measurement. This is a considerably different from the next mass spectrometer discussed, the Fourier Transform Ion Cyclotron Resonance Mass Spectrometer.

2.2.2 Fourier transform ion cyclotron resonance mass spectrometry

Fourier Transform - Ion Cyclotron Resonance Mass Spectrometry (FT-ICR-MS, FTMS) operates on a physically different principle than time-of-flight. A Fourier Transform Mass Spectrometer does also measure the m/z value of ions, but now based on the cyclotron frequency of the ions in a magnetic field. Ion cyclotron resonance was first used for nuclear physics experiments in the 1930's.⁷⁶ In the 1970's Comisarow and Marshall⁷⁷ published the first application of the Fourier transformation to image charge detection. Since then the use of Fourier based mass spectrometry has increased dramatically, especially due to the mass resolution and mass accuracy of these instruments. This next paragraph will briefly discuss the fundamentals of FTMS, before continuing to the practical applications used in this thesis. More information on this technique can be found in these papers⁷⁸⁻⁸⁰.

2.2.3 FT-ICR-MS theory

The main component of FTMS is a high and homogeneous magnetic field. Ions moving in that magnetic field start to rotate with a frequency that is inversely proportional to their m/z ratio, due to the Lorentz force, see Equation 2.1. The rotation is called cyclotron motion.

$$\omega_c = \frac{z}{m}B \quad (2.1)$$

The cyclotron frequency (ω_c) is proportional to the magnetic field (B). By measuring the frequency of the rotation the m/z ratio of the ions in the magnetic field can be calculated. The rotation of the ions can be measured using detection electrodes located around the circular path of the ions.

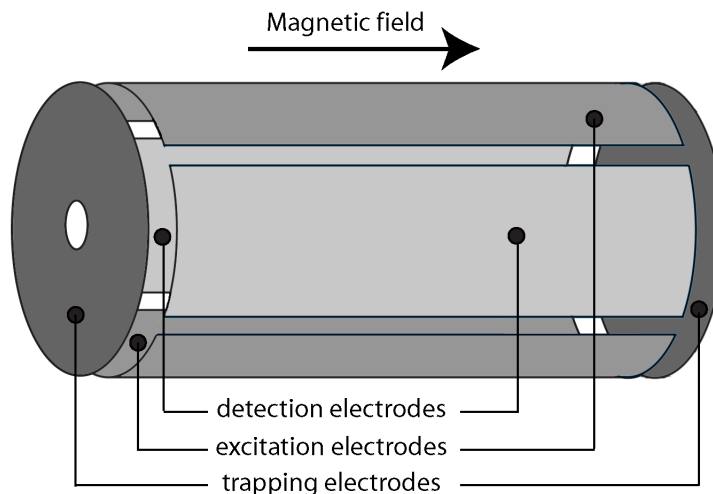


Figure 2.4: Drawing of an ICR-cell. The ions enter through the hole in the front. They are trapped in the direction of the magnetic field by the trapping plates. The excitation plates are used to excite the ions before detection and the image current through the detection plates is measured and amplified to obtain a mass spectrum.

Ions passing by the electrodes will induce an image charge. Since the ions are rotating, the amount of image charge in the electrodes will change with time creating a changing potential on the detection electrodes. The frequency of this potential change is the same as the rotational frequency of the ions. Figure 2.4 shows a typical measurement setup for detection ions within a magnetic field: the ICR-cell.

In this figure two detection electrodes are shown on each side of the ICR-cell. The electrodes will each have a modulated image charge potential that is exactly 180° out-of-phase. The potential differences between the detection electrodes is measured, amplified and Fourier transformed. Besides the detection electrodes, there are four other electrodes present in the ICR-cell, two trapping electrodes and two excitation electrodes. The function of these plates will be discussed next.

A good measurement of the cyclotron frequency requires the ions to be confined in the ICR-cell for prolonged periods of time. The magnetic field will trap the ions in the radial direction and the trapping plates depicted in Figure 2.4 are used to trap the ions in the lateral direction. This is achieved by putting an energy barrier on the electrodes, creating a potential well that confines the ions. The ions exhibit a trapping motion in the lateral direction, with a frequency ω_t determined by Equation 2.2

$$\omega_t = \sqrt{\frac{zV_t}{md^2}} \quad (2.2)$$

V_t is the applied trapping potential and d the length of the ICR-cell. The lateral trapping potential also produces a radial field, creating a force component on the ions directed outward, opposite to that of the Lorentz force:

$$E = \frac{rV_t}{2d^2} \quad (2.3)$$

r is the distance from the cell center. The extra force influences the ion cyclotron motion from Equation 2.1. The ion equation of motion becomes (equating the centrifugal force to the combined magnetic and electric force):

$$m\omega^2 r = zB\omega r - z\frac{rV_t}{2d^2} \quad (2.4)$$

This quadratic equation has two solutions:

$$\omega_+ = \frac{\omega_c}{2} + \sqrt{\left(\frac{\omega_c}{2}\right)^2 - \frac{\omega_t^2}{2}} \quad (2.5)$$

$$\omega_- = \frac{\omega_c}{2} - \sqrt{\left(\frac{\omega_c}{2}\right)^2 - \frac{\omega_t^2}{2}} \quad (2.6)$$

where ω_c is the "unperturbed" cyclotron frequency and ω_t is the trapping frequency. The trapped ions thus exhibit two circular motions with different frequencies: ω_+ , which is slightly lower than the unperturbed cyclotron frequency and ω_- which is a low frequency motion. This last motion is also called the magnetron motion of the ions. The magnetron motion is undesired. It causes a shift in the observed frequency from the ideal value and it can cause sidebands to appear when the magnetron radius becomes significant compared to the radius of the cyclotron orbit.

Ions that are trapped and rotating inside the ICR-cell do not produce a net signal on the detection electrodes, because the radius of motion is small and the ions move incoherently. To measure an ICR-signal the ions need to rotate close to the detection plates and rotate coherently as a single bunch. The excitation electrodes in Figure 2.4 are used for excitation, prior to detection. An alternating electric field over the excitation electrodes with a frequency equal to that of the cyclotron frequency of the ions will excite these ions to cyclotron orbits of increasingly larger radii. Moreover, the initial ion cloud will be excited coherently and move in-phase around the ICR-cell after excitation. Now the ion cloud produces a measurable image potential. This is visualized in Figure 2.5.

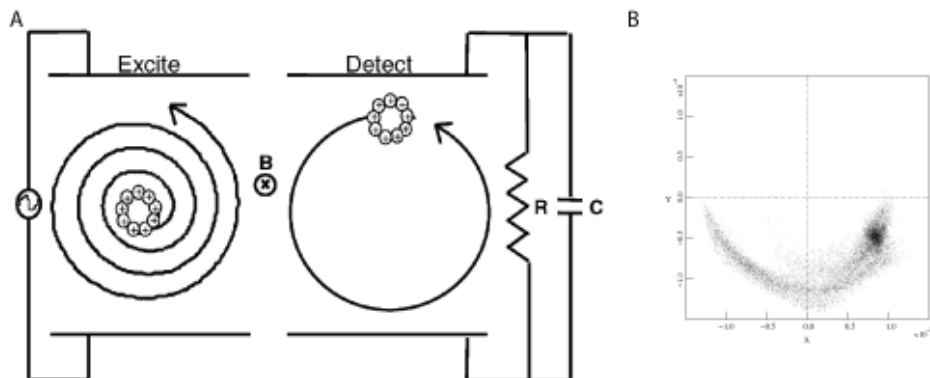


Figure 2.5: A) the ion cloud on the left side, is excited to coherent ion motion by a RF-pulse on the excitation plates. Subsequently it is detected by a measurement circuit connected to the detection plates. *Adapted from: Marshall⁸¹* B) simulations show that after excitation the coherence of the ion package gradually decays due to the formation of a comet-like structure.

It is possible to excite ions of different cyclotron frequencies (i.e. different m/z) sequentially, by changing the excitation frequency. Ions with cyclotron frequencies different from the excitation frequency will not be influenced by that excitation (the off-resonance excitation averages out). The final cyclotron radius obtained by the ions depends linearly on the excitation time:

$$r = \frac{E_0 t_{exc.}}{2B} \quad (2.7)$$

where r is the final cyclotron radius, $t_{exc.}$ is the excitation time and E_0 is the amplitude of the electric field. The orbital radius is independent of the m/z value of the ions and equal excitation times for different m/z ions will lead to equal cyclotron radii. After excitation the electrical signal in the detection plates is measured with respect to time (the transient). The measured signals scale with the charge state of the ions. When performing yield calculations of ions the measured signal must be corrected for the charge state. Throughout this thesis all yield calculations are corrected for charge state unless otherwise stated.

To determine the frequency of rotation from the transient, it has to be Fourier transformed, hence the name of the method. The longer it is possible to measure the transient signal the more precise the frequency determination (and thus the m/z value) will be. One of the major characteristics of this measurement is that, in theory, the measurement does not have to end. The

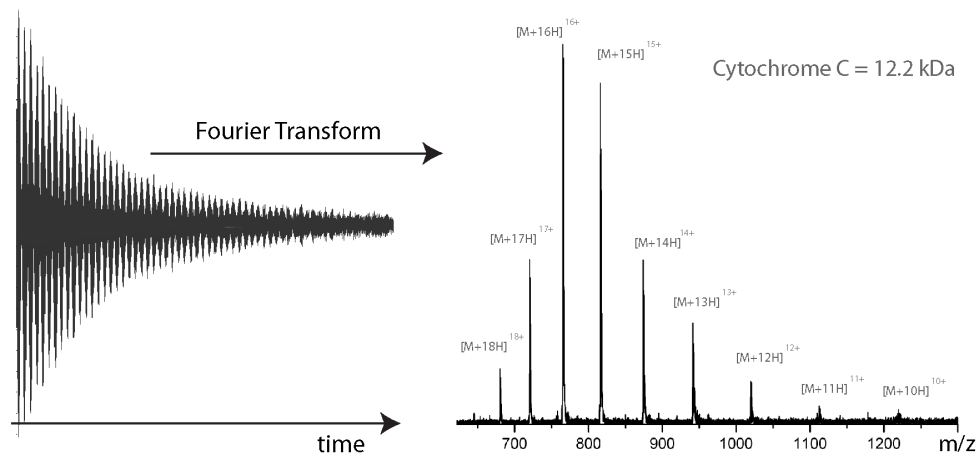


Figure 2.6: The left-hand-side of the figure shows the time signal obtained from image current detection. The beat pattern is caused by interference of ion signals with different cyclotron frequencies. To obtain the mass spectrum (frequency spectrum) from the time signal, it has to undergo a Fourier transformation.

ions move freely in vacuum and are not stopped at a certain position as is the case with time-of-flight measurement. This creates possibilities for very precise measurements of ion m/z . In practice the ion signal decays due to loss of coherence of the ions packets, caused by collisions with background gas and Coulomb repulsion between the ions. A shorter transient leads to increased peak widths. A typical transient is shown in Figure 2.6. The beat pattern arises from summing the time signals generated by ions with different cyclotron frequencies. Applying a Fourier transformation to the transient will render the frequency spectrum that can be readily calibrated to the m/z spectrum. The transient is also called the Free Induction Decay (FID) signal.

A second major characteristic of FTMS is the fact that after the time signal is damped out, the ions are still trapped inside the magnetic field. The detection is non-destructive. This means the same ion cloud can be measured over and over again, until the ions are lost from the ICR-cell. An ion trapped in an ICR-cell can be manipulated using various techniques. Ion-molecule and/or ion-electron reactions can be performed on the ions from which the reaction products are subsequently measured. The versatility of the FTMS is further increased by the possibility to selectively eject ions within specific m/z windows, and performing reactions on the remaining ions. These features give the FTMS MS^n capabilities, see section 2.2.5.

A difference to keep in mind between time-of-flight mass spectrometry and Fourier based mass spectrometry is the delay time between activation

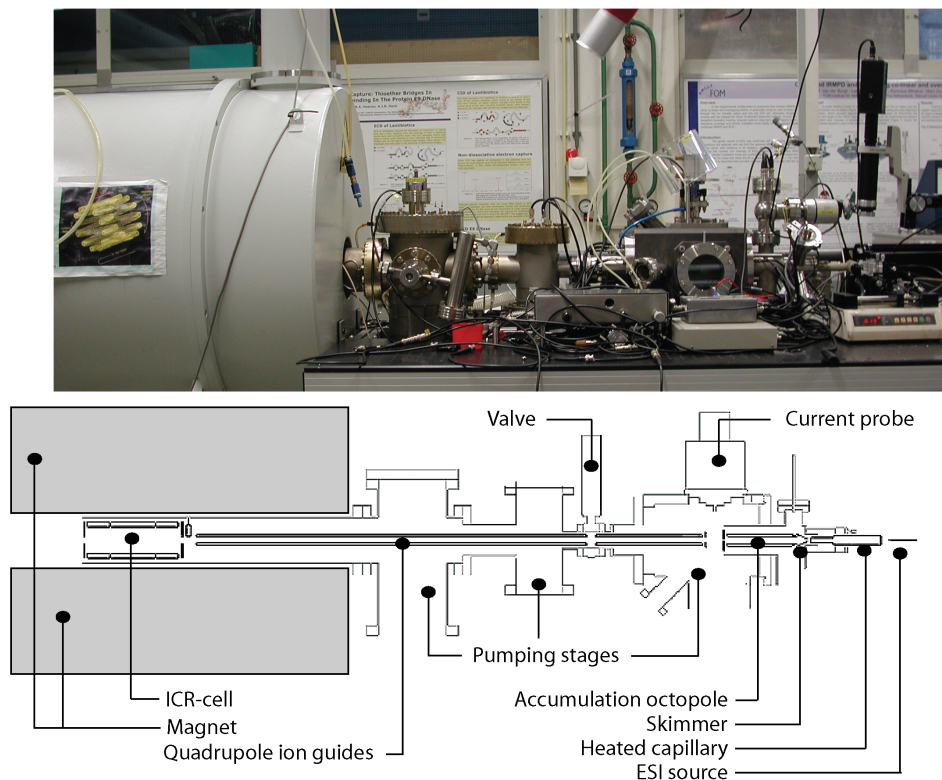


Figure 2.7: Photo and cross section of the FTMS instrument at AMOLF. The ion source is located on the right. Via transport quadrupoles and pumping stages, the ions are brought into the ICR-cell for analysis located inside the magnet on the left.

of the ions and mass analysis. In the FTMS this period is much longer (ms to seconds) than in the ToF MS (μs), giving meta-stable ions more time to decay and hence the same kind of measurement can produce different results when performed on a FTMS or on a ToF MS.

2.2.4 FT-ICR-MS experimental setup

The main component of this machine is a high magnetic field, created by a superconducting coil. The FTMS at AMOLF is a highly modified Bruker APEX 7.0e.⁸² A photo is shown in Figure 2.7 along with a schematic view of the instrument. The front end is on the right showing the atmospheric

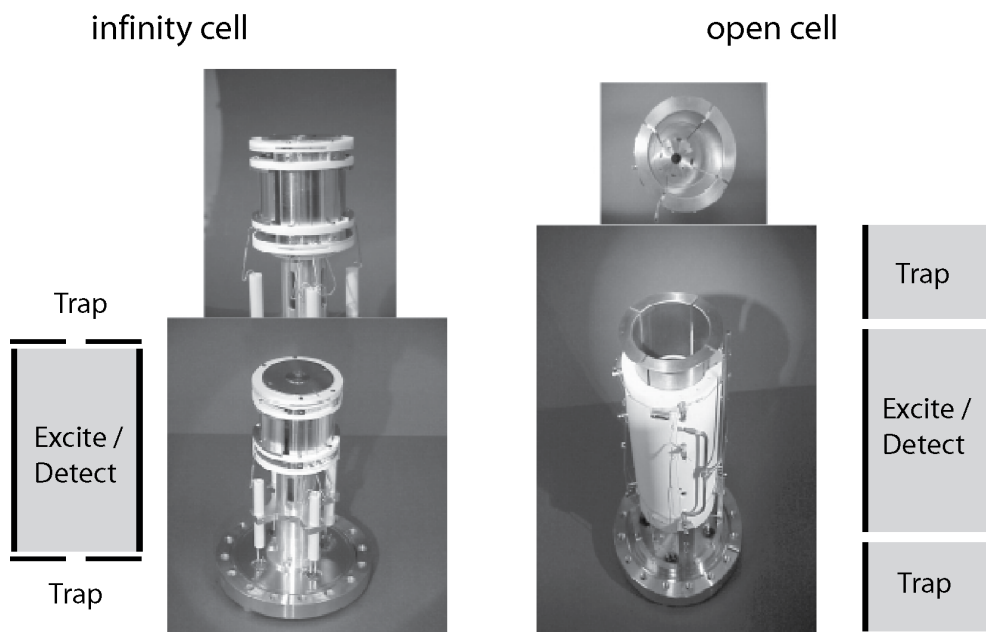


Figure 2.8: These two ICR-cells are available for use at AMOLF: the infinity cell and the open ended cell. Both cell types are used in this thesis.

pressure ESI source. The source is linear in contrast to the orthogonal source of the q -ToF and has a heated capillary to aid desolvation of the ions. After desolvation the ion bundle is cleaned by passing it through a skimmer. Ions can be accumulated in the octopole located behind the skimmer.⁸³ The octopole can also be operated in transfer mode for accumulation of ions inside the ICR-cell. To aid transfer of the high mass ions into the mass spectrometer, the pressure in the source region (in this case the octopole) is raised to 2-3mbar. A probe, located behind the octopole, can be inserted into the ion beam to measure the actual ion current. Via sequential pumping stages the ions are transported to the ICR-cell inside the magnet using quadrupoles. At AMOLF two different ICR-cell configurations can be used, a so-called infinity cell and a so-called open cell. Both cells are shown in Figure 2.8. The open cell has a higher loading capability for ions, but is also more sensitive to noise. The open cell is also equipped with a heating and cooling mechanism, useful for manipulation of the trapped ion cloud.⁸⁴⁻⁸⁷ Both cells are used in this thesis.

The FTMS is operated with home-built software and electronics. A control program called Arbitrary Waveform Generator (AWG),⁸² is used for the design and generation of any desired sequence of pulses and voltages.

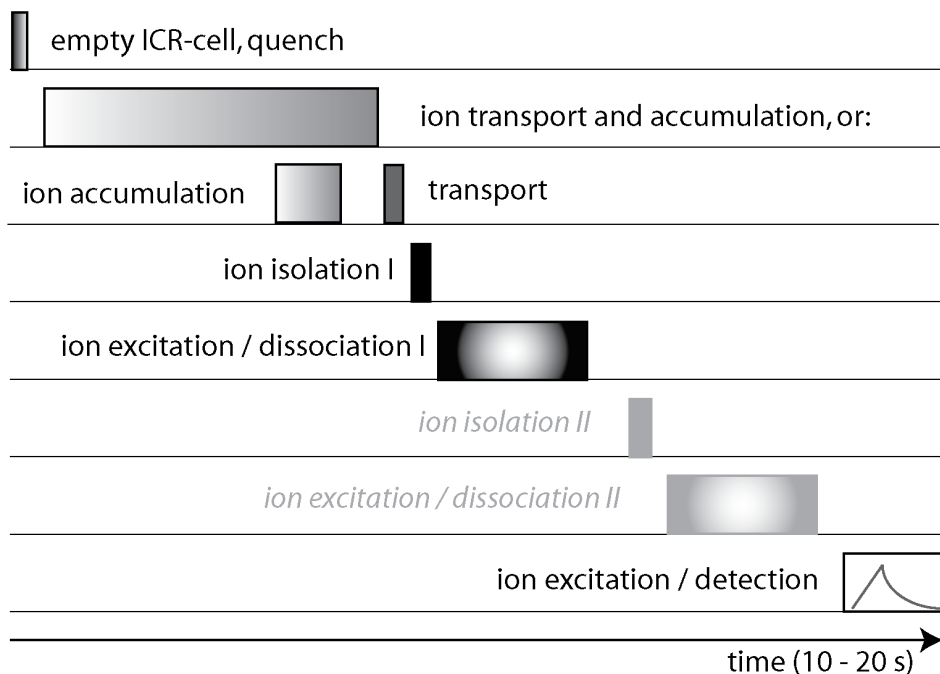


Figure 2.9: Time view of the events occurring sequentially during one measurement cycle. First the ICR-cell has to be emptied from ions remaining from a previous measurement. The clean cell is then loaded with new ions, either by transport and accumulation in the ICR-cell (second row) or by ion accumulation in the source octopole and subsequent transport of the ion bunch to the ICR-cell (third row). These ions can be directly measured (MS^1). They can also be subsequently isolated and manipulated in one (MS^2 or tandem MS) or multiple steps (MS^n). After manipulation the resulting ion cloud is excited and detected.

This program controls all voltages on the system. A typical time-line example of such an output is given in Figure 2.9.

2.2.5 Tandem mass spectrometry with the FT-ICR-MS

As briefly mentioned, FT-ICR-MS is perfectly suited for performing multistage MS experiments on the same ions. Once the primary ion cloud originating from the sample is trapped in the magnetic field, gas-phase experiments can be performed on these ions. In most cases, however, it is desired to perform the experiments only on ions of a specific m/z range, i.e. one specific charge state or conformation of a protein. This can be achieved by ejecting all unwanted ions from the ICR-cell using the excitation elec-

trodes. Ions can be ejected by selectively over-exciting them, so that they hit the cell wall. Thus over-exciting all frequencies except the desired one, will remove all unwanted ions from the ICR-cell. With the software that has been designed at AMOLF, it is possible to select specific mass ranges in the mass spectrum and subsequently create a tailored waveform for ejection of the selected mass range. This is done by creating so-called SWIFT pulses (Stored Waveform Inverse Fourier Transform).⁸⁸ This creates a inverse Fourier transform of the desired m/z (frequency) excitation spectrum using a quadratic phase scrambling method. The excitation signal will now eject all unwanted ions and leave the desired ions untampered with.

The isolated ions can subsequently be activated via various techniques to induce physical and chemical reactions.⁸⁹⁻⁹¹ Some of these techniques are detailed in the next paragraphs. The reaction product ions can be analyzed and, if desired, a second isolation-activation round can be performed analyzing the fragments of fragments, and a third, and so on. This is what is meant by MS^n capabilities of FT-ICR-MS instruments. The next paragraphs will explain the activation techniques used in this thesis, some of them use isolation before activation, whereas others activate the entire ion population.

Nozzle-skimmer dissociation

This is an ion activation technique that is performed in the source region of the mass spectrometer, without any prior isolation of specific ions. Immediately after generation of the ions and passing through the heated capillary, the ions can be accelerated by raising the voltage of the capillary compared to the voltage of the skimmer. The ions will subsequently collide with the cooling gas having a higher kinetic energy than under normal conditions and transform this kinetic energy into internal energy. This technique is called Nozzle-Skimmer Collision Activated Dissociation (NS-CAD). The higher internal energy will result in the decay of the ions if the dissociation threshold is reached. The internal energy accumulated is determined by the acceleration potential multiplied by the charge of the particular ion and the efficiency of converting kinetic energy into internal energy via collisions. A major characteristic of this technique is that the ions need not be completely desolvated before excitation. This means there might be more interaction with buffer molecules during the activation in comparison to activation in the ICR cell. Activation occurs on a much shorter time scale than activation inside the ICR cell, because the pressures are much higher in the source than in the ICR cell. Finally the resulting products still have to be transported to the ICR cell, which might result in additional losses of specific ion fragments.

Collision activated dissociation

Collision Activated Dissociation (CAD) is performed on ions trapped in the ICR-cell.^{92,93} The ions can be selectively activated using an excitation pulse of corresponding frequency on the excitation electrodes. The kinetic energy of these ions is increased by the excitation, see equation 2.8.

$$K.E. = \frac{q^2 V_{p-p}^2 T_{excite}^2}{8d^2 m} \quad (2.8)$$

Here q is the charge of the ion in Coulombs, V_{p-p} the peak-to-peak excitation voltage in volts, T_{excite} the excitation time in seconds, d the ICR-cell diameter and m the mass of the ion in kg. After excitation, the ions collide with a collision gas, like Argon or Xenon, which is passed to the ICR cell via a valve. Collisions convert the kinetic energy of the ions into internal energy, eventually inducing dissociation of the ions. To decrease the complexity of fragment analysis, the parent ions can be isolated before activation, removing all other ions from the ICR-cell. All ions present in the resulting (fragment) spectrum originate from dissociation of the parent species. Typically, the kinetic energy is transformed into internal energy via several high energy collisions, within a relatively short time period.

Sustained off-resonance collision activated dissociation

High mass ions have a large number of degrees of freedom in their rovibrational modes. The internal energy built-up is distributed over the modes, resulting in a higher overall internal energy built-up needed for dissociation. For these higher mass ions a single excitation with CAD might not be enough to reach the energy threshold for any decay channel. There is also a possibility to excite them continuously using Sustained Off-Resonance Irradiation Collision Activated Dissociation (SORI-CAD).⁹³⁻⁹⁵ Using this method activation is slower, but can be continued for longer periods of time. SORI-CAD uses a specific frequency for excitation, as with CAD, only now it is slightly off-resonance with the frequency of the desired parent ion. This means the excitation will move in- and out-of-phase with the movement of the ions creating a modulation in the kinetic energy of the parent ions. This is visualized in Figure 2.10

Compared to CAD the maximum obtained kinetic energy is lower, but the excitation can be continued indefinitely. With CAD the excitation energy is limited by the physical properties of the cell. During excitation, the ions are collided with collision gas again. A disadvantage of SORI-CAD is that possible fragment ions with a m/z value that corresponds to the frequency of excitation will be ejected from the ICR cell because they are in resonance. This results in a blind spot in the mass spectra after excitation.

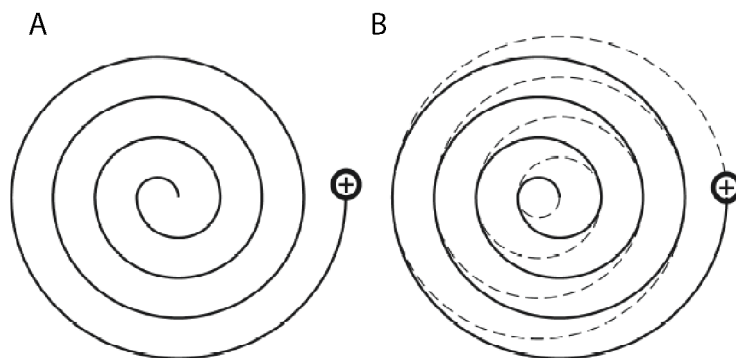


Figure 2.10: Schematic view of the ion trajectory with on resonance excitation (A) and off resonance excitation (B). Using off resonance excitation, the ion radius and thus the ion kinetic energy is modulated. The radius in (B) is exaggerated; in practice, the maximum radius using SORI is much smaller than the radius after excitation using CAD.

A remedy is to perform the experiment twice whereby the second frequency excitation offset is opposite to the offset in the first experiment.

Infrared multiphoton dissociation

Proteins in the gas-phase can absorb and irradiate photons. The energy of the photons is released into the ro-vibrational states of the protein. Irradiating the proteins with multiple IR photons thus heats up the ions and increases the internal energy. This is called Infrared Multiphoton Dissociation (IRMPD).^{96,97} Activation is more gentle than using collisions (CAD) and results in a slower heating of the analyte ions. Using this activation method the ions will be triggered to fragment via the lowest-energy decay channel.

The setup used for IMRPD in this thesis is shown in Figure 2.11. The trapped ions are irradiated from the rear end of the ICR cell with laser light originating from a CO₂-laser, which is focused into the cell for optimum transfer efficiency. The laser is aligned by opening the front end of the mass spectrometer and arranging the various mirrors such that the laser light exits at the front end of the mass spectrometer. Using this alignment scheme, the laser beam passes through several diaphragms along the ion-optical path. This assures good overlap of the laser beam with the ion cloud inside the ICR cell.

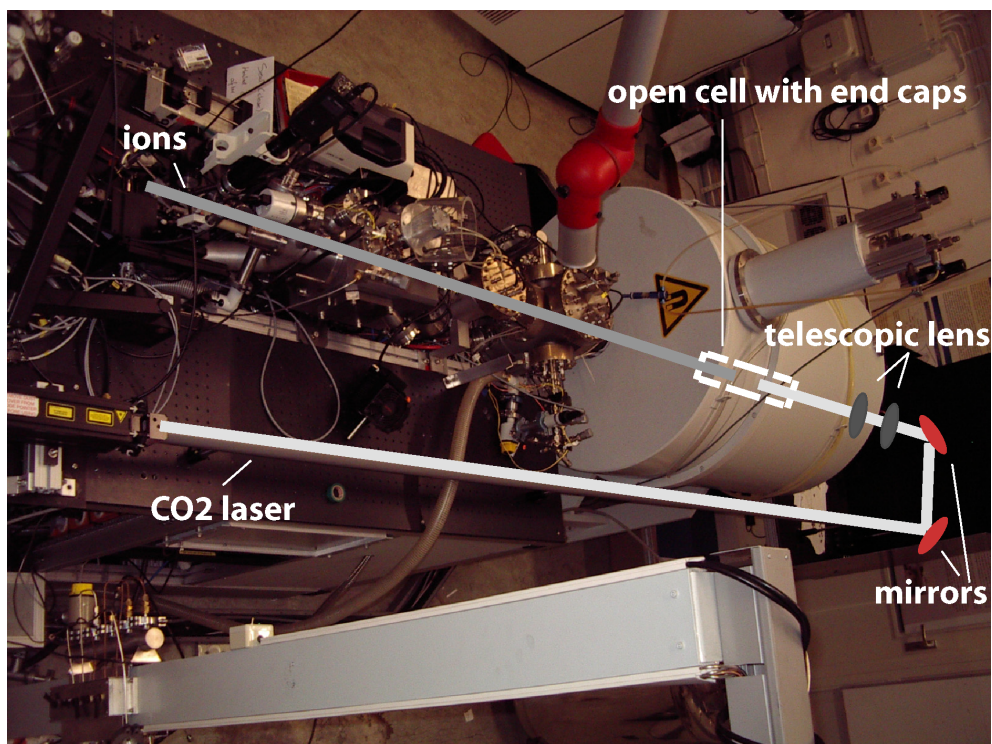


Figure 2.11: Using IRMPD the ions are trapped in the open ended cell and irradiated from the back end with CO₂ laser light. The laser light is focussed with a telescopic lens onto the entrance diaphragm for maximum transmission into the ICR-cell.

Electron capture dissociation

Positively charged proteins trapped inside the ICR cell, can be subjected to irradiation with low-energy electrons. The electrons (negatively charged) can be captured by the positively charged sites on the proteins. This is called Electron Capture Dissociation (ECD).⁹⁸⁻¹⁰² Upon recombination of the positive and negative charge an average energy of approximately 6eV is released into the molecule. This energy can be used to break covalent backbone bonds of the proteins. The energy released upon recombination is not distributed into ro-vibrational states of the protein, but is used locally. That is why this activation method is considered to be non-ergodic.^{98,103} Various experimental approaches have led to the formation of a theory for the mechanism of ECD based on the "hot hydrogen" model. This theory states that the electron is captured at the site of a solvated proton. Fast cleavage is subsequently caused by the transfer of the H[•] to sites with high

hydrogen radical affinity. These sites are for example: carbonyl oxygens, sulfide bonds, and tryptophan residues.¹⁰⁴

ECD is now routinely used in proteomics, to obtain very high sequence coverages.^{105,106} ECD can also be used for identifying post-translational modifications (PTMs). ECD lends itself very well for the analysis of PTMs, because labile bonds are preserved in ECD. PTM sites can easily be observed from mass spectra after ECD. Besides leaving the labile PTM bonds intact, ECD also leaves relatively weak hydrogen bonds intact.^{107,108} For analysis of larger proteins ECD seems to be less suitable because electron capture for these proteins only results in charge reduction without evidence for significant backbone fragmentation. McLafferty suggested that backbone fragments are formed, however, but remain noncovalently bound to the protein.¹⁰⁹ A solution to this problem is to pre-activate the ions before electron irradiation, so-called activated ion (AI-) ECD. Pre-activation of the ions will decrease the higher order structure and increase the amino acid sequence coverage.^{109,110} Another way to reveal backbone fragments that are still attached to the protein is to apply a light post-activation to the ion inducing detachment of the fragments. In contrast to the other studies, in this thesis the first time observation of dissociation of non-covalent bonds due to electron capture is shown (Chapter three).

To be able to perform ECD an electron dispenser cathode is situated at the rear end of the ICR cell. Upon heating electrons from the cathode are emitted into the ICR cell, where they are confined by the magnetic field (as are the positive protein ions). By tuning the overlap between the positive ion cloud and the electron cloud ECD is obtained. Besides physical alignment, also the kinetic energy of the electrons has to be tuned for optimum capture efficiency. For the experiments done in this thesis the optimum electron energy was determined to be $\pm 3\text{eV}$. For a more elaborate treatment of ECD the reader is referred to chapter two of¹¹¹.

2.2.6 Protein fragmentation

Gas-phase activation of protein (complexes) ions can lead to unimolecular dissociation of both the non-covalent bonds, as well as the covalent bonds. Dissociation of the non-covalent bonds leave the backbone of the subunit intact, whereas covalent dissociation results in backbone cleavage. Backbone bond cleavage can occur at various sites along the amino acid chain. The possible cleavages are depicted in Figure 2.12.^{112,113}

Usually CAD and IRMPD lead to b- and y-fragment ions and ECD leads to c- and z•-fragments. The z-fragment has in effect obtained the captured electron at the end of the dissociation reaction.

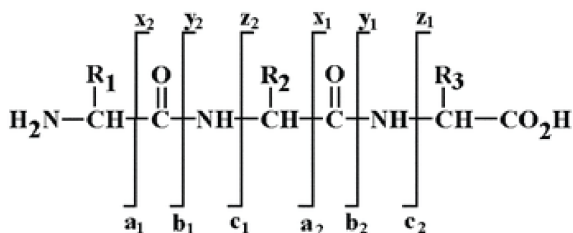


Figure 2.12: Overview of possible backbone cleavage sites and the accompanying nomenclature.

2.3 Temperature controlled ESI

As mentioned in the previous section, activation and dissociation of proteins can be achieved in the gas-phase inside the mass spectrometer. Biologists are usually more interested in the behavior of proteins upon perturbation *in vitro*. There are various methods for perturbing proteins *in vitro*, e.g. manipulation the pH of the solution, adding chemical or biological reagents and thermal manipulation. The effects of *in vitro* manipulation are often analyzed using mass spectrometry. Analyzing pH and chemical/biological manipulation with MS does not pose many difficulties, since the sample is in equilibrium after manipulation. Analyzing thermal manipulation with MS is more difficult, since the equilibrium shifts when the sample is returned to room temperature before ESI and mass analysis. Measuring thermal manipulation with MS therefore requires accurate temperature control of the sample up to the moment of ESI. To be able to analyze thermal manipulation *in vitro* in the mass spectrometer, we have developed a ESI setup in which the sample solution temperature can be accurately controlled (following the example of¹¹⁴). The temperature of the sample can be precisely controlled up to the moment of spraying. As will be shown in Chapter five, using this ThermoProbe temperature dependent effects on proteins can be accurately monitored by MS.

2.3.1 Technical data thermoprobe

A photograph of the ThermoProbe is shown in Figure 2.13. The core of the probe consists of a Peltier element, current controlled by a Eurotherm controller. One side of the Peltier element is connected to a heat sink, whereas the other side is connected to an aluminum block that holds the spray needle. Depending on the direction of the current, the Peltier element heats or cools the aluminum block. Inside the block is a Pt100 resistance for feedback on the actual local temperature inside the block. Two different spray needles can be used: electrospray needles attached to a syringe pump

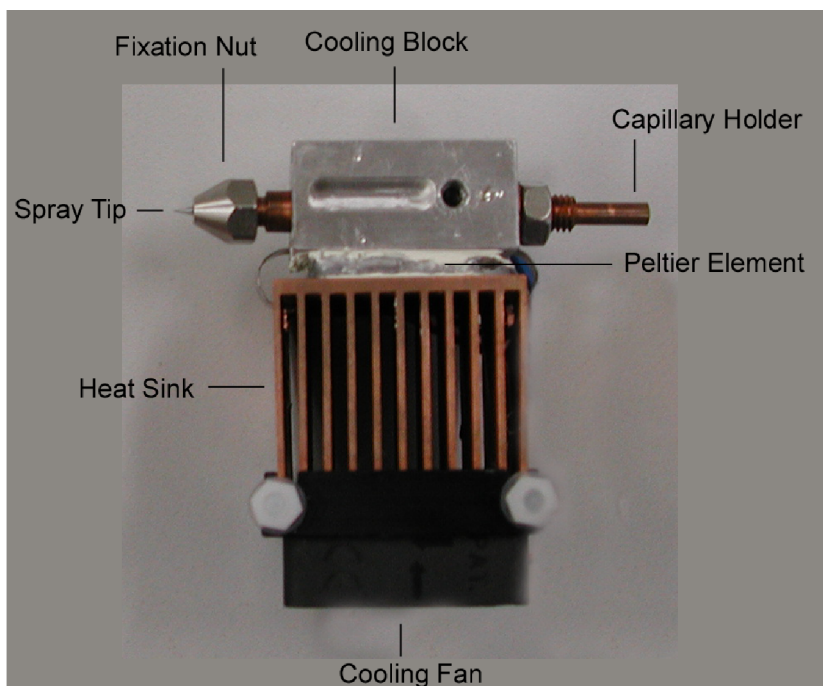


Figure 2.13: Photo of the ThermoProbe. The functional parts of the ThermoProbe are indicated.

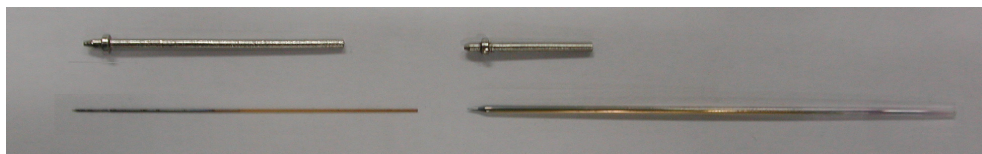


Figure 2.14: Pictures of the two metal capillaries constructed for the two different spray needles. Below the capillaries the fused silica needles are shown.

for continuous flow (microspray), or nanospray needles containing a small static reservoir of sample (nanospray). For these two spray needles metal capillary sleeves have been developed, to assure good contact between the aluminum block and the spray needle, see Figure 2.14.

The sample is either heated or cooled while passing through the needle, right before entering the mass spectrometer. Since both the end of the metal capillary sleeve and the fixation nut will be very close to the orifice of the mass spectrometer, care has to be taken not to cause discharge and not to disturb the electrical field that is necessary to achieve good desolvation

and ionization. For in-line ESI sources (as present on the FT-ICR-MS used for this thesis) this is not a problem, but for orthogonal sources (like the Z-spray source mounted on the Micromass q-ToF or LCT), this poses a problem. For these sources the capillary sleeve and sampling cone are in very close proximity. To be able to perform well with these sources the sleeves are coated with a thin isolating urethane layer. The insulating coating provides better focus of the electric field on the spray tip and prevents discharge between the sleeve and the sample cone.

For calibration of the actual sample temperature inside the needle, the nanospray needle is used. The electrospray needles are too small to fit a thermocouple for calibration. It is assumed that the temperature inside these smaller diameter electrospray needles will be between the temperature of the aluminum block and the temperature inside the nanospray needles. To measure the calibration, a K-type thermocouple (diameter 0.256mm) was fitted inside this needle, along with the sample. The calibration curve is shown in Figure 2.15, demonstrating accurate control of the temperature in the needle tip. For the measurements reported in this thesis the syringe pump with the electrospray needles are used. The spray tip gets clogged when using these protein samples with the nanospray needles at elevated temperatures.

2.4 Gas-phase vs. solution-phase

Using the techniques discussed above, it is possible to perform both solution-phase and gas-phase manipulation of samples and it is of interest to see how the two approaches compare. In this paragraph the theoretical considerations that need to be taken into account when comparing gas-phase to solution-phase effects are discussed. To measure biological molecules by mass spectrometry, they are removed from their natural environment *in vivo* and evaporated into the gas-phase. The most natural environment for proteins is *in vivo*. Proteins *in vivo* are difficult to analyse, because the biological environment intervenes with the measurements. Some techniques for analysis *in vivo* are: fluorescent labeling, Føster Resonance Energy Transfer (FRET) spectroscopy, optical microscopy, confocal microscopy. Although these methods are very useful, exact cause-effect relationships are difficult to asses, as there are a lot of parameters that are not under the control of the experimentalist. For these reasons scientists often remove proteins from their natural environment to have better control over the parameters. The proteins are extracted from cells and dissolved in solvents: *in vitro*. The advantage of better experimental control is counteracted by the difficulty of relating behavior found *in vitro* to biological significant behavior *in vivo*.

For mass spectrometry this holds even more so, because proteins are

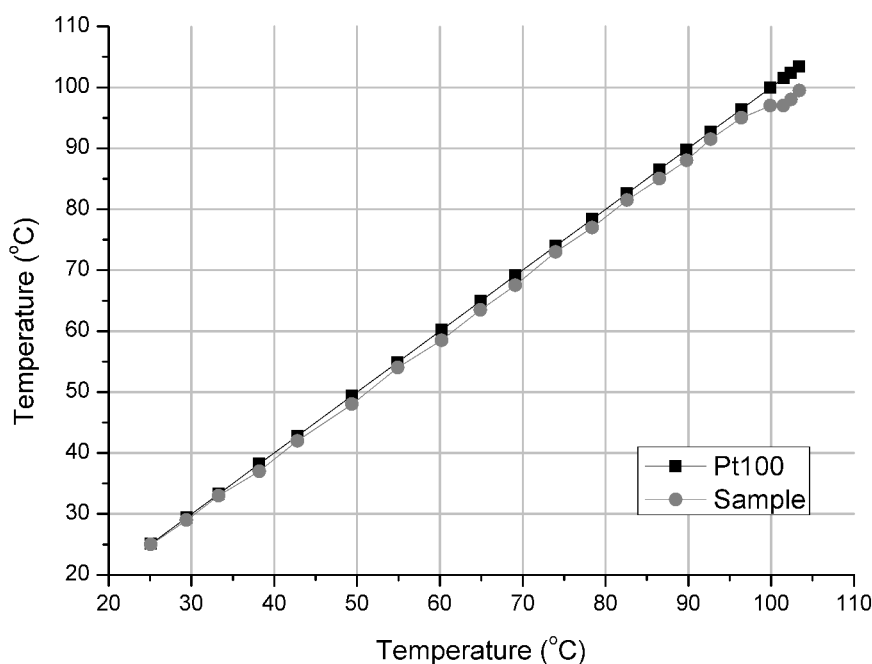


Figure 2.15: Calibration of actual sample temperature compared to the read-off from the Pt100 resistance located inside the aluminum block. At 95°C the deviation from the set temperature is still less than 2°C.

first extracted from cells and subsequently evaporated into the gas-phase (from *in vivo* > *in vitro* > *in vacuo*), where the surrounding environment is completely absent. This allows for very nice experimental control and possibility of specific analyses. However, to a large extent, the function of proteins is determined by its environment. Removing the environment and neighbouring molecules will complicate transfer of the findings in the gas phase to normal functioning of the proteins *in vivo*. By removing the solvent when using mass spectrometry the interactions between the solvent and the proteins are lost.

There are a lot of static electrical interactions within proteins, between proteins and between proteins and their environment. Most of the biological functions of proteins rely on these kinds of interactions. The three dimensional shape of a protein is among other things determined by such interactions, both within the molecule itself and with its environment. The

environment contains usually mostly water, but some (parts of) proteins reside in lipid membranes. Water has a large dipole moment and a large dielectric constant. This means that any polar areas of the molecule will orient itself towards the water when solvated, this is known as hydrophilic interaction. Non-polar sites of the molecules will turn away from the aqueous surroundings and turn to the inside of the molecule, controlled by hydrophobic interactions. In this manner water induces and controls the conformation of the protein *in vivo* and *in vitro*. Hydrogen bonding to water molecules competes with internal hydrogen bonding when the protein is solvated. Removing the solvent, removes the competition and allows for more extensive internal hydrogen bonding. Proteins in the gas-phase may thus be more condensed than when dissolved (in a polar buffer). Moreover the (proton) charges on the molecules present in solution will be shielded from each other and the rest of the molecule by the water molecules. Removing the water will lead to less shielding and more elaborate interactions between the charges and the rest of the molecule, possibly leading to unfolding and denaturation of the protein.

The question arises whether the conformation adopted by the protein in the gas-phase (without solvent and loaded with charges) still resembles its conformation in the solution-phase. Many experiments investigate gas-phase conformations and their relation to conformations *in vivo*.¹¹⁵⁻¹¹⁹ ESI made soft-ionization possible (see paragraph 2.1), allowing multimeric protein complexes to be transferred into the gas-phase intact. This creates possibilities for so-called native mass spectrometry.^{118,120,121} Molecular dynamics simulations and theory also increase our understanding of hydration effects on the conformation of ions.¹²²⁻¹²⁵ Increasingly more experiments are directed towards studying partially solvated systems and the effects of increasing/decreasing hydration on the conformation.^{116,126-129} The onset of ion mobility mass spectrometry in the recent years has opened new possibilities for studying gas-phase conformations of proteins.^{115,130} Using ion mobility MS it is possible to separate ions in the gas-phase based on their cross-section (i.e. conformation), allowing ions of equal m/z but different conformation to be separated before mass analysis.

Besides the interaction with surroundings, the effect of evaporation on the internal temperature of the protein also needs to be taken into account. When evaporating the proteins, expansion into the gas-phase will cool the protein ions. The cooling is counteracted by the applied potentials that accelerate the ions, causing collisions with background gas and heating the ions by converting kinetic energy into internal energy. Usually evaporation is facilitated by a heated capillary or cone, also influencing the temperature of the ions. The resulting energy distribution of the ions (and accompanying effective internal temperature) might be very different from the solution-

phase, having its effect on the conformation of the molecules.

The area of gas-phase protein conformation is thus under vivid investigation, and it will be long before final things are said on this matter.

2.4.1 Implications for this research

The proteins used in this thesis form noncovalent heptameric ring structures *in vivo* and *in vitro*. In the gas-phase this conformation is retained (see Chapters three, four, and five) and activation reactions will be applied to these protein ions using the techniques described above. It will be investigated how the complexes dissociate into their constituent parts and the role the gas-phase conformation plays in that matter. The behavior of the two different proteins will be examined. The interpretation of the results of the techniques will be discussed, along with the applicability of using these methods to study such proteins. Possible relations to the solution-phase behavior of the proteins are also addressed (Chapter five). Analyzing the solution-phase behavior by gas-phase MS will give insight into the overall effect the evaporation and ionization process has on the (conformational) state of the analyte. In the end of the thesis the solution-phase activation will be compared to the gas-phase activation, whereby the effect of removing the solvent on the behavior of the proteins is very clear.

ECD as structural probe for noncovalent gas-phase protein assemblies

Abstract

Electron capture dissociation (ECD) of proteins in Fourier Transform Ion Cyclotron Resonance (FT-ICR) mass spectrometry (MS) usually leads to charge reduction and backbone-bond cleavage, thereby mostly retaining labile, intramolecular non-covalent interactions. In this report, we evaluate ECD of the 84kDa non-covalent heptameric gp31 complex and compare this with sustained off-resonance irradiation collisionally activated dissociation (SORI-CAD) of the same protein. Unexpectedly, the 21+ charge state of the gp31 oligomer exhibits a main ECD pathway resulting in a hexamer and monomer, disrupting labile, intermolecular noncovalent bonds and leaving the backbone intact. Unexpectedly, the charge separation over the two products is highly proportional to molecular weight. This indicates that a major charge redistribution over the subunits of the complex does not take place during ECD, in contrast to the behavior observed when using SORI-CAD. We speculate that the ejected monomer retains more of its original structure in ECD, when compared to SORI-CAD. ECD of lower charge states of gp31 does not lead to dissociation of noncovalent bonds. We hypothesize that the initial gas-phase structure of the 21+ charge state is significantly different from the lower charge states. These structural differences result in the different reaction pathways when using ECD.

Rimco B.J. Geels, Saskia M. van der Vies, Albert J.R. Heck, and Ron M.A. Heeren, *Analytical Chemistry*, 2006, 78(20), 7191-7196.

3.1 Introduction

Since the late 1990s Electron Capture Dissociation¹⁰⁴ (ECD) has been available as a tool for structural analysis in Fourier Transform Ion Cyclotron Resonance Mass Spectrometry (FT-ICR-MS). To date, ECD is routinely used for top-down sequencing and identification of the post-translational modifications, such as sulfide bridges, phosphorylation and methylation.^{110,131–135} During an ECD experiment, low-energy electrons are injected into the ICR-cell and captured by multiply-protonated ions, resulting in the release of approximately 2-6eV of recombination energy into the ion.^{104,136} Typically, the capture of one or more electrons leads to the rapid dissociation of covalent backbone bonds, resulting in the formation of c and z · fragment ions.¹⁰⁵

The ECD process has so far been studied using peptides and proteins with a molecular mass up to 50kDa,^{109,110} but not yet for protein complexes or proteins with a higher molecular mass. There is still an active debate about the exact mechanisms of ECD.^{106,136–142} The early research demonstrated that ECD leads to rapid dissociation of the backbone close to the site of electron capture, not necessarily fragmenting the weakest bonds in the molecule. In line with this observation, ECD has been found to often preserve labile noncovalent bonds,¹⁰⁹ for instance in cytochrome C¹⁴³ and vancomycin complexed with diacetyl-L-Lys-D-Ala-D-Ala.¹⁴⁴ This makes ECD a potentially useful technique for examining interaction sites in larger, noncovalent protein complexes.

In this report, we use ECD to study the interaction sites in the large gp31 heptameric protein complex from bacteriophage T4. The protein complex has a molecular mass of 84kDa and consists of seven identical subunits that are noncovalently linked together and form a dome-like structure with 7-fold symmetry. Gp31 is a co-chaperonin that bacteriophage T4 uses in concert with the GroEL chaperonin of the host bacterium *Escherichia coli* in order to fold its viral capsid protein.^{23,31,40,57,59,145} The structure of gp31 is analogous to the *E. coli* co-chaperonin GroES, but is somewhat larger to accommodate the viral capsid protein inside the chaperonin complex. In contrast to the expectations, ECD of the gp31 co-chaperonin leads exclusively to noncovalent bond dissociation for one particular charge state, with a remarkable charge distribution over the two fragments.

3.2 Experiment

The experiments were performed using a modified Bruker APEX 7.0e FT-ICR-MS equipped with an infinity cell⁸², as described in detail in chapter two. Experimental control hard- and software were developed in-house and have been described elsewhere.⁸² Elevated pressure in the source octopole

facilitated transfer of the large intact protein complexes into the gas phase and to the ICR cell. Ions were directly gas-assisted accumulated inside the ICR cell with typical accumulation times of 10-12s. Individual charge states of the gp31 heptamer were isolated using SWIFT pulses⁸⁸ and subsequently irradiated with low energy electrons. ECD settings were optimized for maximum fragmentation. The optimal electron energy was determined to be $\sim 0.3\text{eV}$. A Heatwave STD134 heated cathode, mounted at the back end of the cell on axis and operated at 1.3A, 7.5W, dispensed electrons into the ICR cell. Electrons emitted from the cathode passed through the cell once and were collected on the end plate. Electron irradiation times used in the experiments varied between 2 and 3s. During ECD and measurement of the ions, trapping plate voltages were lowered to 1.5V.

In addition to ECD, Collision Activated Dissociation (CAD) and Sustained Off-Resonance Irradiation Collision Activated Dissociation (SORI-CAD) experiments were also performed, as described in detail in chapter two. CAD was performed on the ECD products to determine their composition. SORI-CAD was used on the native gp31 heptameric species to compare SORI-CAD pathways with ECD pathways.¹⁴⁶ SORI-CAD was performed with a +1000 Hz offset and Argon collision gas, using procedures described previously.¹³¹

The gp31 heptamer was purified as described previously.⁵⁸ The protein was buffer exchanged to a 1mM ammonium acetate buffer, pH 6.8, by using ultra filtration filters with a cut-off of 5000Da (Millipore, Bedford). Final concentration of gp31 in the spray sample was $13.5\mu\text{M}$. Protein concentration is given based on the gp31 monomer.

3.3 Results and discussion

3.3.1 ECD leads to dissociation of noncovalent bonds for specific charge states of gp31 heptamers

Figure 3.1 shows an ESI FT-ICR-MS spectrum of heptameric gp31. Indicated in the figure are the visible charge states. Along with the spectrum, the X-ray crystal structure is of gp31 presented, showing the circular arrangement of the seven noncovalently bound subunits.⁵⁷ Heptamer charge states 18+ through 21+ were isolated separately and subjected to ECD under identical experimental conditions. The results are shown in Figure 3.2.

Remarkably, ECD of gp31 did not result in backbone fragmentation, for all the different charge states that were examined. There are no peaks in the spectra corresponding to backbone fragments. The $[M_7 + 21H]^{21+}$ species shown in Figure 3.2a exhibited two pathways under ECD. First, multiple electron capture without fragmentation occurs, creating lower charged radical heptamer species. This is reaction I shown in Table 3.1.

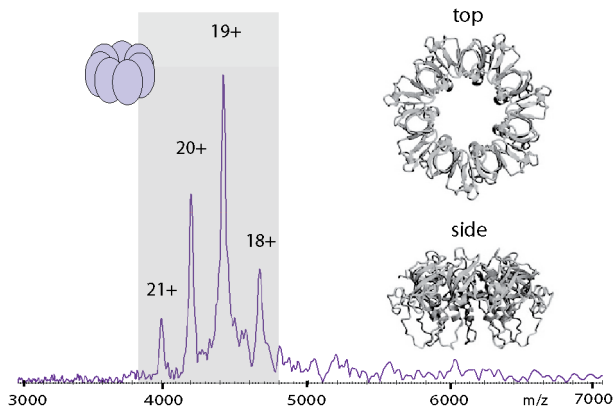


Figure 3.1: ESI FT-ICR-MS spectrum of the gp31 co-chaperonin complex. Around $4250m/z$ the charge states 18+ through 21+ of the heptamer are visible. The donut-shaped cartoon represents heptameric gp31. Only the (native) heptameric form of gp31 was present. On the right, the X-ray crystal structure of the heptameric gp31 is shown⁵⁷ (PDB accession code: 1G31).

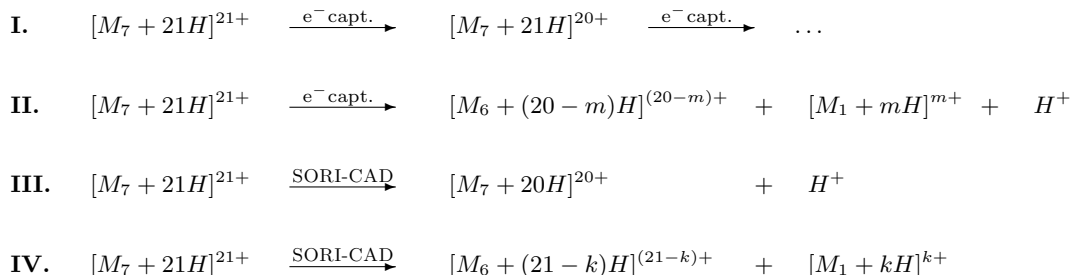


Table 3.1: Reaction pathways of gp31 21+ upon activation using ECD (I and II) or SORI-CAD (III and IV). (I) Electron capture leads to charge reduction of the complex without fragmentation, creating a radical complex. (II) Electron capture leads to dissociation of the complex creating a hexamer and a monomer. The radical H-atom either resides with the hexamer or the monomer. (III) SORI-CAD leads to charge reduction via ejection of a positive charge. Resolution is not sufficient to ascertain the identity of the ejected fragment. In the reaction this particle is symbolized by H^+ . (IV) SORI-CAD leads to dissociation of the complex creating a hexamer and a monomer. The charge states of the ejected monomers in reactions II and IV are different. In (II) $m = 2-3$ and in (IV) $k = 7-9$.

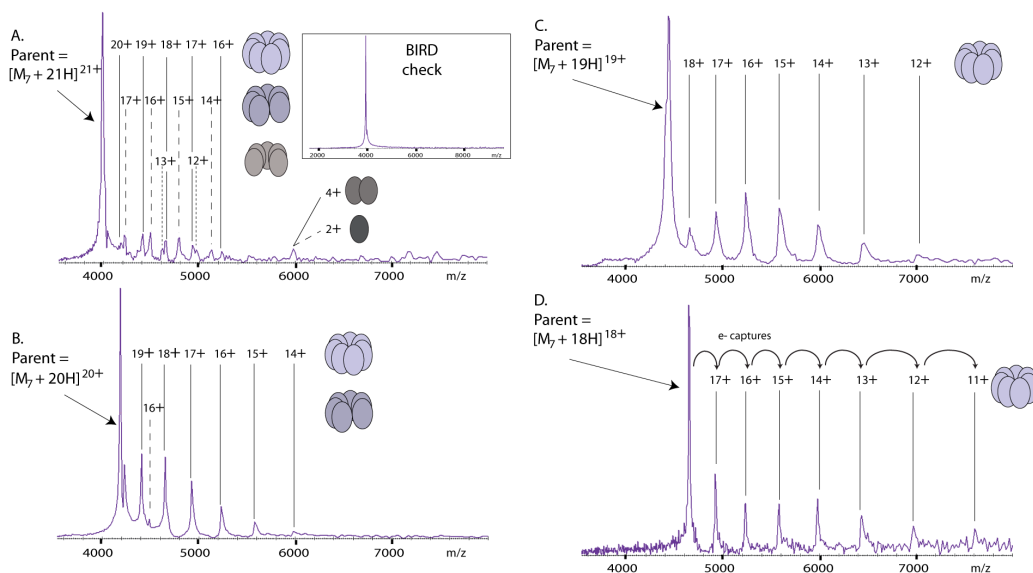


Figure 3.2: ECD spectra of the different charge states of the intact gp31. The peaks in the spectra are annotated with corresponding charge states and cartoon representations of the oligomeric state. All mass-selected parent ions were subjected to ECD for 3s. (A) The most abundant fragment ions correspond to lower charged heptamers as well as smaller oligomers, indicating that ECD of $[M_7 + 21H]^{21+}$ causes prominent charge reduction and dissociation. (B) ECD of $[M_7 + 20H]^{20+}$ results in prominent charge reduction and minor dissociation. (C, D) ECD of parent species $[M_7 + 19H]^{19+}$ and $[M_7 + 18H]^{18+}$ results only in charge-reduced heptamer species. In (D), the subsequent electron captures are also indicated, showing seven subsequent electron captures. The inset in (A) shows a reference spectrum with the electron gun on and electrons repelled from the ICR cell. This spectrum confirms that fragmentation does not occur due to Blackbody Infrared Radiative Dissociation (BIRD) from the heated cathode.

Second, electron capture followed by dissociation of noncovalent bonds, creating hexamer and monomer fragments (the observation of pentamer and dimer fragments is discussed below). This is reaction II in Table 3.1. Reaction II may occur either upon first electron capture or after multiple electron captures. The resulting ECD products from reaction II may again be susceptible to subsequent electron capture(s).

The $[M_7 + 20H]^{20+}$ species, shown in Figure 3.2b, also exhibited both pathways, although the pathway following reaction II from Table 3.1 is much less prominent than for the $[M_7 + 21H]^{21+}$ species, visible only by the 16+ hexamer peak. ECD of species $[M_7 + 19H]^{19+}$ and $[M_7 + 18H]^{18+}$, shown in Figure 3.2c and 3.2d, only followed reaction I leading to charge

reduction. For the latter two precursor ions reaction I occurred up to seven times before the ion signal disappeared, creating ions of charges down to 12+ and 11+ respectively. The release of up to seven times the recombination energy into the molecule thus does not result in any visible dissociation of noncovalent bonds or cleavage of backbone bonds. ECD on large proteins leading to charge reduction without fragmentation has been shown before.^{106,139} ECD leading to dissociation of small, noncovalently bound peptide complexes has also been demonstrated.¹⁴⁴ However, ECD of large, noncovalently bound protein complexes resulting in dissociation of intermolecular noncovalent bonds has never been shown before to the knowledge of the authors. Moreover, the fact that it only occurs for specific charge states makes this observation even more interesting.

To confirm that dissociation of the noncovalent bonds was not due to thermal activation by blackbody IR photons emitted by the heated cathode, a reference spectrum was obtained (Figure 3.2a, inset). This spectrum reveals there was no fragmentation when the heated cathode was on and the electrons were repelled from the ICR cell, revealing that the observed dissociation is truly electron capture induced.

3.3.2 Pentamer species of gp31 originate via dimer ejection from the heptamer

Pentamers with charge states 12+ and 13+ were seen to be formed in the ECD experiment on the $[M_7 + 21H]^{21+}$ ions, as shown in Figure 3.2a. They were generated in a one-step reaction analogous to reaction II, but now with the ejection of a dimer instead of a monomer. Subsequent ejection of two monomers can be excluded, because the fragment hexamers from ECD of $[M_7 + 21H]^{21+}$ were observed not to dissociate further upon electron irradiation, as illustrated in Figure 3.3a. The 15+ hexamer fragment from Figure 3.2a was isolated and subjected to a second round of ECD, i.e., MS³. For this species only reaction I occurred, i.e., charge reduction without dissociation of noncovalent bonds. Isolation and subsequent ECD of the 5975 m/z fragment peak, as shown in Figure 3.3b, revealed that this ion signal originated, at least partly, from dimeric ions. This observation confirms that the pentamers from Figure 3.2a originate through dimer ejection from the heptamer.

3.3.3 ECD products have not had backbone cleavage

As stated previously, backbone fragmentation without dissociation of the fragment from the complex did not occur. Further evidence for this is provided in Figure 3.4a, which shows the result of resonant CAD of the 15+ hexamer fragment that originated from ECD of $[M_7 + 21H]^{21+}$. CAD resulted in fragmentation analogous to reaction IV from Table 3.1. All CAD

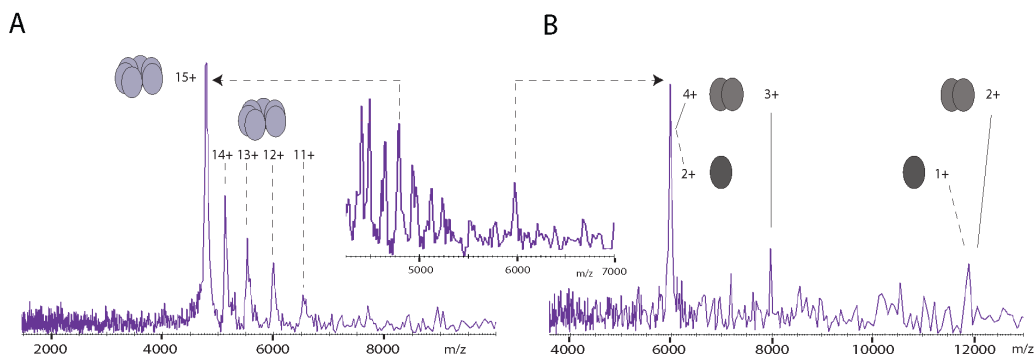


Figure 3.3: ECD MS³ spectra of the $[M_7 + 21H]^{21+}$ gp31 species. In the middle spectrum the 4250-7000 m/z mass region from Figure 3.2a is reproduced, i.e., the first ECD step. From this spectrum, the peaks at 4780 m/z and 5975 m/z were mass-selected and examined. (A) ECD of the 15+ hexamer fragment at 4780 m/z . After ECD the major peak in the spectrum corresponds to the 15+ hexamer "parent". The other peaks present correspond to charge-reduced species of the hexamer. ECD of the hexamer does not result in any dissociation. (B) ECD of the 5975 m/z fragment peak. Electron capture resulted in monomers and dimers of low charge states, as indicated. The presence of dimers and monomers after ECD confirms that the "parent" 5975 m/z peak consisted of both monomers and dimers.

products corresponded to monomers and pentamers without any visible mass losses. From this we infer that the backbone of the CAD parent, the 15+ hexamer ECD fragment, was intact. Resonant CAD on the 2+ monomer fragment that originated from ECD of $[M_7 + 21H]^{21+}$ did not result in any c and z ions (data not shown), indicating that the backbone of the 2+ monomer ECD fragment, was intact.

3.3.4 Multiple electron capture before dissociation

We stated that the $[M_7 + 21H]^{21+}$ complex either dissociated upon the first electron capture, or after multiple electron captures. The occurrence of the second option is confirmed by the spectrum in Figure 3.4b. In this experiment the 5975 m/z fragment peak from the first ECD step was isolated and subjected to a subsequent ECD step, the same as was done to obtain the spectrum in Figure 3.3b. Contrary to the results in Figure 3.3b, in Figure 3.4b, mostly heptamers and hexamers are present after ECD. This reveals that the parent peak composition at 5975 m/z , was different for the two experiments. In the second experiment, this peak consisted mostly of $[M_7 + 21H]^{14+}$ ions, whereas for the experiment shown in Figure 3.3b it consisted mostly of 2+ monomers and 4+ dimers.

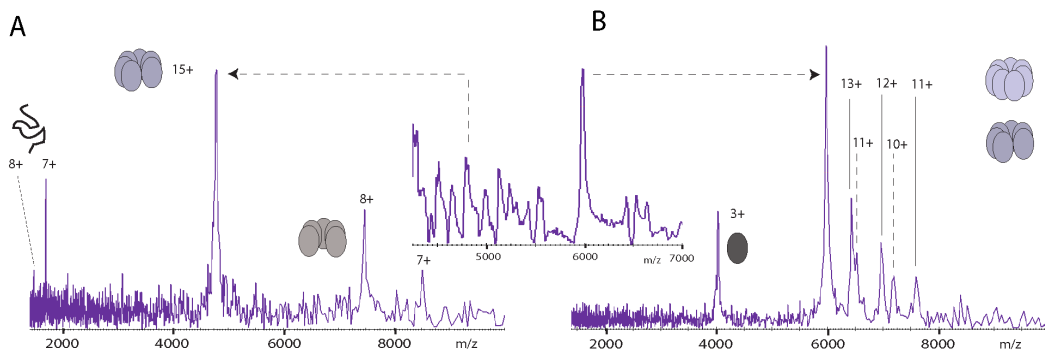


Figure 3.4: ECD and CAD MS³ spectra of the $[M_7 + 21H]^{21+}$ gp31 species. The middle spectrum shows a result of ECD of the $[M_7 + 21H]^{21+}$ gp31 species, focussed on the 4250-7000 m/z region. Peaks at 4780 and 5975 m/z were isolated and examined. (A) CAD of the 15+ hexamer fragment at 4780 m/z leading to dissociation of noncovalent bonds to produce a highly-charged (i.e., unfolded, as indicated by the cartoon) monomer and corresponding pentamer. There are no peaks corresponding to small backbone fragments. (B) ECD of the 5975 m/z product. Heptamers and hexamers are present as ECD products, indicating that the mass-selected "parent" contained the $[M_7 + 21H]^{14+}$ species. The 3984 m/z peak is identified as a 3+ (folded) monomer, since a charge-state distribution corresponding to an oligomer is not present. Part of the $[M_7 + 21H]^{14+}$ thus dissociated into a hexamer and a monomer, confirming the possibility of dissociation after multiple electron capture.

The appearance of the 3+ monomer at 3984 m/z in Figure 3.4b, together with the heptamers and hexamers at higher masses confirm that the second ECD step dissociated the noncovalent bonds in the $[M_7 + 21H]^{14+}$ species. Thus sequential reactions I created the $[M_7 + 21H]^{14+}$ species, which subsequently dissociated via reaction II.

3.3.5 Comparison of ECD with SORI-CAD reveals different dissociation mechanics

Dissociation of noncovalent bonds in protein complexes can also be achieved by other activation methods such as (SORI-)CAD or InfraRed Multi-Photon Dissociation (IRMPD).^{89,147-149} A comparison of the observed fragments created by activation with ECD or with SORI-CAD reveals that charge states of the generated species differ, suggesting that the dissociation mechanism for ECD is different from that in SORI-CAD. In Figure 3.5, the 21+ ECD spectrum from Figure 3.2a is compared with the results obtained from SORI-CAD of that same species. With SORI-CAD, two breakdown pathways are identified. In the first pathway, charge reduction

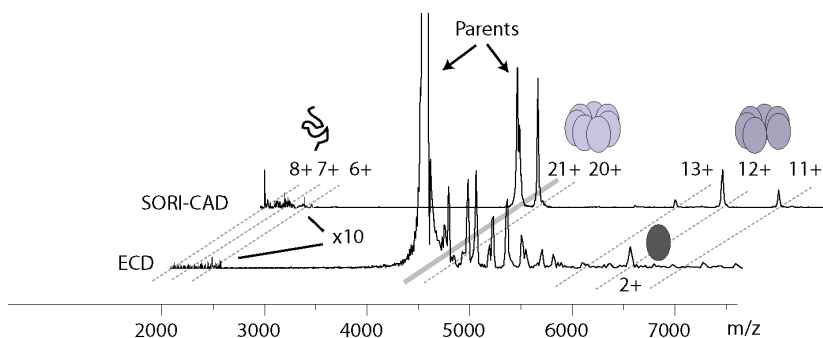


Figure 3.5: Tandem MS spectra of the gp31 co-chaperonin using two different activation techniques: ECD and SORI-CAD. The ECD spectrum of Figure 3.2a is reproduced here. The lower m/z range is multiplied 10 times to show that peaks here are present for SORI-CAD, but are absent with ECD. SORI-CAD resulted in heptamers, hexamers and monomers of the indicated charge states, showing that both SORI-CAD reactions from Table 3.1 occurred. Even though both ECD and SORI-CAD resulted in dissociation of non-covalent bonds into the same oligomeric species, the charge separation over the fragments was significantly different.

of the activated heptamer is observed. After which, the charge-reduced heptamer (now 20+) was no longer activated and did not react further. This behavior corresponds to reaction III in Table 3.1. In the second pathway, the activated complex dissociated into a highly charged monomer and corresponding hexamer. This corresponds to reaction IV from Table 3.1.

In our experiment, ECD leads to symmetric charge separation over the fragments, while SORI-CAD leads to asymmetric charge separation. This disparate charge distribution has been observed numerous times in CAD experiments of protein complexes. It is believed that Coulombic forces drive the dissociation, which proceeds via the partial unfolding of a single subunit from the complex. While this subunit unfolds, a charge redistribution takes place. When the monomer is sufficiently unfolded and charged, Coulombic repulsion is thought to lead to expulsion of the highly charged monomer.^{147–153}

The charge redistribution to the ejected monomer, as seen with SORI-CAD, is absent in the case of ECD. Therefore, dissociation of noncovalent bonds via ECD is thought not to alter the underlying structure of the monomer. The monomer dissociation from the complex using ECD is rapid relative to dissociation with SORI-CAD, otherwise the Coulomb forces would redistribute charges to the monomer during ejection. The observed rapid dissociation with ECD can be interpreted as supporting

the nonergodic dissociation mechanism for ECD, but the data are not conclusive on this matter.

3.3.6 Gas-phase structure determines ECD pathway

In summary, we have shown the dissociation of species $[M_7+21H]^{21+}$, $[M_7+20H]^{20+}$, and $[M_7+21H]^{14+}$ upon electron capture, while no dissociation was observed for the $[M_7+19H]^{19+}$, $[M_7+18H]^{18+}$, $[M_7+19H]^{14+}$, and $[M_7+18H]^{14+}$ species, as visible in Figure 3.2c and 3.2d. We hypothesize that different gas-phase structures of the various gp31 heptamer species determine the behavior with ECD. Variations in ECD behavior between proteins have been attributed to conformational differences.^{137,154} It has been shown that gas-phase structures of a single protein differ between specific charge states and even differ for the same charge state.¹¹⁹ Increasing Coulomb repulsion through an increase of the number of charges on the ion during the evaporation process induces conformational changes. It is thought that for heptamer charge states up to 20+ the Coulomb repulsion is not large enough to inflict serious structural deformations from the 7-fold symmetric ring arrangement. However, the 21+ heptamer experiences significant Coulomb repulsion and at least part of the gas-phase population has undergone a conformational change away from the 7-fold symmetry. As a result, we conclude that the overall structure exhibits a deformation that makes it susceptible to dissociation by ECD.

One can imagine that, during ECD, electron capture at or close to the structurally deformed site will lead to rapid dissociation of the complex, whereas electron capture at sites away from the deformation will only lead to charge reduction. The actual dissociation event is still caused by a single electron capture. To account for the dissociation of the $[M_7+21H]^{14+}$ species with ECD in Figure 3.4b, we postulate that charge reduction by electron capture in the gas-phase will not lead to a structural rearrangement back to the 7-fold symmetric ring but will leave the ion susceptible to dissociation upon a next electron capture.

The analytical results and the hypothesis on the influence of conformation are schematically summarized in Figure 3.6. The structural deformation for the 21+ charge state is visualized as a dislocation of one subunit. Contrary to ECD, for SORI-CAD, the complex is slowly heated up and the original gas-phase structure is not relevant for the eventual breakdown pathway.

3.4 Conclusion

ECD of the noncovalent gp31 co-chaperonin complex does not lead to cleavage of covalent backbone bonds as has been observed for monomeric proteins, but instead to rapid disassembly of the complex for which multiple

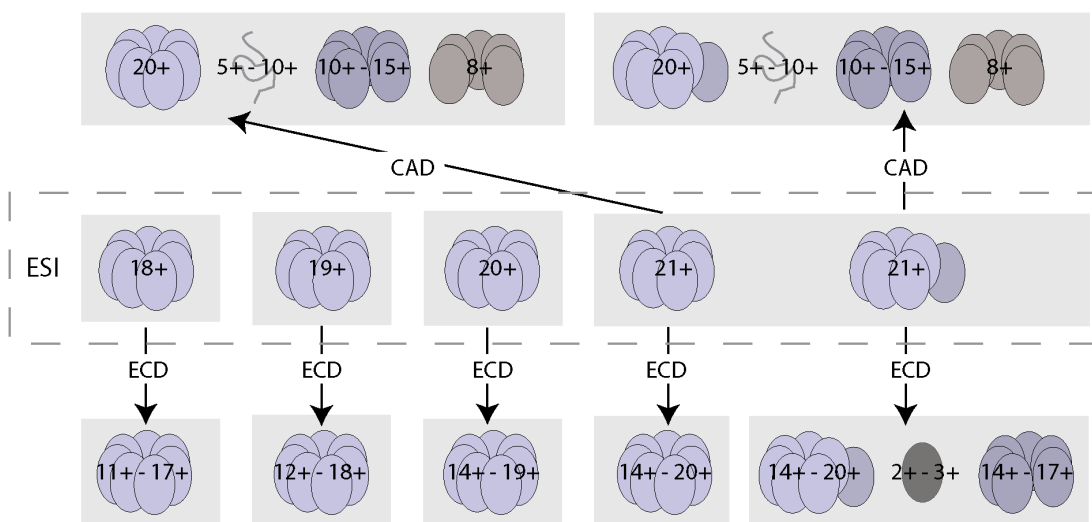


Figure 3.6: Schematic representation of the hypothesis that different gas-phase structures for the 21+ charge state of gp31 cause the different pathways observed for ECD. The center of the figure shows the charge states and structures after ESI. These species are subject to ECD (the arrows downward) with the resulting species dependent on the parent structure, or they are subject to SORI-CAD (the arrows upward) with the resulting species not dependent on the parent structure. The scheme also shows that the ejected monomer remains relatively more folded when using ECD than when using SORI-CAD.

noncovalent intermolecular interactions have to be broken. The backbones of the subunits remain intact and the ejected subunit does not unfold during dissociation from the complex. These observations are very different from what has been reported for ECD on smaller, monomeric proteins. We conclude that the 21+ charge state of the complex has a gas-phase structure that is different from that of the lower charge states, allowing ECD to dissociate noncovalent bonds. This conclusion implies that the underlying differences in gas-phase structure lead to the observed different dissociation pathways for ECD, but not for (SORI-)CAD. This thus indicates that the conformation of a protein plays a crucial role in ECD.

3.5 Acknowledgement

We would like to thank Esther van Duijn for kindly providing the protein samples. This research is part of the research program of the "Stichting voor Fundamenteel Onderzoek der Materie (FOM)", which is financially

3. ECD AS STRUCTURAL PROBE FOR NONCOVALENT GAS-PHASE PROTEIN ASSEMBLIES

supported by the "Nederlandse organisatie voor Wetenschappelijk Onderzoek (NWO)". This work is part of the FOM/ALW program "Physical Biology II" under project number 01FB12-1.

Comparative gas-phase activation of two similar noncovalent heptameric protein complexes: gp31 and GroES

Abstract

Using electrospray ionization, noncovalently bound protein complexes can be transferred intact into the gas-phase and analyzed and manipulated in a mass spectrometer. Here two large (70 - 80kDa) similar noncovalent protein complexes, gp31 and GroES, both cochaperonin of GroEL in *Escherichia coli*, were manipulated and compared inside a mass spectrometer using several gas-phase activation techniques. Nozzle-skimmer dissociation and (sustained off-resonance irradiation) collision-activated dissociation were performed using a quadrupole time-of-flight mass spectrometer and a Fourier transform ion cyclotron resonance mass spectrometer. Dissociation of these heptameric complexes mainly results in hexamers and monomers. There are no significant differences in gas-phase stability between the two complexes, but their fragmentation pathways exhibit considerable differences. Charge division over the fragments and overall charge losses during dissociation of the complexes differ clearly between GroES and gp31. These effects also differ between the various activation techniques, demonstrating that the different activation techniques yield complementary data. Combined, the different activation techniques are used to elucidate the dissociation mechanism and the degree of unfolding of the ejected monomer from the complex. The different behavior of the two protein complexes is rationalized to be dependent on the gas-phase structures of gp31, GroES and their fragmentation products.

Rimco B.J. Geels, Saskia M. van der Vies, Albert J.R. Heck, and Ron M.A. Heeren, *International Journal of Mass Spectrometry*, 2007, 265(2-3), 159-168.

4.1 Introduction

Electrospray ionization (ESI) can be used to transfer noncovalently bound complexes into the gas-phase for intact protein complex analysis in a mass spectrometer. ESI is a soft ionization method that retains labile quaternary associations of protein complexes.^{147,155,156} Very small complexes, such as protein ligand interactions, up to intact ribosomes have been examined with ESI.¹⁵⁷⁻¹⁵⁹ The structure and gas-phase stability of these complexes can be examined by means of ion activation techniques. By trapping the intact complexes in a Fourier Transform - Ion Cyclotron Resonance - Mass Spectrometer (FT-ICR-MS), the complexes can be examined and manipulated for extended periods of time. This creates possibilities for ion activation via InfraRed Multi-Photon Dissociation (IRMPD), Surface Induced Dissociation (SID), Electron Capture Dissociation (ECD), Blackbody Infrared Radiative Dissociation and Sustained Off-Resonance Irradiation Collision Activated Dissociation (SORI-CAD) or on-resonance CAD.^{89,160,161} Non-covalent protein complexes of increasingly larger masses are subject to structural analysis by Mass Spectrometry.^{40,153} Activation and dissociation analysis of over 50kDa complexes is now routinely done. In this paper we report on two noncovalent complexes, GroES and gp31, which have been subjected to gas-phase stability experiments.

Both gp31 and GroES are cochaperonin of the GroEL protein in *Escherichia coli*. In *E. coli* many proteins need the GroEL-GroES chaperonin machinery to be able to fold into their biologically active native state.²³ GroEL functions as the folding cage, the so-called Anfinsen cage,¹⁶² and GroES is the lid of this cage. The chaperonin complex is involved in the folding of approximately 15% of all the *E. coli* proteins.¹⁶³ These proteins vary greatly in size and function, illustrating the versatility of this chaperonin complex. This broad functionality of the complex is the main reason why it is being studied very extensively.^{18,164-167}

E. coli can get infected by Bacteriophage T4. As part of the reproduction of the bacteriophage, its major capsid protein, gp23, needs to fold into its native state. To achieve the native state, the chaperonin machinery of the *E. coli* cannot be used, i.e., gp23 cannot fold with the help of the normal GroEL-GroES complex. The GroES lid of the folding cage has to be substituted by the bacteriophage-encoded protein gp31.⁵⁷ Gp31 shows structural similarity to GroES. Both are noncovalent complexes of seven identical subunits arranged in a circular fashion, exhibiting seven-fold symmetry. The gp31 heptamer is slightly heavier (84kDa) than GroEL (73kDa). The origin of this functional difference has been investigated extensively.^{55,56} It is believed that the difference in function arises from a difference in structure between the two protein complexes.³¹ The size of the folding cage for the GroEL-gp31 complex is somewhat larger than that of the GroEL-GroES complex. This enlargement allows for the accommodation

of the relatively large gp23 (56kDa), which is close to the upper size limit of proteins that can be accommodated by GroEL-GroES chaperonin and will probably not fit into this folding cage.⁵⁶ The crystal structures of the two proteins are reproduced in Figure 4.1. Besides the increase in cavity size, there are other structural differences visible between GroES and gp31. Gp31 has a large mobile loop that might have other functions than just assisting in the size increment of the folding cage. In addition the roof loop that is present in GroES is missing in gp31, which might allow the formation of a larger folding cage.

Using native mass spectrometry of noncovalent complexes,¹⁶⁸ possible with FT-ICR-MS and quadrupole Time-of-Flight (q-ToF) mass spectrometry, it is possible to uncover additional differences between the two complexes. For instance, differences in the stability and structure of the complexes in the gas-phase can become apparent when activating these molecules in the mass spectrometer. In this paper we report on the analysis of both complexes in the gas-phase using nozzle-skimmer dissociation, on-resonance CAD and SORI-CAD. These techniques are all based on collisional activation, but the activation and analyses timescales of the experiments vary. These techniques will render complementary information on collisional activation of the protein complexes.

4.2 Experiment

Both co-chaperonins, gp31 and GroES were over-expressed in *E. coli* strain MC1009¹⁶⁹ and purified as described previously.^{58,170,171} The proteins were buffer exchanged to a 1mM ammonium acetate buffer, pH 6.8, by using ultra filtration filters with a cut-off of 5000Da (Millipore, Bedford). Final concentrations of gp31 and GroES in the spray sample were 13.5 μ M and 28 μ M respectively. Protein concentrations are given based on the gp31 and GroES monomer. Denatured solutions of gp31 and GroES consist of 14 μ M protein dissolved in a buffer of water (29%), methanol (69%) and acetic acid (2%). The experiments were performed using a modified Bruker APEX 7.0e FT-ICR-MS equipped with an infinity cell⁸², as described in detail in chapter two. Experimental control hard- and software were developed in-house and have been described elsewhere.⁸² Elevated pressure in the source octopole (\sim 2mbar) facilitated transfer of the large intact protein complexes into the gas phase and to the ICR cell.¹⁷² Ions were accumulated inside the ICR cell using gas-assisted trapping with typical accumulation times of 10-12 seconds. Individual charge states of the protein heptamers were isolated using SWIFT pulses.⁸⁸ Nozzle-Skimmer (NS)-dissociation was performed by scanning the capillary voltage from 0V to 300V while keeping the skimmer voltage constant at 25V. The dissociation is thus actually "capillary-skimmer dissociation", but it is

comparable to what is commonly called NS-dissociation in orthogonal-acceleration time-of-flight mass spectrometry. We will use NS-CAD to refer to this technique. Ions are accelerated out of the capillary-skimmer region where they collide with neutral air molecules. The pressure in this region is on the order of 10^{-2} mbar. The activated ions and their dissociation products are subsequently transported to the ICR-cell and analyzed. CAD and SORI-CAD experiments were also performed. In CAD the SWIFT isolated charge states were excited on-resonance for increasing amounts of time, where after the activated ions collide with neutral Argon gas. In SORI-CAD the ions were excited off-resonance to produce ions with varying kinetic energy.¹⁷³ SORI-CAD was performed with a +1000Hz offset and Argon collision gas, using procedures described previously.¹³¹ SORI-CAD is a slow-heating technique that only activates the lowest energy decay channel, whereas on-resonance CAD activates the ions in a much shorter time period. On-resonance CAD is usually thought not to be able to add enough internal energy to large ions / ion complexes to allow fragmentation. Longer excitation via SORI-CAD is necessary to achieve the threshold activation energy for dissociation, as described in detail in chapter two. As it turns out, both techniques deliver enough energy to dissociate the complex and the results of both techniques can be compared. CAD was also performed using a q-ToF I instrument from Micromass. This mass spectrometer is adapted for tandem mass spectrometry on macromolecular protein complexes.¹⁷⁴ The source pressure was elevated to 8mbar to cool the ions and facilitate ion transfer into the gas-phase.⁷³⁻⁷⁵ Selected parent charge state ions were accelerated into the collision quadrupole and the resulting fragments analyzed with the ToF system. Results of all the activation techniques were compared. The timescales with respect to activation and analyses times for the various techniques differ. For the various (on-resonance) CAD experiments, the activation of the protein complexes is fast, via several energetic collisions, whereas the activation with SORI-CAD proceeds slower, via multiple low-energy collisions. After activation the analysis times also differ between the q-ToF and the FT-ICR-MS. The time-of-flight measurement of the activation products proceeds within milliseconds, whereas analysis in the FT-ICR-MS takes several seconds.

4.3 Results and discussion

In Figure 4.1 on the left-hand-side, the plain mass spectra for gp31 and GroES are shown, together with their crystal structures. The solution phase K_d of GroES is estimated to be 1.10^{-38} M⁶.¹⁷⁵ For the molarities used in these experiments the equilibrium is almost completely to the heptameric form. For gp31 no measurement of the solution phase dissociation constant

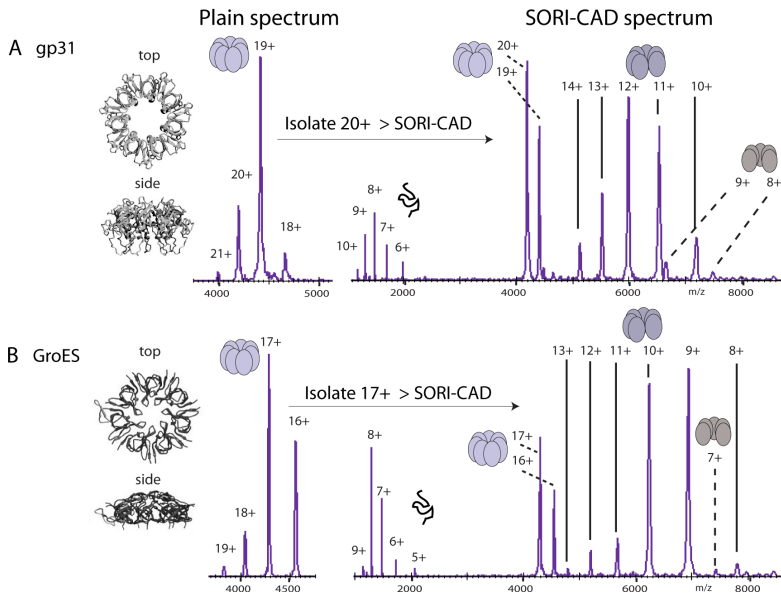


Figure 4.1: A) Plain spectrum obtained for the gp31 noncovalent heptamer on the left side, flanked by the crystal structure,⁵⁷ revealing the seven-fold symmetry of the protein complex. The result of isolation of the 20+ charge state and subsequent SORI-CAD is shown on the right hand side of the top graph. Visible are the remaining parent, a charge stripped heptamer, fragment hexamers and pentamers at the high-mass end and at the low-mass end highly charged, unfolded monomers. B) Plain spectrum obtained for the GroES noncovalent heptamer. Here the 17+ charge state is isolated and collision-activated. The cartoons next to the peaks in the spectra indicate the stoichiometry of the various species.

exists, but considering the similarity between the two complexes it can be expected that the equilibrium for gp31 will also be shifted to the heptameric complex. Gel filtration experiments confirm that at concentrations between $10\mu\text{M}$ and $25\mu\text{M}$ gp31 is in its heptameric form (unpublished data). The gas-phase data confirm that the equilibrium is completely towards the heptameric form, showing only the heptamer stoichiometry in the plain mass spectra.

On the right-hand-side of Figure 4.1, typical SORI-CAD breakdown diagrams of one specific charge state are shown. Gp31 and GroES exhibit similar behavior upon activation. Activation of the parent ion leads to charge reduction of the parent peak as is visible in the spectrum where the heptamer peak has one less charge. Most likely this lost charge is a charged adduct like sodium or ammonium, present in the solution. It is unlikely that protons are knocked off the complex. The resolution of the spectra

is not sufficient to determine the nature of the lost charge carrier. While other groups have reported the loss of a negative charge upon activation of large complexes,^{145,176} in the experiments in this paper loss of a negative charge has not occurred. Besides charge reduction, the parent heptamer can also fragment upon activation. Fragmentation proceeds via ejection of a subunit from the complex, leaving behind a hexamer. The ejected monomer carries away a disproportionately large share of the total number of charges. This disparate charge distribution has been observed numerous times in CAD experiments of protein complexes.^{147–150,152,153,177} It is believed that Coulombic forces drive the dissociation, which proceeds via the partial unfolding of a single subunit from the complex. While this subunit unfolds, a charge redistribution takes place. When the monomer is sufficiently unfolded and charged, Coulombic repulsion is thought to lead to expulsion of the highly-charged monomer. The unfolded monomers appear at the low mass/charge region of the spectrum. The pentamers present in the spectrum can originate via ejection of a dimer from the complex or via subsequent ejection of two monomers. Although dimers are not visible in the spectra, it cannot be concluded that dimer ejection has not occurred, because the dimers probably fall apart into two monomers after ejection.

CAD experiments of the proteins on the FT-ICR-MS and the q-ToF I also resulted in both charge reduction of the parent species and dissociation of the complex into hexamers and highly charged monomers mostly.

4.3.1 Thermodynamic stabilities of GroES and gp31 are comparable

Comparison of the thermodynamic stabilities of the two complexes was done via collision activation experiments on the q-ToF I. For gp31 individual charge states were isolated in separate experiments (19+ up to 22+) and subject to CAD. The same was done for various charge states of GroES (18+ up to 20+). The survival yields of the parent ions were calculated for all collision energies used in the experiment. The survival yield was calculated by dividing the ion count of the remaining parent after activation by the total ion count of the remaining parent plus fragment species. The constructed survival yield diagrams for all parent charge states are shown in Figure 4.2. The collision voltages (V_{coll}) are scaled with the charges (q) of the various parent ions to obtain the kinetic energy ($E_{kin,lab}$) with which the ions enter the collision cell ($E_{kin,lab} = q * V_{coll}$). As is immediately evident from this figure, with increasing charge state the gas-phase complexes are thermodynamically less stable. Less kinetic energy is needed to achieve 50% survival yield for the higher charged ions.^{178,179} Considering the difference in thermodynamic stability of GroES and gp31, the data show that for the same parent charge state, the 50% survival yields are comparable within error. Any apparent difference in stability is caused by different number of

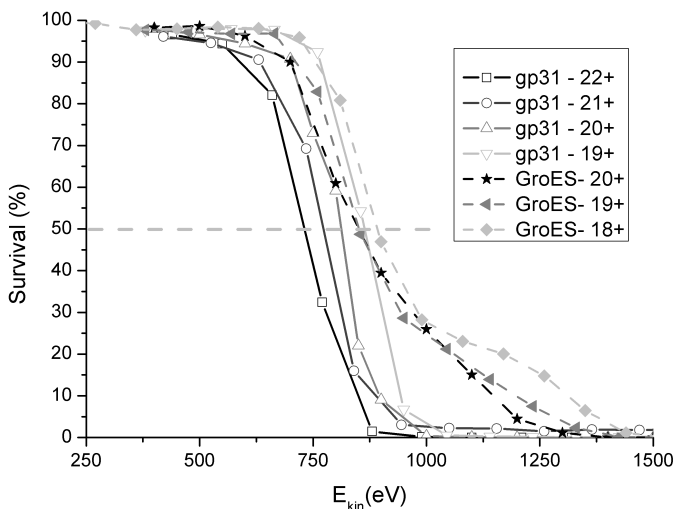


Figure 4.2: Breakdown diagrams constructed for the various parent charge states of gp31 and GroES. The breakdown diagrams are constructed by calculating the survival percentage of heptamer compared to all activation products present. The survival percentages are shown as a function of kinetic energy with which the parent enters the collision cell. The 50% survival yield points show a trend to lower kinetic energies for higher charge states, compensating for less Coulombic repulsion within the complex for lower charge states. The differences in 50% survival yield points between the two species can be explained by this charge-effect and do not indicate any intrinsic thermodynamic stability difference between the two proteins in the gas-phase.

charges on the protein complexes in the gas-phase. The total interaction strength between the subunits for GroES and gp31 is thus comparable, demonstrating that the difference in function of the two complexes *in vivo* cannot be directly related to differences in their gas-phase thermodynamic stability.

4.3.2 The different activation mechanisms result in comparable breakdown diagrams

The q-ToF collisional activation measurements are compared with survival yield curves constructed from activation measurements using on-resonance CAD, SORI-CAD and NS-CAD on the FT-ICR-MS. In Figure 4.3a the gp31 20+ charge state is visualized and in Figure 4.3b the 19+ GroES

charge state survival yield curves are shown. The 19+ and 20+ charge states are chosen, because they lie closest to the average parent heptamer charge in the NS-CAD experiment. To be able to compare the survival yields of the parent ions for the various experiments in one graph, scaling factors for the degree of activation are needed. Throughout the rest of the paper in the graphs the 50% survival yield points using the various activation methods will be aligned. The alignment procedure is done via Equations 4.1a and 4.1b, creating a new dimensionless quantity: I_{act} , the activation intensity,

$$I_{act} = \frac{E_{kin,lab}}{C_{50}} \quad \text{NS - CAD, q-ToF - CAD and FTMS - CAD} \quad (4.1a)$$

$$I_{act} = \frac{N_{SORI} \cdot \langle E_{kin,lab} \rangle}{C_{50}} \quad \text{FTMS SORI - CAD} \quad (4.1b)$$

Here: $E_{kin,lab}$ = the resulting laboratory frame kinetic energy of the parent after activation (for NS-CAD the "average" parent), $\langle E_{kin,lab} \rangle$ = the average laboratory frame kinetic energy during SORI activation, N_{SORI} = total number of SORI cycles and C_{50} = the scaling factor aligning the 50% survival yield points. The C_{50} values for all experiments are given in Table 4.1. Comparing the kinetic energies needed to achieve 50% survival yield for the on-resonance CAD experiment in the FT-ICR-MS with that needed for the CAD experiment in the q-ToF, somewhat higher kinetic energy is needed in the FT-ICR-MS for both protein complexes. First, ions in the q-ToF were internally hotter than in the FT-ICR-MS before activation, resulting in higher kinetic energy needed for dissociation in the FT-ICR-MS.¹⁸⁰ Second, collision gas pressure used in the FT-ICR-MS was lower than in the q-ToF, resulting in a slower kinetic energy to internal energy conversion resulting in a greater InfraRed (IR) loss. Both factors contribute to the higher kinetic energy needed for dissociation in the FT-ICR-MS. Concerning IR-losses, due to the slow-heating process of SORI-CAD, the effect of IR-loss during activation with this technique becomes considerable and is clearly visible in the decreased slope of the breakdown diagrams. For the q-ToF CAD, FT-ICR-MS on-resonance CAD and NS-CAD the survival yield diagrams have comparable shapes.

These figures also do not reveal any significant difference in gas-phase thermodynamic behavior of the two complexes. In the following paragraphs, however, we will show that, despite the comparable stability of the two protein species using the different activation techniques, there are major differences between techniques and species concerning dissociation mechanics.

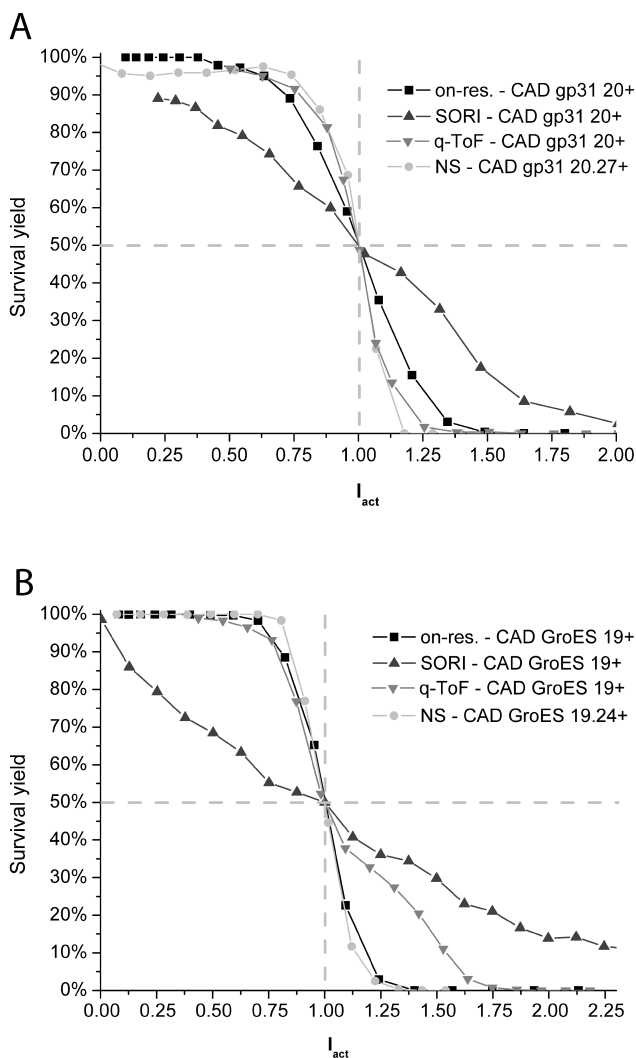


Figure 4.3: A) CAD of the gp31 20+ heptamer for the various activation methods indicated. For NS-Activation it is not possible to isolate a charge state beforehand. The average charge state of the heptamers at 0V NS-Activation is 20.27. This is closest to the 20+ charge state for the other activation experiments. The spectra have been linearly aligned at zero activation and 50% survival yield. B) CAD of the GroES 19+ heptamer. The average parent heptamer charge state at 0V NS-Activation of GroES is: 19.24. This is compared to the 19+ charge states in the other activation experiments.

4. COMPARATIVE GAS-PHASE ACTIVATION OF TWO SIMILAR NONCOVALENT HEPTAMERIC PROTEIN COMPLEXES: GP31 AND GROES

C ₅₀ values	<i>Gp31</i>				<i>GroES</i>				
	<i>22+</i>	<i>21+</i>	<i>20+</i>	<i>19+</i>	<i>20+</i>	<i>19+</i>	<i>18+</i>	<i>17+</i>	<i>16+</i>
NS-CAD	3700				3675				
q-ToF CAD	730	778	796	864	830	870	929		
on-res CAD		1466	1090	1205		950	1130	1175	1950
SORI-CAD		17463	17603	19210		19210	26963	17463	30037

Table 4.1: Overview of the C₅₀-scaling values (in eV) used in Equations 4.1a and 4.1b to align the 50% survival yield points in figures 3, 5 and 6 of this paper.

4.3.3 Dissociation pathways for GroES and gp31 exhibit differences

Activation of the noncovalently bound protein complexes resulted in fragment species with two distinct characteristics: stoichiometry and charge. The experimental results do not indicate that the stoichiometries of the fragment species differ, but the distributions of charges over the various fragments for the different activation techniques show that the dissociation mechanisms of the two complexes differ. The stoichiometric fragmentation pathway of the two complexes, is reproduced in Figure 4.4a. This figure shows the parent heptamer dissociating into a hexamer and a monomer. The hexamer has relatively low charge and the (partially) unfolded monomer has relatively high charge. In the next sections the average charge states of the hexameric and monomeric fragments, resulting from dissociation as in Figure 4.4a, will be further analyzed.

Charge state of ejected monomer depends on activation technique, parent charge and parent species

As stated earlier, it is commonly believed that the ejection of the monomer from the complex proceeds via Coulomb-induced unfolding of the monomer and corresponding migration of charge carriers onto the unfolding monomer. Table 4.2 shows the average charge of the ejected monomers at 50% survival yield for all experiments and species together. It also shows the average charge of monomers present in a mass spectrum of denatured gp31 and GroES. The average charge state is calculated by weighing the charge states in the spectra with their intensities. The charge state of the denatured form of the proteins is considerably higher than those of the ejected monomers during activation. Since we are assuming Coulomb-induced unfolding, this means the Coulomb repulsion is not further reduced by migrating more charges onto the monomer (considering the fact that the supply of charges is limited by the parent charge) and consequently the monomer is less unfolded as compared to the denatured protein. During dissociation the

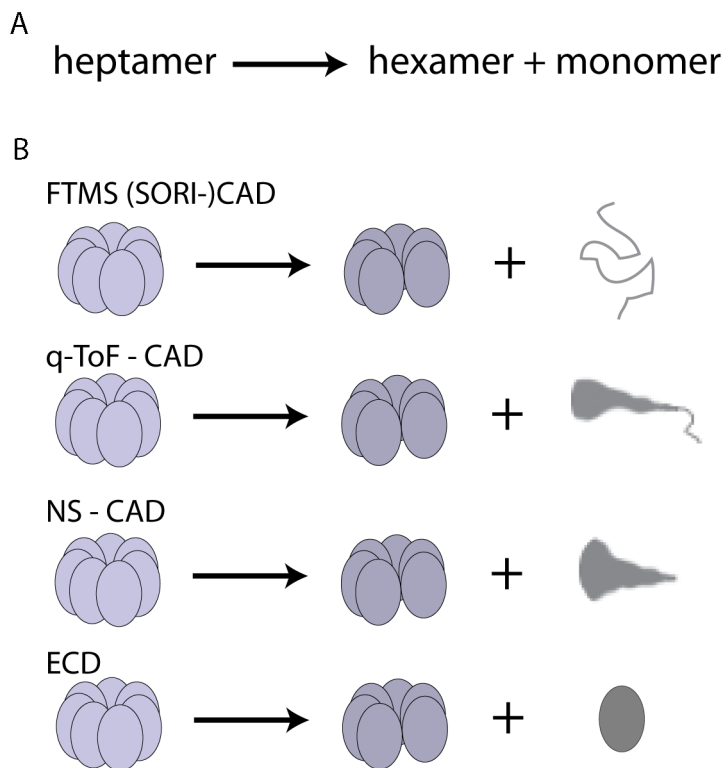


Figure 4.4: A) The major dissociation pathway for both the GroES heptamer and the gp31 heptamer. This pathway holds for all examined charge states and activation mechanisms. It indicates dissociation of the noncovalent parent heptamer into a hexamer and a monomer. The hexamer has a relatively low charge and the monomer has a relatively high charge. This picture is incomplete. Our measurements reveal the effect the activation technique has on the charge states of the fragmentation products. B) A more detailed representation of the fragmentation products after dissociation. The various activation techniques result in different degrees of unfolding and charging of the monomer.

4. COMPARATIVE GAS-PHASE ACTIVATION OF TWO SIMILAR NONCOVALENT HEPTAMERIC PROTEIN COMPLEXES: GP31 AND GROES

<i>Species</i>	<i>Parent Charge</i>	<i>q-ToF CAD</i>	<i>FT-ICR-MS</i>		
			<i>on-res. CAD</i>	<i>SORI-CAD</i>	<i>NS-CAD</i>
gp31 monomer	22	7.3	-	-	6.0
	21	7.7	7.9	8.1	
	20	7.4	8.1	8.4	
	19	7.3	8.1	8.3	
	denatured	11.2			
GroES monomer	20	6.9	-	-	5.0
	19	7.3	8.2	7.9	
	18	7.3	7.8	7.9	
	17	-	7.4	7.4	
	16	-	7.0	7.0	
	denatured	9.9			

Table 4.2: Overview of average monomer charge states. The table shows the average monomer charges at 50% survival yield for the various collisional activation techniques, as well as the average charge of the monomers in the mass spectrum of the denatured protein. All indicated charge states have an error of ± 0.2 .

charges are located at the sites with the highest gas-phase basicity. Table 4.2 also reveals the variation of the monomer charge with the different parent protein species and charges and with the activation technique chosen.

Charge state of the ejected monomer relates to the extent of unfolding

In Figure 4.5, for the gp31 21+ parent and the 19+ parent for GroES, the average charges of the monomer and hexamer fragments are shown, along with their combined charge as a function of increasing activation. The other investigated parent charge states (19+ and 20+ gp31 and 18+ GroES) exhibit similar behavior and are not reproduced in this figure. The on-resonance CAD experiments using the FTMS and the CAD experiments using the q-ToF show comparable evolution of the combined charge of the fragment hexamer and monomer, whereby the combined charge is somewhat lower for the q-ToF CAD than for the FTMS on-resonance CAD. Interestingly, the charges are differently distributed over the hexamer and monomer. In the q-ToF CAD experiment, the monomer takes away fewer charges than in the FTMS on-resonance CAD experiment. Since the monomer charge states differ, this suggests that the degree of unfolding of the monomer is different for both experiments because otherwise the charge migration onto the monomer would have been the same. The time frame of activation and the total analysis time is shorter for the q-ToF than for the FTMS; which is also indicated by the higher kinetic energy needed

for dissociation in the FT-ICR-MS. The data indicates that the monomer is already ejected from the complex in the q-ToF experiment before the Coulomb-induced unfolding has reached the same degree of unfolding as with the FTMS on-resonance CAD experiment.

Around the 50% survival yield point, there is only a slight difference in monomer charge between on-resonance CAD and SORI-CAD on the FTMS. The q-ToF CAD experiment has slightly lower charged monomers, for most parent charge states; see also Table 4.2. Despite the fact that SORI-CAD slowly heats the protein complex and thus probably would also allow for more extensive unfolding of the monomer, the monomer charge is not higher than for the FTMS on-resonance CAD experiment. This means the Coulomb-induced unfolding has reached equilibrium before dissociation occurred. The ejected monomer charge can therefore be seen as an indicator of the degree of unfolding of the monomer.

In an earlier study we observed no charge redistribution to the ejected monomer in ECD experiments, while a monomer was also ejected from the gp31 protein complex.¹⁸¹ This was attributed to the shorter time-scale of dissociation for the ECD experiment compared to the (SORI-)CAD experiment. This observation agrees well with the differences in activation time and resulting charge redistribution that we observe in the experiments discussed in this paper. Overall, our findings show that changing the mechanism of activation can influence the degree of unfolding of the ejected monomer.

Figure 4.4b shows a schematic representation of these effects. Going from no charge carrier rearrangement ("no" unfolding) to some charge rearrangement ("some" unfolding) to even more charge migration to the monomer ("more" unfolding), by using ECD, NS-CAD, q-ToF CAD, and FTMS on-resonance CAD and FTMS SORI-CAD respectively.

Activation of complexes results in overall charge loss

In Table 4.3, the average charges of the remaining hexamers are given. Since the average monomer charge and the average hexamer charge do not add up to the parent charge, charge is somehow lost in the process. Table 4.4 show these charge deficits from the various measurements. For GroES there is only a small charge deficit present for the 19+ parent at the 50% survival yield point in the FTMS SORI-CAD experiment. For gp31 charge deficits are present in the FTMS experiments for the higher charged parents and seem to increase with increased charge state.

Table 4.4 also shows that for the q-ToF CAD experiment there is no charge loss at the 50% survival yield point. The average charge states for the q-ToF experiments from tables 4.2 - 4.4 together show that charging of the monomer is restricted by the degree of unfolding of the monomer during dissociation using CAD in the q-ToF. In Table 4.2 all monomers arising

4. COMPARATIVE GAS-PHASE ACTIVATION OF TWO SIMILAR NONCOVALENT HEPTAMERIC PROTEIN COMPLEXES: GP31 AND GROES

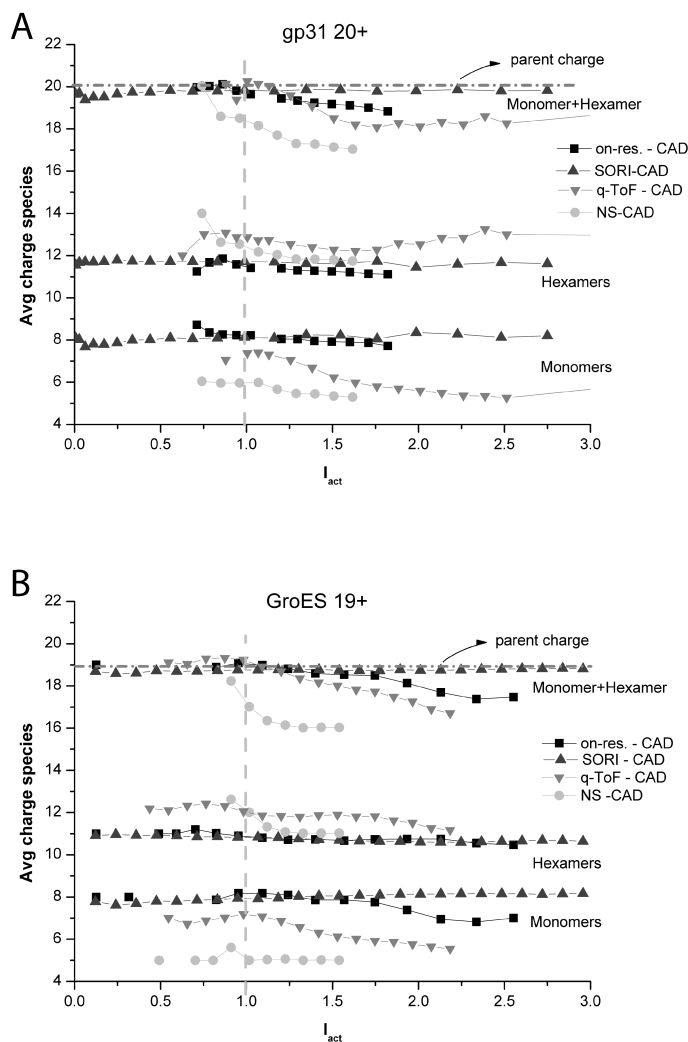


Figure 4.5: Evolution of the average charge of the dissociation products, monomers and hexamers, with increasing activation of the parent heptamer, for the gp31 20+ parent charge state (A) and the GroES 19+ parent charge state (B). The parent charge states not shown exhibit similar behavior. All activation techniques are shown in one graph. For NS-CAD the average parent charge state is 20.27 for gp31 and 19.24 for GroES. The 50% survival yield point is indicated by the vertical dashed bar in each graph. Also the combined charges of the monomer + hexamer are shown in the figure, to visualize the overall charge loss with increasing activation.

<i>Species</i>	<i>Parent Charge</i>	<i>q-ToF</i>	<i>FT-ICR-MS</i>		
		<i>CAD</i>	<i>on-res. CAD</i>	<i>SORI-CAD</i>	<i>NS-CAD</i>
gp31 hex- amer	22	14.6	-	-	12.5
	21	13.8	12.0	12.2	
	20	12.9	11.6	11.5	
	19	12.1	10.8	10.6	
GroES hex- amer	20	13.0	-	-	12.0
	19	11.9	10.9	10.8	
	18	11.2	10.2	10.1	
	17	-	9.7	9.6	
	16	-	9.0	9.1	

Table 4.3: Overview of average hexamer charge states. The table shows the average hexamer charges at 50% survival yield for the various collisional activation techniques. All indicated charge states have an error of ± 0.2 .

<i>Species</i>	<i>Parent Charge</i>	<i>q-ToF</i>	<i>FT-ICR-MS</i>		
		<i>CAD</i>	<i>on-res. CAD</i>	<i>SORI-CAD</i>	<i>NS-CAD</i>
gp31 charge deficit	22	0.1	-	-	1.8
	21	-0.5	1.1	0.7	
	20	-0.3	0.3	0.2	
	19	-0.4	0.1	0.1	
GroES charge deficit	20	0.1	-	-	2.2
	19	-0.2	-0.1	0.2	
	18	-0.5	0.0	0.0	
	17	-	-0.1	0.0	
	16	-	0.0	-0.1	

Table 4.4: Overview of the charge deficits. The charge deficits are the differences between the average monomer charge + average hexamer charge and the parent heptamer charge. It is calculated for each activation method and charge state. All indicated charge deficits have an error of ± 0.3 .

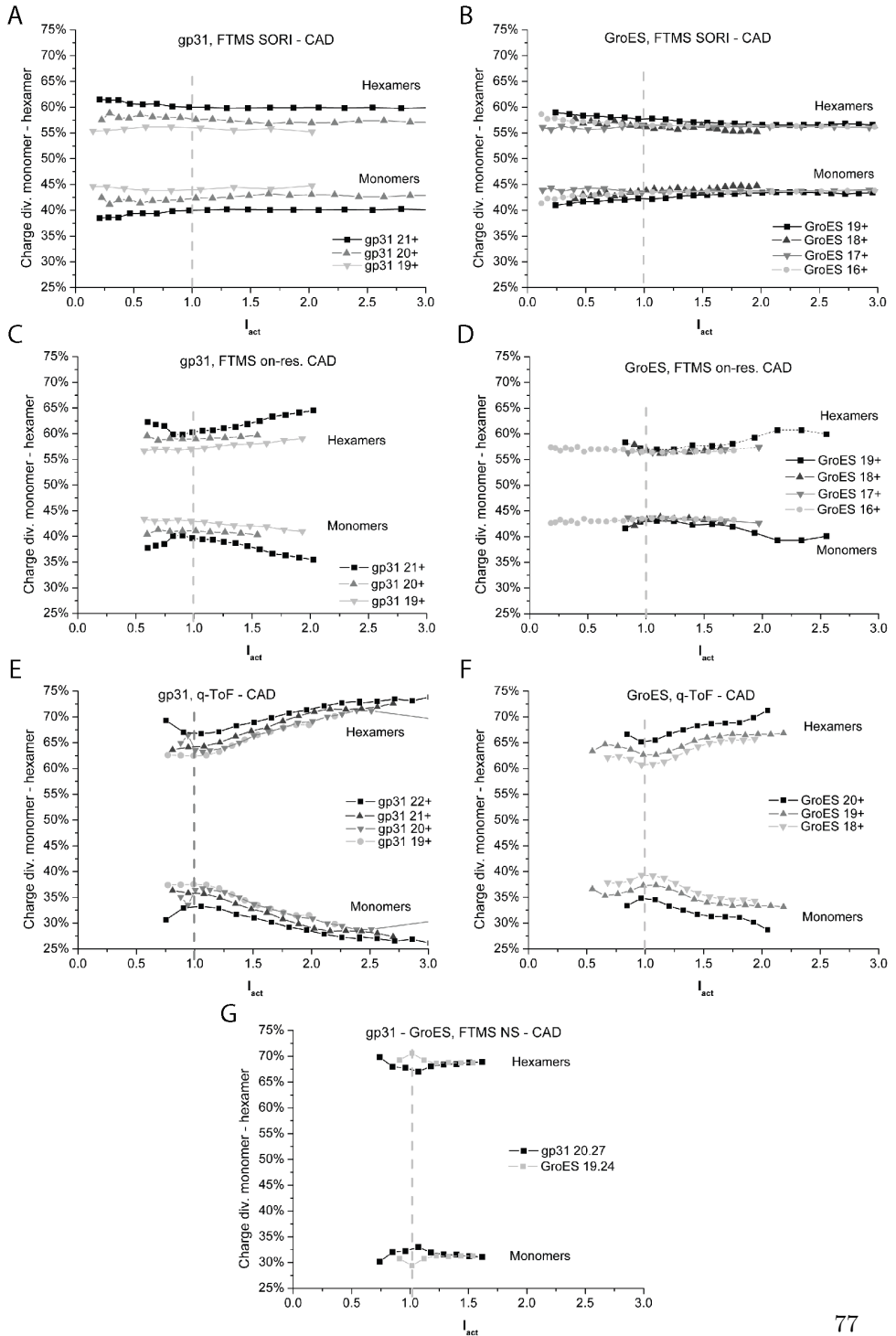
from differently charged parents are approximately equally charged. This means the extra charge with increasing parent charge is not redistributed to the ejecting monomer. Monomer charges when using FTMS on-resonance CAD and SORI-CAD are however higher, indicating that in this case the monomer is unfolded more extensively.

Loss of charge happens during or after dissociation of the complex

Since the experiments also showed charge stripping without dissociation upon activation (see Figure 4.1) it is presumable that at least part of the

charge loss of the fragments has already occurred well before the onset of dissociation. This is actually not the case, because we observe no difference in dissociation pathway between a charge stripped parent and a parent with fewer charges by itself. For instance, the 21+ gp31 parent with a charge deficit of 2 would be indistinguishable from the 19+ parent without a charge deficit. From Figure 4.6 it becomes clear that dissociation of these two parents does not yield the same fragment species in the presented experiments. In this figure the charge division between the monomers and hexamers is shown with increasing activation for all activation techniques. In Figure 4.6c it can be seen that dissociation of the gp31 21+ parent never yielded the same distribution of charges over the fragments as dissociation of the 20+ and 19+ parents. With increasing activation for the (on-resonance) CAD experiments, the charge loss increased, as shown in Figure 4.5 by the decreasing combined monomer and hexamer charge. The charge division over the fragments (Figure 4.6c) with increasing activation (i.e. increasing charge deficits) actually diverges from a charge division over the fragments measured for the lower charge states. This confirms that charge stripping and subsequent equilibration does not occur before dissociation, implying that the charge stripping cannot be seen separate from the dissociation of the complex.

Figure 4.6: Evolution of the charge division over the dissociation products, monomers and hexamers, with increasing activation of the parent heptamer. Per species and activation technique all charge states are shown in one graph. The graphs are aligned using equations 4.1a and 4.1b. The 50% survival yield point is indicated by the vertical dashed bar in each graph. The bottom graph combines the results of NS-CAD for both proteins.



Charge stripping is a kinetic effect

Figure 4.5 shows that with growing activation in (on-resonance) CAD the combined fragment charge decreases (i.e. an increasing charge deficit), while for the SORI-CAD experiment the combined fragment charge remains approximately constant. In SORI-CAD the average internal energy is increased with "continuous low kinetic energy and multiple (soft) collisions", not resulting in more charge loss. This is contrary to (on-resonance) CAD, where the kinetic energy at the start of the collision cascade is increased, resulting in harder collisions and more charge loss. This difference indicates that the charge stripping is a kinetic effect. The charge deficit increases with increasing parent charge state for all experiments. This increasing charge loss is largely accounted for by fewer charges on the ejected monomer. This is evident from the observed decrease in monomer charges (Figure 4.5) while the hexamer charge remains relatively constant. This becomes even more clear in Figure 4.6c, 4.6d and 4.6e which shows that the relative charge on the hexamers is increasing compared to the monomer charge. NS-CAD has the highest charge deficit, relative to the average parent charge. While the lowest monomer charge states are achieved with NS-CAD, the hexamer charge states remain comparable to the results for the other FTMS experiments (Figure 4.5). Despite the fact that NS-CAD exhibits the largest charge losses, the charge loss is more equally divided over the hexamer and monomer fragment than for the other activation mechanisms that show charge losses. This is shown in Figure 4.6f, where the charge division between the fragments during NS-CAD only slightly changes with increasing activation, while the charge loss increases with increasing activation (Figure 4.5). This does not agree with the diverging charge divisions in Figure 4.6c, 4.6d and 4.6e when charge loss increases. The exact origin of the charge losses with the ejected monomer and, partly, the fragment hexamer thus remains to be determined.

Difference gp31 and GroES

Besides the effects of different experimental techniques and parent charge states on the charge states of the fragmentation products, the two different protein complexes exhibit different behavior.

This study shows that using various activation techniques it is possible to induce different effects on the GroES and gp31 proteins. With rapid, energetic activation, as in NS-CAD, the behavior of the protein complexes is comparable with respect to charge loss and division over the fragments. Going to a relatively more gentle activation mechanism, the q-ToF CAD, GroES starts showing less charge loss than gp31. This trend continues when using FTMS on-resonance CAD, even gentler activation. When using SORI, the most gentle activation technique used in this paper, also for gp31

the amount of charge loss decreases.

The major differences between the two complexes using these experiments pertain to the effects of charge loss during activation/dissociation. We hypothesize that this loss is related to the structure of the ejected monomer, which is likely to be partially unfolded. The different structure and charging of the parents cause different dissociation pathways to become activated for the two protein complexes, resulting in different divisions of the charge over the fragment hexamers and ejected monomers and the amount of charge loss.

Despite the fact that the denatured average charge state for gp31 monomers is 11+, while the maximum charge state of the monomers formed via dissociation is around 8+, it seems that the monomer cannot be loaded to higher charge states during dissociation. Not even for the slowest activation technique used in this paper (SORI-CAD), will the monomer be unfolded enough to accommodate the maximum number of charges. For GroES the same is applicable, although less pronounced.

The GroES monomer loading is also limited around 8 charges, while the hexamer charge still increases with increasing parent charge.

The lower parent charge states for GroES are the prime cause of the different behavior under the different activation techniques. The monomers will reach their maximum loading capacity only for the highest GroES parent charge state in the FTMS on-resonance CAD and SORI-CAD experiments. For the q-ToF CAD experiment, both the gp31 monomer and the GroES monomer have reached their maximum loading capacity.

4.4 Conclusion

In this study gas-phase differences between two highly similar large non-covalent protein complexes were examined, in an effort to relate their functional in vivo differences to differences in gas-phase stability and/or structure. The experiments reveal that there is no significant difference between the gas-phase stability of the two proteins. From this we deduce that the difference in function of the two complexes in vivo does not depend on the inter subunit interaction strength. Comparison of the different activation techniques with respect to the effects on charge distribution over the fragments proves to be interesting. The maximum loading capacities of the ejected monomers are obtained and the correlation is shown between the time frame of activation and the degree of unfolding of the ejected monomer.

The investigation into the dissociation pathways for the two protein complexes revealed differences with respect to charge distribution over the dissociation products and with respect to the extend of charge loss during dissociation. There are no differences for NS-CAD and small differences

for q-ToF CAD, but differences between the two complexes become more apparent with the more gentle activation mechanisms, FTMS on-resonance CAD and FTMS SORI-CAD. These differences indicate that there are structural features of the two complexes that are significantly different and that control the dissociation pathway. The major discriminants of the dissociation pathway are the parent charge state and the ability of the unfolded monomer to take up charges.

4.5 Acknowledgement

We thank Esther van Duijn for kindly providing the protein samples. This research is part of the research programme of the "Stichting voor Fundamenteel Onderzoek der Materie (FOM)", which is financially supported by the "Nederlandse organisatie voor Wetenschappelijk Onderzoek (NWO)". This work is part of the FOM/ALW program "Physical Biology II" under project number 01FB12-1.

Solution-phase and gas-phase thermal activation of the co-chaperonins GroES and gp31 probed by mass spectrometry

Abstract

Native electrospray ionization mass spectrometry can be used to study static and dynamic solution-phase stoichiometry of protein complexes in the gas-phase. A thermally controlled electrospray setup was employed to analyze conformational and stoichiometric changes of protein complexes at varying temperature. Conformational changes result in changing charge state distributions at a specific stoichiometry, provides insight into the conformational and stoichiometric changes that occur during the thermal denaturing process, something that cannot be resolved by conventional methods such as fluorescence spectroscopy. Both native electrospray ionization mass spectrometry and fluorescence spectroscopy were employed to analyse the oligomeric chaperonin complexes (GroES and gp31). We report that thermal dissociation temperatures of the complexes are similar using both techniques and that thermal denaturing of GroES and gp31 proceeds via intermediate steps of all oligomeric forms down to the monomer. There is no evidence of a transiently stable unfolded heptamer. With each intermediate step, the subunits of the complex are increasingly more unfolded, as is apparent from an increase of the charge per subunit in the complex. It is also possible to infer the role of hydration on the thermal dissociation of the complexes by comparing the solution-phase thermal activation to gas-phase thermal activation using IRMPD. Using gas-phase activation the smaller oligomers are not seen, only down to the pentamer, where after the complex seems to dissociate completely, demonstrating clearly that conformational changes of GroES and gp31 due to heating in solution are significantly influenced by the presence of solvent molecules.

Rimco B.J. Geels, Stephane Calmat, Albert J.R. Heck, Saskia M. van der Vies, and Ron M.A. Heeren, *Analytical Chemistry*, in preparation.

5.1 Introduction

Noncovalent association of monomeric proteins into biologically active oligomeric conformations is a vital part of many biological functions. Oligomeric complexes occur in a range from very large, heterogeneous assemblies, e.g. ribosomes to small homogeneous assemblies, e.g. alcohol dehydrogenase. Noncovalent association of the monomer subunits is essential for their proper biological function. Noncovalent association of multiple subunits seems to be preferred over covalently linked subunits.¹⁸² At physiological concentrations, the oligomeric state is energetically preferred since covalent linkage often complicates folding kinetics. It might also be that error rates in transcription create serious problems in fabrication of large amino acid chains, multiple smaller subunits are then more reliable. Another possible argument mentioned in the literature is that the native state is only reached through induced folding of the subunits upon association.^{183–186} Multisubunit complexes also give the cell the possibility to use different subunits in more than one way, allowing for dynamic control of biological processes. Generally, more complex functions require larger and more sophisticated multi subunit protein complexes, like the chaperonins. To fully understand the biological relevance of noncovalent complexes a thorough understanding of the actual association process of these complexes is necessary.

The GroEL-GroES chaperonin complex assists non-native proteins in attaining their native state by isolating the protein from its environment and actively using hydrophobic interactions to help fold the substrate protein.^{18,23} The folding cycle of GroEL-GroES is very dynamic and complex with many conformational changes occurring during the folding cycle. Since many conformational changes are apparently needed, the question arises how flexible and dynamic GroES is and how it actually associates itself. GroES is a heptamer consisting of 7 identical 10kDa subunits arranged in a circular fashion. The necessity of oligomerization over un-associated monomers is part of the quest. Association of folded monomers into a native heptamer seems entropically very unfavorable. The association of GroES and various other cpn10 family members, has been the subject of numerous such studies.^{175,182–195}

The theory on how the association of the GroES heptamer proceeds has changed drastically over the last ten years. In 1995 Zondlo *et al.*¹⁷⁵ first suggested a two-step process whereby monomer first folds to its native state and subsequently associates via a single step into the native heptamer.¹⁷⁵ Later Donald *et al.*¹⁸⁸ refined this model by revealing multiple steps in the association process of GroES *in vitro*, which was supported by others.¹⁸³ Besides the investigations into the association steps, several studies have been performed on the folding equilibria of the monomers in relation to their monomer-heptamer equilibrium. Boudker *et al.*¹⁸⁷

showed that it is thermodynamically unfavorable for the monomers to be folded before they associate and provided evidence for induced folding during association of the monomeric subunits. Since then multiple studies have investigated the thermodynamics of unfolding and refolding of GroES *in vitro*. In such studies GroES is denatured using temperature, urea or guanidine-hydrochloride.^{183,189,191} Changes in the protein can be monitored by fluorescence, circular dichroism (CD), cross-linking, isothermal calorimetry (ITC) and X-ray scattering.^{190,192,193,195} By using point-mutations in the amino-acid sequence of the monomers and identifying vital residues for association scientists have also tried to investigate the interplay between folding and association.¹⁹⁰

The general consensus of the reported studies appears to be that the un-associated monomers exist mainly as unfolded monomers and a small part as partially folded monomers. Under appropriate concentrations i.e. in the presence of certain concentrations of guanidium hydrochloride or urea, a non-native heptamer is formed. This species can be transforming into the native heptamer upon changing the conditions to more physiological relevant conditions. This evidence is based either on best-fits of experimental data or on molecular dynamics simulations. The species mentioned have not been observed directly (via NMR, X-Ray or Mass Spectrometry). The non-native heptamer has been suggested to be a necessary intermediate in the formation of native heptameric cpn10 (GroES in *E. coli*).¹⁸⁶ The findings on the conformation and stoichiometry of the protein complex depend greatly on the denaturing method used. The association/dissociation pathways of the various cpn10 homologues differ somewhat with respect to intermediates and association/folding speeds and may reflect the difference in amino acid sequence of the different homologues.^{193,194}

All these investigations reveal that the details of the association process of GroES are difficult to elucidate. None of the papers described details of the exact association steps of GroES. Most of them imply a single association step of seven subunits in one step. However, Donald *et al.*¹⁸⁸ and Bascos *et al.*¹⁸³ have provided evidence for extra association steps, using mass spectrometry and fluorescence/CD respectively. Interestingly, the two papers do not agree on the association steps. The bottleneck in the process as described by Donald *et al.* seems, undoubtedly, the three-body association of the three dimers, which would mean that the dimer form should be a very abundant species. There is no evidence of this in the literature. CD, ITC and fluorescence spectroscopy are all indirect methods of determining the stoichiometry of the different forms of the protein in the sample. This might explain why the intermediate oligomeric forms of the cpn10s are not observed. We have used mass spectrometry combined with thermal manipulation to induce unfolding/dissociation intermediates of GroES and gp31 in solution-phase and in the gas-phase.

Gp31 is an analog of GroES, which is used by bacteriophage T4 during

morphogenesis in *E. coli*. As part of the reproduction of the bacteriophage, its major capsid protein, gp23, needs to fold into its native state, which the chaperonin machinery of the *E. coli* cannot do, i.e., gp23 cannot fold with the help of the normal GroEL-GroES complex. The GroES co-chaperonin has to be substituted by the bacteriophage-encoded protein gp31.⁵⁷ Gp31 shows structural similarity to GroES. Both are noncovalent complexes of seven identical subunits each, arranged in a circular fashion with seven-fold symmetry. The gp31 heptamer has a slightly bigger mass (84kDa) than GroES has (72kDa).⁵⁷ The origin of this functional difference has been investigated extensively.^{46,55,56} It is believed that the difference in function arises from a difference in structure between the two protein complexes.³¹ The size of the folding cage in the GroEL-gp31 complex is somewhat larger than that of the GroEL-GroES complex. This enlargement may allow for the accommodation of the relatively large gp23 capsid protein (56kDa), which is close to the upper size limit of proteins that can be accommodated by GroEL-GroES chaperonin.⁵⁶ Besides the increase in cavity size in the GroEL-gp31 complex there are other structural differences visible between GroES and gp31 co-chaperonins.⁵⁷ Gp31 has a longer mobile loop that is thought to allow the size increment of the folding cage. However, additionally, gp31 may affect parts of the folding cycle. Interestingly, the roof loop that is present in GroES is missing in gp31, which might be required for the formation of the observed larger folding cage.

Mass spectrometry has two distinct characteristics that can be very useful for determining characteristics of the dissociation mechanisms of GroES and gp31. First, the stoichiometry of protein complexes is easily determined.^{40,181,188,196} and second, the charge state of proteins in the mass spectrometer can be related to their gas-phase structure.¹¹⁹ For example, unfolded proteins tend to attain a higher charge state during the electrospray process than do folded proteins.¹⁹⁷⁻¹⁹⁹ A subject of discussion concerns the relation between the stoichiometric states of the proteins in the gas-phase and their states in the more physiological solution-phase.^{119,200,201} The absence of solvent in the gas-phase has a profound influence on the structure of the protein and the collisional cooling of ions during and after evaporation can influence stoichiometry of the complexes.¹²⁵ To gain insight into these effects, the solution-phase thermal activation of GroES and gp31 was compared to gas-phase thermal activation using fluorescence spectroscopy and mass spectrometry respectively.

To this end a temperature controlled electrospray ionization setup was developed, based on the one described by Benesh *et al.*¹¹⁴ Details of this device are explained in the materials sections. With this temperature controlled probe, the temperature of the sample can be tuned in the range of 3-100°C and is maintained right up to the electrospray of the protein sample. The effect of sample temperature changes as observed in

the mass spectrum will provide detailed information about the prevailing stoichiometric state of the sample. The results will be compared to thermal activation of GroES and gp31 monitored by tyrosine fluorescence.

5.2 Experiment

Both co-chaperonins, gp31 and GroES were over-expressed in *E. coli* strain MC1009¹⁶⁹ and purified as described previously.^{58,170,171} The proteins were transferred to 5mM ammonium acetate, pH 6.8, by using ultra filtration filters with a cut-off of 5000Da (Millipore, Bedford). The concentration of gp31 and GroES in the sample was 12.5 μ M. Protein concentrations are given based on the gp31 and GroES monomer. To perform the solution-phase thermal activation experiments, a temperature controlled electrospray setup was developed.¹¹⁴ A cross-section of the device is shown in Figure 5.1a. To have a proper control over the sample temperature up to the exact moment of spraying, the spray needles used are fit inside a metal capillary, shielding from the lower environment temperature at the tip end, as is indicated in the figure. The prevailing sample temperature inside the tip was calibrated with the readout temperature of the Pt100 resistance using a small thermocouple fitting inside the spray needle. The tip temperature is only marginally lower than the set temperature and is maximally 2 degrees lower at 90°C.

The mass spectrometry experiments were performed using a modified Bruker APEX 7.0e FT-ICR-MS equipped with an open-ended cell.⁸² Experimental control hard- and software were developed in-house and have been described elsewhere.⁸² Elevated pressure in the source octopole (\sim 2mbar) facilitated transfer of the large intact protein complexes into the gas phase and into the ICR cell.¹⁷² Ions were accumulated inside the source octopole and subsequently transported to the ICR cell using gated trapping with typical accumulation times of 2-3 seconds in the octopole. To perform the gas-phase thermal activation experiments, the ion cloud trapped inside the ICR cell was irradiated with infrared photons, so-called InfraRed Multi-Photon Dissociation (IRMPD). A scheme of the IRMPD setup is shown in Figure 5.1b. A CO₂ laser from Synrad, model: J48-2SW, was focused onto the hole of a diaphragm located at the rear end of the open cell via a telescopic lens setup, passing through a ZnSe window, obtained from Viewport with an antireflection coating. The irradiation power and time can thus be controlled. Individual charge states of the protein heptamers were isolated using SWIFT pulses⁸⁸ generated using AWG3 software²⁰² and subject to IRMPD. Fluorescence measurements were performed on a Varian Cary Eclipse Fluorescence Spectrophotometer (1cm cell). Excitation was at 280nm with 5nm excitation and emission slits. Thermal manipulation was performed using a water-cooled peltier device, Varian Single Cell Peltier

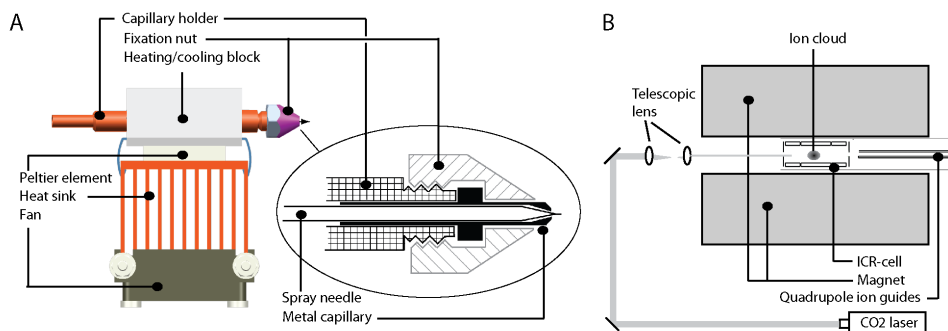


Figure 5.1: Schematics of the mass spectrometry setup. Part A shows the lay-out of temperature controlled electrospray device. The inset shows the cross-section of the spray tip. The spray needle is fitted inside the metal capillary to have proper temperature control over the sample up to the exit of the spray needle. Part B shows the lay-out of the InfraRed MultiPhoton Dissociation (IRMPD) setup. The CO₂ laser beam enters the ICR-cell from the back and is focused through the entrance diaphragm of the cell. Alignment of the laser is performed by maximizing the intensity of the dissociation products in the mass spectra.

Accessory. Sample temperature was measured to correspond to the readout temperature of the peltier element within half a degree. The protein sample was allowed to equilibrate at each temperature for two minutes i.e. after the readout temperature reached the set temperature. As a control the temperature-dependent fluorescence spectrum of the ammonium acetate solution was determined. The pH of the solution was also measured separately at various temperatures. The pH decreased to 5.8 for temperatures up to 90°C.

5.3 Results and discussion

5.3.1 Solution-phase thermal dissociation monitored by mass spectrometry

A sample of GroES dissolved in ammonium acetate was analyzed by mass spectrometry at various sample temperatures using the temperature controlled electrospray probe. Mass spectra obtained at three different temperatures are shown in Figure 5.2.

From these kind of mass spectra the various oligomeric species present in the sample are readily determined as indicated in the figure. At room temperature only heptameric GroES is present in the sample. After raising the temperature to 76°C, with 2°C intervals many different oligomeric

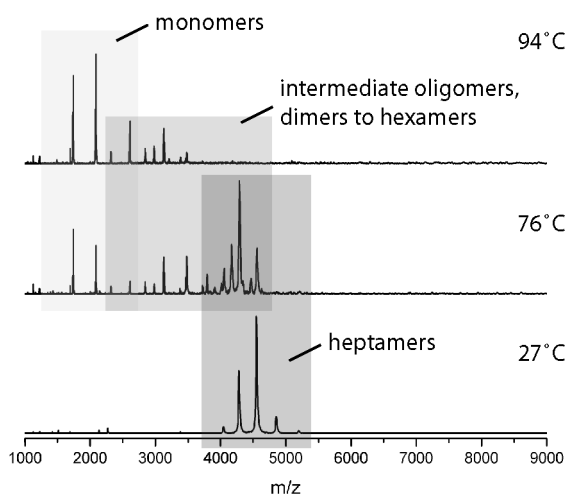


Figure 5.2: GroES mass spectra at different sample temperatures. The bottom graph show only heptamers at temperatures close to room temperature. At higher temperatures (middle graph) the presence of various kinds of intermediate oligomeric species in the sample is evident. At even higher temperature (top graph) mostly monomers remain, along with a small amount of dimers and trimers.

species are present in the sample. Note, that these species are present in solution and are not created during or after electrospray ionization. This is inferred from the fact that gas-phase dissociation leads to entirely different species,¹⁸¹ also shown in the paragraph on gas-phase dissociation. At even higher temperatures mostly monomers remain (Figure 5.2, top spectrum).

In Figure 5.3 the division of the population over the various possible oligomeric states is shown for each measured temperature, for both GroES and gp31. The number of each oligomer was scaled by the number of its constituent subunits, to reflect that one heptamer equals seven monomers, and subsequently normalized. From these graphs it is clear that there is a substantial number of intermediate oligomers. The presence of these intermediate oligomers indicates that they represent stable, temperature dependent conformations. To the knowledge of the authors, only the presence of dimers and hexamers for GroES has been reported explicitly.¹⁸⁸ Other intermediate species have not been observed. Luke *et al.*¹⁹⁴ and Guidry *et al.*¹⁸⁹ report intermediate species appeared to be present in acrylamide gels, but this was attributed to incomplete crosslinking. Also, all the thermal denaturation experiments performed on members of the cpn10-family have not revealed possible intermediate states and only deal

5. SOLUTION-PHASE AND GAS-PHASE THERMAL ACTIVATION OF THE CO-CHAPERONINS GROES AND GP31 PROBED BY MASS SPECTROMETRY

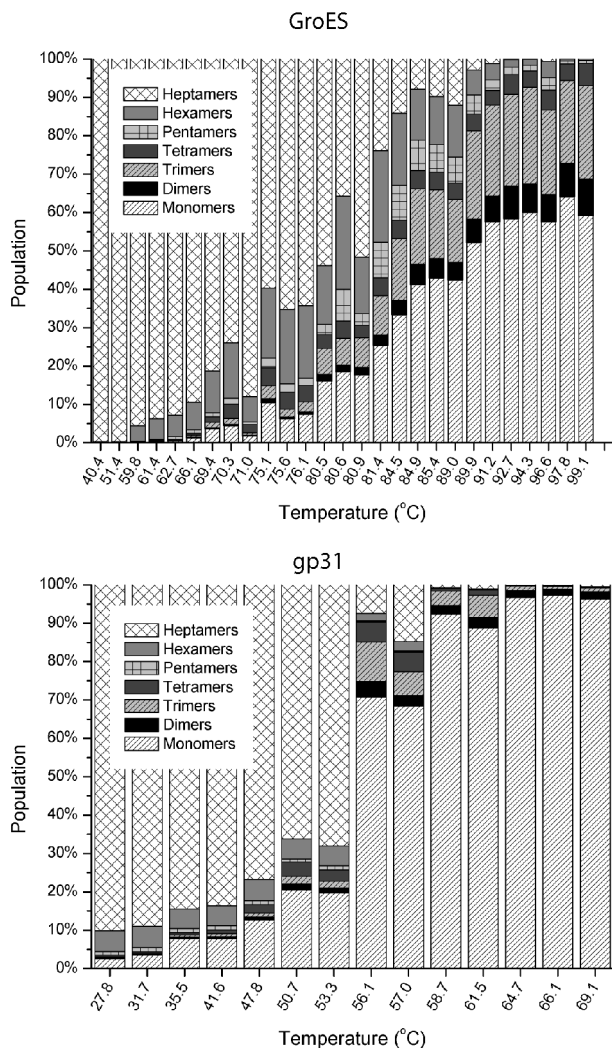


Figure 5.3: Population of the different oligomeric species of GroES and gp31 throughout the temperature range. The numbers are calculated by scaling the relative ion counts of the species by the number of constituent subunits and subsequently normalizing. At intermediate temperatures a significant population of oligomeric species in between the monomer and the heptamer is evident.

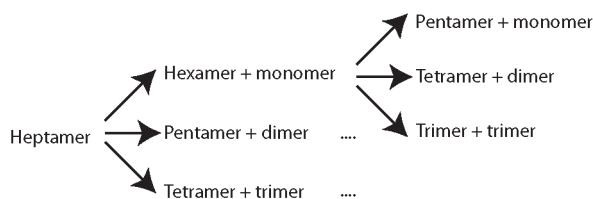


Figure 5.4: Possible thermal solution-phase dissociation pathways of GroES and gp31. Starting from a stable heptamer, with increasing temperature lower oligomers are created via ejection of a monomer or higher oligomer from the complex. These intermediate oligomers form stable intermediates in the thermal dissociation pathway. Eventually, at high temperatures only monomers will remain.

with the heptamer to monomer transition.^{185,187,189,190} From these data it is evident that thermal denaturation of GroES and gp31 in solution-phase cannot be seen as a two-state process. From subunit exchange experiments with wild-type and mutant cpn10s¹⁹⁰ and subunit exchange between GroES and gp31 performed in our lab (no exchanges observed, data not shown) it can be inferred that the heptamers form stable structures up to high temperatures. The hexamers and lower oligomers present at increasing temperature thus have to originate from dissociation of a monomer or higher oligomer from the heptameric complex. They do not stem from a heptamer that first dissociated into monomers and then reassembled into the lower oligomer. Thermal denaturation of GroES and gp31 thus proceeds via sequential steps from the native heptamer down to monomers via sequential ejection of one or more subunits.

The possible dissociation pathways are summarized in Figure 5.4. The fact that throughout the temperature range there is a pronounced presence of intermediate oligomers indicates that the free energy of all these conformations at a certain temperature is comparable. It is not until at high temperature that the entropy term of the free energy substantially outweighs the enthalpy of oligomerization resulting in monomers mostly. For gp31 it can be argued that the entropy term has a bigger influence than in the case of GroES, since the abundance of intermediate oligomers in that case is much less and the temperature of disassembly is much lower, see also Figure 5.5.

Figure 5.5 visualizes the thermal breakdown diagrams. The difference in midpoint temperature (as a measure of the survival yield of heptameric GroES and gp31) is clear. The value, 79°C, for the thermal midpoint of GroES is a little higher than those found by other methods on GroES or *hm-cpn10*, as determined by fluorescence, CD and differential scanning calorimetry (DSC).^{185,187,189,190} A thermal midpoint temperature for gp31

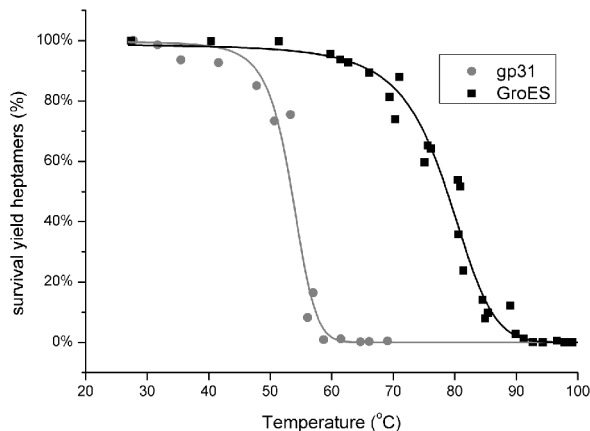


Figure 5.5: Thermal dissociation survival yield graph of GroES and gp31. In this figure the survival yield of the heptamers is plotted against the temperature. The survival yield is calculated as the number of subunits accommodated in heptamers in terms of the total number of subunits present and normalized. Thermal midpoint temperatures of gp31 and GroES are approximately 55°C and 79°C respectively. The lines are meant to guide the eye.

has as far as we know not been published in the literature. In order to establish whether the values obtained by mass spectrometry are comparable to other methods, thermal dissociation curves for both GroES and gp31 were recorded using fluorescence spectroscopy.

5.3.2 Thermal denaturation probed with fluorescence spectroscopy

GroES has one tyrosine pointing inward into the dome-shaped lid.^{31,57} Gp31 has three tyrosines, one of which resembles the location of the tyrosine in GroES and one of which is located at the inter subunit boundary. Using fluorescence it is possible to probe the effects of thermal activation on the local surroundings of the tyrosines. The effects of sample temperature on the fluorescence spectra are shown in Figure 5.6.

Two effects are visible in the spectra of Figure 5.6a. First, the overall fluorescence intensity decreased with increasing temperature. Second, the lay-out of the spectra changes, i.e. a shift of the fluorescence maximum and an overall flattening of the peak in the fluorescence spectrum. Figure 5.6b shows the integrated fluorescence intensities as a function of temperature. Analysis of the slopes of these graphs revealed a single major transition

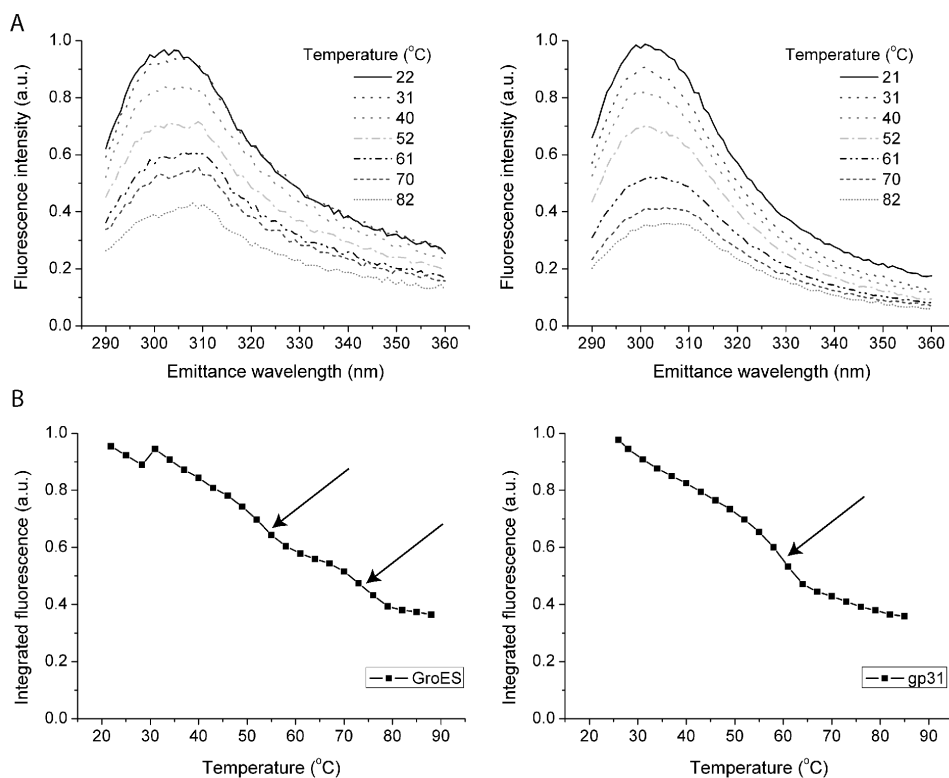


Figure 5.6: Thermal fluorescence measurements of GroES and gp31. Part A shows the change in the fluorescence spectra at various temperatures. Part B shows the evolution of the integrated fluorescence intensity with temperature. The arrows indicate transition midpoints. For GroES there are two transitions apparent from the fluorescence measurements. Thermal midpoints of these measurements are 52°C and 74°C for GroES (left panels) and 59°C for gp31 (right panels).

for gp31, with midpoint temperature 59°C, but also indicates two smaller transitions for GroES with midpoint temperatures 52°C and 74°C. The transitions are indicated in the figure. The midpoint temperature of gp31 agrees rather well with the midpoint temperature determined by mass spectrometry (55°C vs. 59°C) and the midpoint temperature of the second transition of GroES also corresponds well with the mass spectrometry data (78°C vs. 74°C).

The large difference in transition temperatures for the two species is clearly present with both techniques. The origin of the double transition for GroES is unclear from fluorescence data alone. However, our mass

spectrometry data revealed that the thermal denaturing of GroES cannot be seen as a two-step process, but involving all intermediate oligomers. Since every transition to the next intermediate oligomer has an influence on the fluorescence of the tyrosines, the interpretation of the fluorescence measurement is seriously complicated. The gradual nature of the transition for GroES makes interpretation of the fluorescence data difficult. The two minor transitions evident from the fluorescence cannot be readily related to the species identified by mass spectrometry. The first transition occurs at 52°C, where the only species present in the mass spectrum is the heptamer, indicating a change in the local environment of the Tyrosine while remaining heptameric. The second transition however coincides well with the midpoint temperature as determined by mass spectrometry. The intermediate species present in the mass spectra for gp31 are much less abundant compared to the mass spectra for GroES. This explains why the gp31 fluorescence spectrum still clearly shows one major transition (from the heptamer to the monomer) at the corresponding temperature. Despite the fact that the exact thermal unfolding/disassembly process remains unclear, it is shown that the process cannot be viewed as a two (or three, with intermediate unfolded heptamers or folded monomers) step transition, as has previously been done repeatedly.

5.3.3 Probing the folding state of the species using mass spectrometry

As discussed in the introduction, in the literature various possible disassembly pathways of cpn10s have been proposed and validated by measurements. In many of these pathways an unfolded heptamer or unfolded monomer is present. This interpretation is primarily based on the fact that probing methods such as CD and Fluorescence are more sensitive to unfolding of subunits than to disassembly of oligomers. However, mass spectrometry data can also give insight into the folding state of the species present, by means of the average charge the species acquire during the electrospray process. Basically, a more extended, i.e. unfolded, molecule will acquire more charges during electrospray ionization than a more compact molecule.^{196,201,203} For example, the unfolding transition of hen egg white lysozyme has been accurately determined.¹¹⁴ The presence of an unfolded heptamer intermediate or a change of folded to unfolded monomer should be evident from the average charge state in the mass spectra. The average charges of the various species in the mass spectra are, however, independent of temperature. The values of the average charges are given in Table 5.1.

For each increasingly smaller oligomer the average charge per subunit increases, indicating a less compact structure. An unfolded heptamer would acquire many more charges per subunit than the 2-2.5 in this measurement, since the charge on the single monomers is approximately 6. If the unfolded

	monomer	dimer	trimer	tetramer	pentamer	hexamer	heptamer
GroES	5.6±0.1	4.0±0.1	3.3±0.3	2.9±0.5	2.7±0.2	2.5±0.1	2.4±0.1
gp31	5.9±0.1	4.4±0.2	3.6±0.5	3.5±0.5	2.8±0.4	2.7±0.2	2.7±0.1

Table 5.1: Overview of the average charge of the various oligomeric species during the thermal activation experiments in solution and monitored by mass spectrometry. The average charges are temperature independent. The values for the intermediate oligomers in the case of gp31 are difficult to determine due to their low abundance and thus have considerable error bars.

heptamer is only transiently present in the sample, it will not show up in these mass spectra. The higher charge on every sub sequential lower oligomer cannot be explained just by the increase in surface area due to a reduced interaction with other subunits, but an increase in surface area due to unfolding has to be taken into account. This suggests that the monomer is the most unfolded species in our experiment. The non-changing charge on the monomer also indicates that there is no temperature dependent unfolding of this species during the experiment. For instance for gp31 this suggests a single major transition from the folded (native) heptamer to the (partly) unfolded monomer. Previous experiments performed in our group using 2% acetic acid denatured GroES and gp31¹⁹⁶ indicate that the charge on these denatured monomers is even higher (up to 10-11) charges per monomer. Comparing this to the 6 charges determined for the monomers in the thermal denaturing experiment, suggests that the monomers are not completely unfolded and have considerable residual three-dimensional structure. This is supported by the observation that all thermal denaturing measurements were reversible. If the monomers would have been completely unfolded, one would have expected that lowering the temperature would lead to aggregation of the protein.

From the investigations presented it is clear that the mass spectrometry analysis adds considerable insight into the thermal denaturing of these protein complexes. The analysis can be extended to thermal activation of proteins in the gas-phase by using IRMPD, to probe the disassembly behavior in the absence of solvent.

5.3.4 Gas-phase thermal activation using mass spectrometry

A gas-phase equivalent to solution-phase thermal activation is InfraRed MultiPhoton Dissociation (IRMPD), an activation technique that can be used on ions trapped inside the ICR-cell of a FT-ICR-MS. Prior to activation a precursor ion species can be selected on the basis of their mass/charge value. All ions with other mass/charge ratios are ejected from the ICR-cell in this process. When the remaining ions are irradiated,

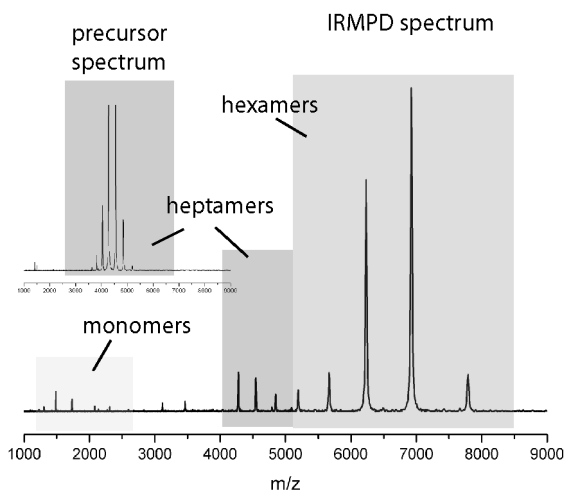


Figure 5.7: Infrared multiphoton dissociation of GroES heptamers. Irradiation of GroES heptamer leads to dissociation of the heptamer into a hexamer and corresponding monomer. The original charge on the heptamer is divided over the hexamer and monomer fragment. The monomer fragments take up a relatively large share of the charges, because they (partly) unfold during ejection. That is why the monomers appear at lower m/z and the hexamers at higher m/z .

they absorb the incoming photons and when their internal temperature reaches a dissociation threshold that specific dissociation occurs. Using this technique, the difference between GroES and gp31 with respect to gas-phase stability can be assessed. In addition, the dissociation pathways of the two proteins can be compared to each other and to the dissociation pathway in solution, giving insight into the role of water molecules in the dissociation process.

In Figure 5.7 a mass spectrum is shown of GroES after activation with IRMPD. The inset shows the spectrum before irradiation when only heptameric species of various charge states were present. For longer irradiation times the layout of the spectrum does not change, only the intensities decrease. Figure 5.7 is clearly different from Figure 5.2 in that there the only lower oligomer created in the dissociation pathway is the hexamer and other lower oligomers are not present. This indicates that when the hexamer dissociates, it dissociates into monomers only or that possibly formed lower oligomers are not stable enough to remain bound. Even for longer irradiation times a substantial amount of hexamer remains, indicating that the hexamer form is a very stable configuration in the gas-phase. As a control experiment, explicit activation of the fragment hexamer using

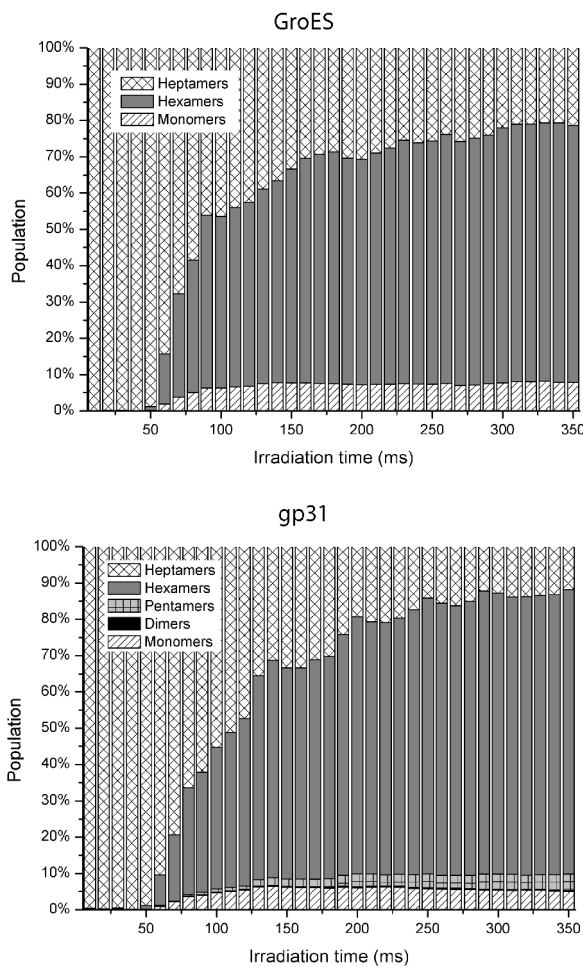


Figure 5.8: Population of the different oligomeric species of GroES and gp31 with increasing irradiation time. The numbers are calculated by scaling the relative ion counts of the species by the number of constituent subunits and subsequently normalizing. There is no substantial population of intermediate oligomers other than the hexamer and pentamer (gp31).

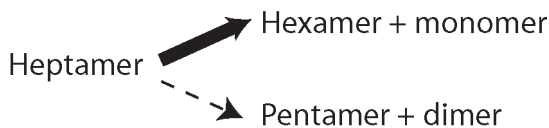


Figure 5.9: Gas-phase breakdown pathways for GroES and gp31. GroES only shows dissociation into a hexamer+monomer, whereas gp31 also exhibits some dissociation into a pentamer+dimer.

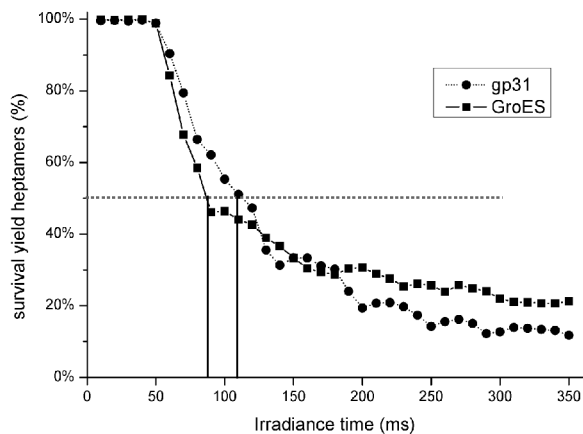


Figure 5.10: Survival yield diagrams of gp31 and GroES using IRMPD. The survival is calculated as the percentage of monomeric subunits accommodated in heptamers to the total number of monomeric subunits present in all species together. The small difference in 50% survival yield is not large enough to state that there is a significant difference in gas-phase thermal stability.

various activation methods was performed, but this did not result in any substantial fragmentation (data not shown).

Figure 5.8 shows population of the different oligomeric species with increasing irradiation times both GroES and gp31 using IRMPD, the gas-phase equivalent of Figure 5.3. Figure 5.9 shows the stoichiometric breakdown pathways and Figure 5.10 shows the breakdown (survival yield) diagrams. Various observations can be made from these figures. First of all, the fragmentation pathways for GroES and gp31 are similar. The difference being that gp31 has some fragmentation to pentamers, whereas the pentamers are absent for GroES. Second, the extend of the formation of intermediate oligomers is approximately equal for both complexes, as

opposed to solution-phase activation, where GroES exhibited a much higher degree of intermediate oligomer formation. Third, the survival yield diagrams do not show a significant difference in gas-phase stability for the two complexes, as opposed to the lower solution-phase stability for gp31.

The absence of a large portion of intermediate oligomers with the gas-phase activation suggests that the conformation of most of the intermediate oligomers is not stable without the interaction with the solvent, since these formed oligomers are stable in solution. Subsequent measurement in the gas-phase of these oligomers does not cause disassembly, indicating that the mechanism of disassembly in the absence of solvent does not lead to the same conformation as in the presence of solvent. The influence of solvent is also apparent from the difference in stability between gp31 and GroES in solution that is absent in the gas-phase. GroES seems to be stabilized better by the solvent than gp31. The lower stability of gp31 can be an advantage for the bacteriophage that uses it. Since less stability means more flexibility, this might be one of the reasons that the gp31-GroEL complex can actually fold gp23, which is too big for the GroES-GroEL complex.⁵⁷

5.4 Conclusion

Monitoring thermal disassembly using mass spectrometry revealed direct evidence of stable temperature-dependent intermediate oligomers in the thermal denaturation for both GroES and gp31. The ability to easily determine stoichiometry makes mass spectrometry combined with temperature controlled electrospray a useful tool for analyzing thermal disassembly of noncovalent protein complexes. The analysis did not reveal any evidence for temperature-dependent unfolding of (intermediate) species in the solution-phase. Thermal stability of gp31 in solution is much lower than that of GroES. The higher versatility of gp31 in the folding of substrates comes at the expense of lower solution-phase thermal stability. The solution-phase thermal stability is influenced greatly by specific interactions with the solvent. That the solvent has different effects on the thermal stabilities for the two protein assemblies become clear when comparing the solution-phase thermal activation to gas-phase thermal activation of isolated complexes.

5.5 Acknowledgement

We thank Marc Duursma for his extensive help with the FT-ICR-MS experiments. We also thank Esther van Duijn for kindly providing the protein samples. This research is part of the research programme of the "Stichting voor Fundamenteel Onderzoek der Materie (FOM)", which is financially supported by the "Nederlandse organisatie voor Wetenschappelijk

5. SOLUTION-PHASE AND GAS-PHASE THERMAL ACTIVATION OF THE
CO-CHAPERONINS GROES AND GP31 PROBED BY MASS SPECTROMETRY

Onderzoek (NWO)". This work is part of the FOM/ALW program "Physical
Biology II" under project number 01FB12-1.

Bibliography

- [1] J.M. Berg, J.L. Tymoczko, and L. Stryer. *Biochemistry*. Michelle Julet, 2002.
- [2] C.M. Dobson and M. Karplus. The fundamentals of protein folding: bringing together theory and experiment. *Current Opinion in Structural Biology*, 9(1):92–101, Feb 1999.
- [3] C.B. Anfinsen. Principles that govern the folding of protein chains. *Science*, 181(96):223–230, Jul 1973.
- [4] L.N. Johnson and D. Barford. The effects of phosphorylation on the structure and function of proteins. *Annual Review of Biophysics and Biomolecular Structure*, 22:199–232, 1993.
- [5] S. Schuchardt and A. Sickmann. Protein identification using mass spectrometry: a method overview. *EXS*, 97:141–170, 2007.
- [6] J. Reinders and A. Sickmann. Modificomics: posttranslational modifications beyond protein phosphorylation and glycosylation. *Biomolecular Engineering*, 24(2):169–177, Jun 2007.
- [7] F. Gesellchen, O. Bertinetti, and F.W. Herberg. Analysis of posttranslational modifications exemplified using protein kinase a. *Biochimica et Biophysica Acta*, 1764(12):1788–1800, Dec 2006.
- [8] M.R. Larsen, M.B. Trelle, T.E. Thingholm, and O.N. Jensen. Analysis of posttranslational modifications of proteins by tandem mass spectrometry. *Biotechniques*, 40(6):790–798, Jun 2006.
- [9] R.S.B. Clark, H. Bayir, and L.W. Jenkins. Posttranslational protein modifications. *Critical Care Medicine*, 33(12 Suppl):S407–S409, Dec 2005.
- [10] C.T. Walsh, S. Garneau-Tsodikova, and G.J. Gatto. Protein post-translational modifications: the chemistry of proteome diversifications. *Angewandte Chemie International Edition English*, 44(45):7342–7372, Dec 2005.

- [11] J. Ellis. Proteins as molecular chaperones. *Nature*, 328(6129):378–379, 1987.
- [12] F.U. Hartl. Molecular chaperones in cellular protein folding. *Nature*, 381(6583):571–579, Jun 1996.
- [13] P.T. Lansbury. Evolution of amyloid: what normal protein folding may tell us about fibrillogenesis and disease. *Proceedings of the National Academy of Sciences of the United States of America*, 96(7):3342–3344, Mar 1999.
- [14] C.M. Dobson. The structural basis of protein folding and its links with human disease. *Philosophical transactions of the Royal Society of London. Series B: Biological sciences*, 356(1406):133–145, Feb 2001.
- [15] M. Bucciantini, E. Giannoni, F. Chiti, F. Baroni, L. Formigli, J. Zurdo, N. Taddei, G. Ramponi, C.M. Dobson, and M. Stefani. Inherent toxicity of aggregates implies a common mechanism for protein misfolding diseases. *Nature*, 416(6880):507–511, Apr 2002.
- [16] R.J. Ellis and T.J.T. Pinheiro. Medicine: danger—misfolding proteins. *Nature*, 416(6880):483–484, Apr 2002.
- [17] C. Levinthal. Mössbauer spectroscopy in biological systems, proceedings of a meeting held at allerton house, monticello, illinois. edited by P. DeBrunner, J. Tsibris, and E. Munck, University of Illinois Press, Illinois, :22–24, 1969.
- [18] A.L. Horwich, G.W. Farr, and W.A. Fenton. Groel-groes-mediated protein folding. *Chemical Reviews*, 106(5):1917–1930, 2006. MAY.
- [19] W.A. Houry. Chaperone-assisted protein folding in the cell cytoplasm. *Current Protein and Peptide Science*, 2(3):227–244, Sep 2001.
- [20] A. Brinker, G. Pfeifer, M.J. Kerner, D.J. Naylor, F.U. Hartl, and M. Hayer-Hartl. Dual function of protein confinement in chaperonin-assisted protein folding. *Cell*, 107(2):223–233, Oct 2001.
- [21] K.L. Ewalt, J.P. Hendrick, W.A. Houry, and F.U. Hartl. In vivo observation of polypeptide flux through the bacterial chaperonin system. *Cell*, 90(3):491–500, Aug 1997.
- [22] J.L. Feltham and L.M. Gierasch. Groel-substrate interactions: molding the fold, or folding the mold? *Cell*, 100(2):193–196, Jan 2000.
- [23] P.B. Sigler, Z.H. Xu, H.S. Rye, S.G. Burston, W.A. Fenton, and A.L. Horwich. Structure and function in groel-mediated protein folding. *Annual Review of Biochemistry*, 67:581–608, 1998.

-
- [24] A.L. Horwich, W.A. Fenton, E. Chapman, and G.W. Farr. Two families of chaperonin: physiology and mechanism. *Annual Review of Cell and Developmental Biology*, May 2007.
- [25] J.S. Weissman, Y. Kashi, W.A. Fenton, and A.L. Horwich. Groel-mediated protein folding proceeds by multiple rounds of binding and release of nonnative forms. *Cell*, 78(4):693–702, Aug 1994.
- [26] T.K. Chaudhuri, G.W. Farr, W.A. Fenton, S. Rospert, and A.L. Horwich. Groel/groes-mediated folding of a protein too large to be encapsulated. *Cell*, 107(2):235–246, Oct 2001.
- [27] F.U. Hartl and M. Hayer-Hartl. Molecular chaperones in the cytosol: from nascent chain to folded protein. *Science*, 295(5561):1852–1858, Mar 2002.
- [28] Michael J Kerner, Dean J Naylor, Yasushi Ishihama, Tobias Maier, Hung-Chun Chang, Anna P Stines, Costa Georgopoulos, Dmitriy Frishman, Manajit Hayer-Hartl, Matthias Mann, and F. Ulrich Hartl. Proteome-wide analysis of chaperonin-dependent protein folding in escherichia coli. *Cell*, 122(2):209–220, Jul 2005.
- [29] M.Y. Cheng, F.U. Hartl, J. Martin, R.A. Pollock, F. Kalousek, W. Neupert, E.M. Hallberg, R.L. Hallberg, and A.L. Horwich. Mitochondrial heat-shock protein hsp60 is essential for assembly of proteins imported into yeast mitochondria. *Nature*, 337(6208):620–625, Feb 1989.
- [30] O. Fayet, T. Ziegelhoffer, and C. Georgopoulos. The groes and groel heat shock gene products of escherichia coli are essential for bacterial growth at all temperatures. *Journal of Bacteriology*, 171(3):1379–1385, Mar 1989.
- [31] J.F. Hunt, A.J. Weaver, S.J. Landry, L. Gierasch, and J. Deisenhofer. The crystal structure of the groes co-chaperonin at 2.8 angstrom resolution. *Nature*, 379(6560):37–45, 1996. JAN 4.
- [32] K. Braig, Z. Otwinowski, R. Hegde, D.C. Boisvert, A. Joachimiak, A.L. Horwich, and P.B. Sigler. The crystal structure of the bacterial chaperonin groel at 2.8 a. *Nature*, 371(6498):578–586, Oct 1994.
- [33] Z.H. Xu, A.L. Horwich, and P.B. Sigler. The crystal structure of the asymmetric groel-groes-(adp)(7) chaperonin complex. *Nature*, 388(6644):741–750, 1997.
- [34] R.J. Ellis. Protein folding: importance of the anfinen cage. *Current Biology*, 13(22):R881–R883, Nov 2003.

- [35] D.C. Boisvert, J. Wang, Z. Otwinowski, A.L. Horwich, and P.B. Sigler. The 2.4 Å crystal structure of the bacterial chaperonin groel complexed with atp gamma s. *Nature Structural Biology*, 3(2):170–177, Feb 1996.
- [36] B. Bukau and A.L. Horwich. The hsp70 and hsp60 chaperone machines. *Cell*, 92(3):351–366, Feb 1998.
- [37] V. Grantcharova, E.J. Alm, D. Baker, and A.L. Horwich. Mechanisms of protein folding. *Current Opinion in Structural Biology*, 11(1):70–82, Feb 2001.
- [38] N.A. Ranson, D.K. Clare, G.W. Farr, D. Houldershaw, A.L. Horwich, and H.R. Saibil. Allosteric signaling of atp hydrolysis in groel-groes complexes. *Nature Structural & Molecular Biology*, 13(2):147–152, Feb 2006.
- [39] H.S. Rye, S.G. Burston, W.A. Fenton, J.M. Beechem, Z. Xu, P.B. Sigler, and A.L. Horwich. Distinct actions of cis and trans atp within the double ring of the chaperonin groel. *Nature*, 388(6644):792–798, Aug 1997.
- [40] E. van Duijn, P.J. Bakkes, R.M.A. Heeren, R.H.H. van den Heuvel, H. van Heerikhuizen, S.M. van der Vies, and A.J.R. Heck. Monitoring macromolecular complexes involved in the chaperonin-assisted protein folding cycle by mass spectrometry. *Nature Methods*, 2(5):371–376, 2005. MAY.
- [41] R.L. Baldwin. Energetics of protein folding. *Journal of Molecular Biology*, 371(2):283–301, Aug 2007.
- [42] J.N. Onuchic, Z. Luthey-Schulten, and P.G. Wolynes. Theory of protein folding: the energy landscape perspective. *Annual Review of Physical Chemistry*, 48:545–600, 1997.
- [43] P.E. Leopold, M. Montal, and J.N. Onuchic. Protein folding funnels: a kinetic approach to the sequence-structure relationship. *Proceedings of the National Academy of Sciences of the United States of America*, 89(18):8721–8725, Sep 1992.
- [44] J.D. Bryngelson and P.G. Wolynes. Spin glasses and the statistical mechanics of protein folding. *Proceedings of the National Academy of Sciences of the United States of America*, 84(21):7524–7528, Nov 1987.
- [45] L. Konermann and D.A. Simmons. Protein-folding kinetics and mechanisms studied by pulse-labeling and mass spectrometry. *Mass Spectrometry Reviews*, 22(1):1–26, 2003.

-
- [46] D. Ang, F. Keppel, G. Klein, A. Richardson, and C. Georgopoulos. Genetic analysis of bacteriophage-encoded cochaperonins. *Annual Review of Genetics*, 34:439–456, 2000.
- [47] C.K. Mathews. *An overview of the T4 developmental program*. American Society for Microbiology Press, 1994.
- [48] E. Goldberg, L. Grinius, and L. Letellier. *Recognition, attachment, and injection*. American Society for Microbiology Press, 1994.
- [49] E.S. Miller, E. Kutter, G. Mosig, F. Arisaka, T.i Kunisawa, and W. Ruger. Bacteriophage t4 genome. *Microbiology and Molecular Biology Reviews*, 67(1):86–156, table of contents, Mar 2003.
- [50] V.V. Mesyanzhinov, P.G. Leiman, V.A. Kostyuchenko, L.P. Kurochkina, K.A. Miroshnikov, N.N. Sykilinda, and M.M. Shneider. Molecular architecture of bacteriophage t4. *Biochemistry (Mosc)*, 69(11):1190–1202, Nov 2004.
- [51] C.P. Georgopoulos, R.W. Hendrix, S.R. Casjens, and A.D. Kaiser. Host participation in bacteriophage lambda head assembly. *Journal of Molecular Biology*, 76(1):45–60, May 1973.
- [52] A.L. Hanninen, D.H. Bamford, and J.K. Bamford. Assembly of membrane-containing bacteriophage prd1 is dependent on groel and groes. *Virology*, 227(1):207–210, Jan 1997.
- [53] Y. Ding, R.L. Duda, R.W. Hendrix, and J.M. Rosenberg. Complexes between chaperonin groel and the capsid protein of bacteriophage hk97. *Biochemistry*, 34(45):14918–14931, Nov 1995.
- [54] P.J. Bakkes. *Principles that govern the folding of the bacteriophage T4 major capsid protein*. PhD thesis, 2005.
- [55] P.J. Bakkes, B.W. Faber, H. van Heerikhuizen, and S.M. van der Vies. The t4-encoded cochaperonin, gp31, has unique properties that explain its requirement for the folding of the t4 major capsid protein. *Proceedings of the National Academy of Sciences of the United States of America*, 102(23):8144–8149, 2005. JUN 7.
- [56] D.K. Clare, P.J. Bakkes, H. van Heerikhuizen, S.M. van der Vies, and H.R. Saibil. An expanded protein folding cage in the groel-gp31 complex. *Journal of Molecular Biology*, 358(3):905–911, 2006. MAY 5.
- [57] J.F. Hunt, S.M. van der Vies, L. Henry, and J. Deisenhofer. Structural adaptations in the specialized bacteriophage t4 co-chaperonin gp31 expand the size of the anfinzen cage. *Cell*, 90(2):361–371, 1997. JUL 25.

- [58] S.M. van der Vies. Purification of the gp31 co-chaperonin of bacteriophage t4. *Methods in Molecular Biology: Chaperonin Protocols*, 140:51–61, 2000.
- [59] S.M. van der Vies, A.A. Gatenby, and C. Georgopoulos. Bacteriophage-t4 encodes a co-chaperonin that can substitute for escherichia-coli groes in protein-folding. *Nature*, 368(6472):654–656, 1994. APR 14.
- [60] J.B. Fenn, M. Mann, C.K. Meng, S.F. Wong, and C.M. Whitehouse. Electrospray ionization for mass spectrometry of large biomolecules. *Science*, 246(4926):64–71, Oct 1989.
- [61] M. Dole, L.L. Mack, R.L. Hines, R.C. Mobley, L.D. Ferguson, and M.B. Alice. Molecular beams of macroions. *The Journal of Chemical Physics*, 49:2240–2249, 1968.
- [62] G.I. Taylor. *Proceedings of the Royal Society of London, Series A: Mathematical and Physical Sciences*, 280:383–, 1964.
- [63] J.L. Benesch. *Novel mass spectrometry techniques for the study of small heat shock proteins*. PhD thesis, 2005.
- [64] NewObjective. Website. <http://www.newobjective.com/electrospray/>.
- [65] J.V. Iribarne and J. Thomson. On the evaporation of small ions from charged droplets. *The Journal of Chemical Physics*, 64:2287–2294, 1976.
- [66] J.F. de la Mora. Electrospray ionization of large multiply charged species proceeds via doles’charged residue mechanism. *Analytica Chimica Acta*, 406:93–104, 2000.
- [67] J.F. de la Mora, G.J. Van Berke, C.G. Enke, R.B. Cole, M. Martinez-Sanchez, and J.B. Fenn. Electrochemical processes in electrospray ionization mass spectrometry. *Journal of Mass Spectrometry*, 35(8):939–952, Aug 2000.
- [68] M. Peschke, U.H. Verkerk, and P. Kebarle. Prediction of the charge states of folded proteins in electrospray ionization. *European Journal of Mass Spectrometry*, 10(6):993–1002, 2004.
- [69] P. Kebarle. A brief overview of the present status of the mechanisms involved in electrospray mass spectrometry. *Journal of Mass Spectrometry*, 35(7):804–817, Jul 2000.
- [70] P. Kebarle and M. Peschke. On the mechanisms by which the charged droplets produced by electrospray lead to gas phase ions. *Analytica Chimica Acta*, 406:11–35, 2000.

-
- [71] M. Wilm and M. Mann. Analytical properties of the nanoelectrospray ion source. *Analytical Chemistry*, 68(1):1–8, Jan 1996.
- [72] I.V. Chernushevich, A.V. Loboda, and B.A. Thomson. An introduction to quadrupole-time-of-flight mass spectrometry. *Journal of Mass Spectrometry*, 36(8):849–865, Aug 2001.
- [73] A.N. Krutchinsky, I.V. Chernushevich, V.L. Spicer, W. Ens, and K.G. Standing. Collisional damping interface for an electrospray ionization time-of-flight mass spectrometer. *Journal of the American Society for Mass Spectrometry*, 9(6):569–579, 1998. JUN.
- [74] F. Sobott, H. Hernandez, M.G. McCammon, M.A. Tito, and C.V. Robinson. A tandem mass spectrometer for improved transmission and analysis of large macromolecular assemblies. *Analytical Chemistry*, 74(6):1402–1407, 2002. MAR 15.
- [75] N. Tahallah, M. Pinkse, C.S. Maier, and A.J.R. Heck. The effect of the source pressure on the abundance of ions of noncovalent protein assemblies in an electrospray ionization orthogonal time-of-flight instrument. *Rapid Communications in Mass Spectrometry*, 15(8):596–601, 2001.
- [76] E.O. Lawrence and M.S. Livingston. *Physical Review*, 40:19–35, 1932.
- [77] M.B. Comisarow and A.G. Marshall. *Chemical Physics Letters*, 25:282–283, 1974.
- [78] M.B. Comisarow and A.G. Marshall. The early development of fourier transform ion cyclotron resonance (ft-icr) spectroscopy. *Journal of Mass Spectrometry*, 31(6):581–585, Jun 1996.
- [79] I.J. Amster. Fourier transform mass spectrometry. *Journal of Mass Spectrometry*, 31:1325–1337, 1996.
- [80] A.G. Marshall, C.L. Hendrickson, and G.S. Jackson. Fourier transform ion cyclotron resonance mass spectrometry: a primer. *Mass Spectrometry Reviews*, 17(1):1–35, 1998.
- [81] A.G. Marshall and C.L. Hendrickson. Fourier transform ion cyclotron resonance detection: principles and experimental configurations. *International Journal of Mass Spectrometry*, 215:59–75, 2002.
- [82] T.H. Mize, I. Taban, M. Duursma, M. Seynen, M. Konijnenburg, A. Vijftigchild, C.V. Doornik, G.V. Rooij, and R.M.A. Heeren. A modular data and control system to improve sensitivity, selectivity, speed of analysis, ease of use, and transient duration in an external source fticr-ms. *International Journal of Mass Spectrometry*, 235(3):243–253, 2004. JUL 15.

- [83] I.M. Taban, L.A. McDonnell, A. Römpp, I. Cerjak, and R.M.A. Heeren. Simion analysis of a high performance linear accumulation octopole with enhanced ejection capabilities. *International Journal of Mass Spectrometry*, 244:135–143, 2005.
- [84] S.C. Beu and D.A. Laude. Elimination of axial ejection during excitation with a capacitively coupled open trapped-ion cell for fourier-transform ion cyclotron resonance mass-spectrometry. *Analytical Chemistry*, 64:177–180, 1992.
- [85] S.C. Beu and D.A. Laude. Open trapped ion cell geometries for fourier-transform ion-cyclotron resonance mass-spectrometry. *International Journal of Mass Spectrometry and Ion Processes*, 112:215–230, 1992.
- [86] P. Caravatti and M. Allemann. The infinity cell - a new trapped-ion cell with radiofrequency covered trapping electrodes for fourier-transform ion-cyclotron resonance mass-spectrometry. *Organic Mass Spectrometry*, 26:514–518, 1991.
- [87] G. Gabrielse, L. Haarsma, and S.L. Rolston. Open-endcap penning traps for high-precision experiments. *International Journal of Mass Spectrometry and Ion Processes*, 88:319–332, 1989.
- [88] S.H. Guan and A.G. Marshall. Stored waveform inverse fourier transform (swift) ion excitation in trapped-ion mass spectrometry: Theory and applications. *International Journal of Mass Spectrometry and Ion Processes*, 158:5–37, 1996.
- [89] J. Laskin and J.H. Futrell. Activation of large ions in ft-icr mass spectrometry. *Mass Spectrometry Reviews*, 24(2):135–167, 2005. MAR-APR.
- [90] V.H. Wysocki, K.A. Resing, Q. Zhang, and G. Cheng. Mass spectrometry of peptides and proteins. *Methods*, 35(3):211–222, Mar 2005.
- [91] L. Sleno and D.A. Volmer. Ion activation methods for tandem mass spectrometry. *Journal of Mass Spectrometry*, 39(10):1091–1112, Oct 2004.
- [92] T. Dienes, S.J. Pastor, S. Schurch, J.R. Scott, J. Yao, S.L. Cui, and C.L. Wilkins. Fourier transform mass spectrometry - advancing years (1992 mid 1996). *Mass Spectrometry Reviews*, 15:163–211, 1996.
- [93] M.W. Senko, J.P. Speir, and F.W. McLafferty. Collisional activation of large multiply charged ions using fourier transform mass spectrometry. *Analytical Chemistry*, 66(18):2801–2808, Sep 1994.

-
- [94] A.J.R. Heck, L.J. de Koning, F.A. Pinkse, and N.M.M. Nibbering. Mass-specific selection of ions in fourier-transform ion cyclotron resonance mass spectrometry. unintentional off-resonance cyclotron excitation of selected ions. *Rapid Communications in Mass Spectrometry*, 5:406–414, 1991.
- [95] J.W. Gauthier, T.R. Trautman, and D.B. Jacobson. Sustained off-resonance irradiation for collision-activated dissociation involving fourier-transform mass-spectrometry - collision-activated dissociation technique that emulates infrared multiphoton dissociation. *Analytica Chimica Acta*, 246:211–225, 1991.
- [96] D.P. Little, J.P. Speir, M.W. Senko, P.B. O’Connor, and F.W. McLafferty. Infrared multiphoton dissociation of large multiply charged ions for biomolecule sequencing. *Analytical Chemistry*, 66(18):2809–2815, Sep 1994.
- [97] W. Li, C.L. Hendrickson, M.R. Emmett, and A.G. Marshall. Identification of intact proteins in mixtures by alternated capillary liquid chromatography electrospray ionization and lc esi infrared multiphoton dissociation fourier transform ion cyclotron resonance mass spectrometry. *Analytical Chemistry*, 71(19):4397–4402, Oct 1999.
- [98] F.W. McLafferty, D.M. Horn, K. Breuker, Y. Ge, M.A. Lewis, B. Cerda, R.A. Zubarev, and B.K. Carpenter. Electron capture dissociation of gaseous multiply charged ions by fourier-transform ion cyclotron resonance. *Journal of the American Society for Mass Spectrometry*, 12(3):245–249, Mar 2001.
- [99] R.A. Zubarev, D.M. Horn, E.K. Fridriksson, N.L. Kelleher, N.A. Kruger, M.A. Lewis, B.K. Carpenter, and F.W. McLafferty. Electron capture dissociation for structural characterization of multiply charged protein cations. *Analytical Chemistry*, 72(3):563–573, Feb 2000.
- [100] R.A. Zubarev. Reactions of polypeptide ions with electrons in the gas phase. *Mass Spectrometry Reviews*, 22(1):57–77, 2003.
- [101] K. Håkansson, H.J. Cooper, M.R. Emmett, C.E. Costello, A.G. Marshall, and C.L. Nilsson. Electron capture dissociation and infrared multiphoton dissociation ms/ms of an n-glycosylated tryptic peptic to yield complementary sequence information. *Analytical Chemistry*, 73(18):4530–4536, Sep 2001.
- [102] K. Håkansson, M.R. Emmett, C.L. Hendrickson, and A.G. Marshall. High-sensitivity electron capture dissociation tandem fticr mass

- spectrometry of microelectrosprayed peptides. *Analytical Chemistry*, 73(15):3605–3610, Aug 2001.
- [103] R.A. Zubarev, K.F. Haselmann, B. Budnik, F. Kjeldsen, and F. Jensen. Towards an understanding of the mechanism of electron-capture dissociation: a historical perspective and modern ideas. *European Journal of Mass Spectrometry*, 8(5):337–349, 2002.
- [104] R.A. Zubarev, N.L. Kelleher, and F.W. McLafferty. Electron capture dissociation of multiply charged protein cations. a nonergodic process. *Journal of the American Chemical Society*, 120(13):3265–3266, 1998.
- [105] N.A. Kruger, R.A. Zubarev, D.M. Horn, and F.W. McLafferty. Electron capture dissociation of multiply charged peptide cations. *International Journal of Mass Spectrometry*, 187:787–793, 1999. APR 29 Sp. Iss. SI.
- [106] R.A. Zubarev, D.M. Horn, E.K. Fridriksson, N.L. Kelleher, N.A. Kruger, M.A. Lewis, B.K. Carpenter, and F.W. McLafferty. Electron capture dissociation for structural characterization of multiply charged protein cations. *Analytical Chemistry*, 72(3):563–573, 2000. FEB 1.
- [107] Yongming Xie, Jennifer Zhang, Sheng Yin, and Joseph A Loo. Top-down esi-eed-ft-icr mass spectrometry localizes noncovalent protein-ligand binding sites. *Journal of the American Chemical Society*, 128(45):14432–14433, Nov 2006.
- [108] HanBin Oh, Kathrin Breuker, Siu Kwan Sze, Ying Ge, Barry K Carpenter, and Fred W McLafferty. Secondary and tertiary structures of gaseous protein ions characterized by electron capture dissociation mass spectrometry and photofragment spectroscopy. *Proceedings of the National Academy of Sciences of the United States of America*, 99(25):15863–15868, Dec 2002.
- [109] D.M. Horn, Y. Ge, and F.W. McLafferty. Activated ion electron capture dissociation for mass spectral sequencing of larger (42 kda) proteins. *Analytical Chemistry*, 72(20):4778–4784, 2000. OCT 15.
- [110] Y. Ge, B.G. Lawhorn, M. ElNaggar, E. Strauss, J.H. Park, T.P. Begley, and F.W. McLafferty. Top down characterization of larger proteins (45 kda) by electron capture dissociation mass spectrometry. *Journal of the American Chemical Society*, 124(4):672–678, 2002. JAN 30.
- [111] R. Mihalca. *Structural and conformational aspects of gas-phase peptides probed by electron capture dissociation*. PhD thesis, Utrecht University, 2007.

-
- [112] P. Roepstorff and J. Fohlman. Proposal for a common nomenclature for sequence ions in mass spectra of peptides. *Biomedical Mass Spectrometry*, 11(11):601, Nov 1984.
- [113] K. Biemann. Contributions of mass spectrometry to peptide and protein structure. *Biomedical and Environmental Mass Spectrometry*, 16(1-12):99–111, Oct 1988.
- [114] J.L.P. Benesch, F. Sobott, and C.V. Robinson. Thermal dissociation of multimeric protein complexes by using nanoelectrospray mass spectrometry. *Analytical Chemistry*, 75(10):2208–2214, 2003.
- [115] S.L. Koeniger, S.I. Merenbloom, and D.E. Clemmer. Evidence for many resolvable structures within conformation types of electrosprayed ubiquitin ions. *Journal of Physical Chemistry B*, 110(13):7017–7021, Apr 2006.
- [116] I. Compagnon, J. Oomens, G. Meijer, and G. von Helden. Mid-infrared spectroscopy of protected peptides in the gas phase: a probe of the backbone conformation. *Journal of the American Chemical Society*, 128(11):3592–3597, Mar 2006.
- [117] B.T. Ruotolo and C.V. Robinson. Aspects of native proteins are retained in vacuum. *Current Opinion in Chemical Biology*, 10(5):402–408, Oct 2006.
- [118] R.H.H van den Heuvel and A.J.R. Heck. Native protein mass spectrometry: from intact oligomers to functional machineries. *Current Opinion in Chemical Biology*, 8(5):519–526, Oct 2004.
- [119] F.W. McLafferty, Z.Q. Guan, U. Haupts, T.D. Wood, and N.L. Kelleher. Gaseous conformational structures of cytochrome c. *Journal of the American Chemical Society*, 120(19):4732–4740, 1998. MAY 20.
- [120] I.A. Kaltashov and S.J. Eyles. Studies of biomolecular conformations and conformational dynamics by mass spectrometry. *Mass Spectrometry Reviews*, 21(1):37–71, 2002.
- [121] F. Sobott, M.G. McCammon, H. Hernández, and C.V. Robinson. The flight of macromolecular complexes in a mass spectrometer. *Philosophical transactions of the Royal Society of London. Series A: Mathematical, physical, and engineering sciences*, 363(1827):379–89; discussion 389–91, Feb 2005.
- [122] T. van Mourik. The shape of neurotransmitters in the gas phase: A theoretical study of adrenaline, pseudo-adrenaline, and hydrated adrenaline. *Physical Chemistry Chemical Physics*, 6:2827–2837, 2004.

- [123] G.A. Arteca, C.T. Reimann, and O. Tapia. Proteins in vacuo: denaturing and folding mechanisms studied with computer-simulated molecular dynamics. *Mass Spectrometry Reviews*, 20(6):402–422, 2001.
- [124] P.G. Wolynes. Biomolecular folding in vacuo!!!(?). *Proceedings of the National Academy of Sciences of the United States of America*, 92(7):2426–2427, Mar 1995.
- [125] A. Patriksson, E. Marklund, and D. van der Spoel. Protein structures under electrospray conditions. *Biochemistry*, 46(4):933–945, Jan 2007.
- [126] M.F. Jarrold. Peptides and proteins in the vapor phase. *Annual Review of Physical Chemistry*, 51:179–207, 2000.
- [127] M.N. Blom, I. Compagnon, N.C. Polfer, G. von Helden, G. Meijer, S. Suhai, B. Paizs, and J. Oomens. Stepwise solvation of an amino acid: the appearance of zwitterionic structures. *Journal of Physical Chemistry A*, 111(31):7309–7316, Aug 2007.
- [128] R. L A Timmer and H. J. Bakker. Water as a molecular hinge in amidelike structures. *Journal of Chemical Physics*, 126(15):154507, Apr 2007.
- [129] Y.L.A. Rezus and H.J. Bakker. Observation of immobilized water molecules around hydrophobic groups. *Physical Review Letters*, 99:148301, 2007.
- [130] C.S. Kaddis and J.A. Loo. Native protein ms and ion mobility large flying proteins with esi. *Analytical Chemistry*, 79(5):1778–1784, Mar 2007.
- [131] A.J. Kleinnijenhuis, M.C. Duursma, E. Breukink, R.M.A. Heeren, and A.J.R. Heck. Localization of intramolecular monosulfide bridges in lantibiotics determined with electron capture induced dissociation. *Analytical Chemistry*, 75(13):3219–3225, 2003. JUL 1.
- [132] F.W. McLafferty. Tandem mass spectrometric analysis of complex biological mixtures. *International Journal of Mass Spectrometry*, 212(1-3):81–87, 2001. DEC 20.
- [133] F. Kjeldsen, K.F. Haselmann, B.A. Budnik, E.S. Sorensen, and R.A. Zubarev. Complete characterization of posttranslational modification sites in the bovine milk protein pp3 by tandem mass spectrometry with electron capture dissociation as the last stage. *Analytical Chemistry*, 75(10):2355–2361, 2003. MAY 15.

-
- [134] A.T. Iavarone, K. Paech, and E.R. Williams. Effects of charge state and cationizing agent on the electron capture dissociation of a peptide. *Analytical Chemistry*, 76(8):2231–2238, 2004. APR 15.
- [135] J.J. Cournoyer, J.L. Pittman, V.B. Ivleva, E. Fallows, L. Waskell, C.E. Costello, and P.B. O'Connor. Deamidation: Differentiation of aspartyl from isoaspartyl products in peptides by electron capture dissociation. *Protein Science*, 14(2):452–463, 2005. FEB.
- [136] K. Breuker, H.B. Oh, C. Lin, B.K. Carpenter, and F.W. McLafferty. Nonergodic and conformational control of the electron capture dissociation of protein cations. *Proceedings of the National Academy of Sciences of the United States of America*, 101(39):14011–14016, 2004. SEP 28.
- [137] R. Mihalca, A.J. Kleinnijenhuis, L.A. McDonnell, A.J.R. Heck, and R.M.A. Heeren. Electron capture dissociation at low temperatures reveals selective dissociations. *Journal of the American Society for Mass Spectrometry*, 15(12):1869–1873, 2004. DEC.
- [138] E.A. Syrstad and F. Turecek. Toward a general mechanism of electron capture dissociation. *Journal of the American Society for Mass Spectrometry*, 16(2):208–224, 2005. FEB.
- [139] R.A. Zubarev, N.A. Kruger, E.K. Fridriksson, M.A. Lewis, D.M. Horn, B.K. Carpenter, and F.W. McLafferty. Electron capture dissociation of gaseous multiply-charged proteins is favored at disulfide bonds and other sites of high hydrogen atom affinity. *Journal of the American Chemical Society*, 121(12):2857–2862, 1999. MAR 31.
- [140] F. Turecek. N-c-alpha bond dissociation energies and kinetics in amide and peptide radicals. is the dissociation a non-ergodic process? *Journal of the American Chemical Society*, 125(19):5954–5963, 2003. MAY 14.
- [141] N. Leymarie, C.E. Costello, and P.B. O'Connor. Electron capture dissociation initiates a free radical reaction cascade. *Journal of the American Chemical Society*, 125(29):8949–8958, 2003. JUL 23.
- [142] A. Sawicka, P. Skurski, R.R. Hudgins, and J. Simons. Model calculations relevant to disulfide bond cleavage via electron capture influenced by positively charged groups. *Journal of Physical Chemistry B*, 107(48):13505–13511, 2003. DEC 4.
- [143] D.M. Horn, K. Breuker, A.J. Frank, and F.W. McLafferty. Kinetic intermediates in the folding of gaseous protein ions characterized by electron capture dissociation mass spectrometry. *Journal of the American Chemical Society*, 123(40):9792–9799, 2001. OCT 10.

- [144] K.F. Haselmann, T.J.D. Jorgensen, B.A. Budnik, F. Jensen, and R.A. Zubarev. Electron capture dissociation of weakly bound polypeptide polycationic complexes. *Rapid Communications in Mass Spectrometry*, 16(24):2260–2265, 2002.
- [145] E. van Duijn, D.A. Simmons, R.H.H. van den Heuvel, P.J. Bakkes, H. van Heerikhuizen, R.M.A. Heeren, C.V. Robinson, S.M. van der Vies, and A.J.R. Heck. Tandem mass spectrometry of intact groel-substrate complexes reveals substrate-specific conformational changes in the trans ring. *Journal of the American Chemical Society*, 128(14):4694–4702, 2006. APR 12.
- [146] Y.M.E. Fung, L.F. Duan, and T.W.D. Chan. A comparative study of the collision-induced dissociation and the electron capture dissociation of model peptides using electrospray ionization fourier-transform mass spectrometry. *European Journal of Mass Spectrometry*, 10(4):449–457, 2004.
- [147] A.J.R. Heck and R.H.H. van den Heuvel. Investigation of intact protein complexes by mass spectrometry. *Mass Spectrometry Reviews*, 23(5):368–389, 2004. SEP-OCT.
- [148] F. Sobott, M.G. McCammon, and C.V. Robinson. Gas-phase dissociation pathways of a tetrameric protein complex. *International Journal of Mass Spectrometry*, 230(2-3):193–200, 2003. DEC.
- [149] C. Versluis, A. van der Staaij, E. Stokvis, A. J.R. Heck, and B. de Craene. Metastable ion formation and disparate charge separation in the gas-phase dissection of protein assemblies studied by orthogonal time-of-flight mass spectrometry. *Journal of the American Society for Mass Spectrometry*, 12(3):329–336, 2001. MAR.
- [150] J.C. Jurchen, D.E. Garcia, and E.R. Williams. Further studies on the origins of asymmetric charge partitioning in protein homodimers. *Journal of the American Society for Mass Spectrometry*, 15(10):1408–1415, 2004. OCT.
- [151] J.C. Jurchen, D.E. Garcia, and E.R. Williams. Gas-phase dissociation pathways of multiply charged peptide clusters. *Journal of the American Society for Mass Spectrometry*, 14(12):1373–1386, 2003. DEC.
- [152] M.W.H. Pinkse, C.S. Maier, J.I. Kim, B.H. Oh, and A.J.R. Heck. Macromolecular asserably of helicobacter pylori urease investigated by mass spectrometry. *Journal of Mass Spectrometry*, 38(3):315–320, 2003. MAR.

-
- [153] F. Sobott and C.V. Robinson. Protein complexes gain momentum. *Current Opinion in Structural Biology*, 12(6):729–734, 2002. DEC.
- [154] K. Breuker, H.B. Oh, D.M. Horn, B.A. Cerda, and F.W. McLafferty. Detailed unfolding and folding of gaseous ubiquitin ions characterized by electron capture dissociation. *Journal of the American Chemical Society*, 124(22):6407–6420, 2002. JUN 5.
- [155] J.A. Loo. Electrospray ionization mass spectrometry: a technology for studying noncovalent macromolecular complexes. *International Journal of Mass Spectrometry*, 200(1-3):175–186, 2000.
- [156] K. Benkestock, G. Sundqvist, P.O. Edlund, and J. Roeraade. Influence of droplet size, capillary-cone distance and selected instrumental parameters for the analysis of noncovalent protein-ligand complexes by nano-electrospray ionization mass spectrometry. *Journal of Mass Spectrometry*, 39(9):1059–1067, 2004. SEP.
- [157] K.J. Lightwahl, B.L. Schwartz, and R.D. Smith. Observation of the noncovalent quaternary associations of proteins by electrospray-ionization mass-spectrometry. *Journal of the American Chemical Society*, 116(12):5271–5278, 1994.
- [158] A.A. Rostom, P. Fucini, D.R. Benjamin, R. Juenemann, K.H. Nierhaus, F.U. Hartl, C.M. Dobson, and C.V. Robinson. Detection and selective dissociation of intact ribosomes in a mass spectrometer. *Proceedings of the National Academy of Sciences of the United States of America*, 97(10):5185–5190, 2000. MAY 9.
- [159] S. Zhang, C.K. Van Pelt, and D.B. Wilson. Quantitative determination of noncovalent binding interactions using automated nanoelectrospray mass spectrometry. *Analytical Chemistry*, 75(13):3010–3018, 2003. JUL 1.
- [160] F.M. Fernandez, V.H. Wysocki, J.H. Futrell, and J. Laskin. Protein identification via surface-induced dissociation in an ft-icr mass spectrometer and a patchwork sequencing approach. *Journal of the American Society for Mass Spectrometry*, 17(5):700–709, 2006. MAY.
- [161] J. Laskin and J.H. Futrell. Collisional activation of peptide ions in ft-icr mass spectrometry. *Mass Spectrometry Reviews*, 22(3):158–181, 2003. MAY-JUN.
- [162] R.J. Ellis. Molecular chaperones: Inside and outside the anfinen cage. *Current Biology*, 11(24):R1038–R1040, 2001. DEC 11.

- [163] W.A. Houry, D. Frishman, C. Eckerskorn, F. Lottspeich, and F.U. Hartl. Identification of in vivo substrates of the chaperonin groel. *Nature*, 402(6758):147–154, 1999. NOV 11.
- [164] E. Deuerling and B. Bukau. Chaperone-assisted folding of newly synthesized proteins in the cytosol. *Critical Reviews in Biochemistry and Molecular Biology*, 39(5-6):261–277, 2004. SEP-DEC.
- [165] Z. Lin and H.S. Rye. Groel-mediated protein folding: Making the impossible, possible. *Critical Reviews in Biochemistry and Molecular Biology*, 41(4):211–239, 2006. JUL-AUG.
- [166] A. Richardson, S.J. Landry, and C. Georgopoulos. The ins and outs of a molecular chaperone machine. *Trends in Biochemical Sciences*, 23(4):138–143, 1998. APR.
- [167] Y.C. Tang, H.C. Chang, A. Roeben, D. Wischnewski, N. Wischnewski, M.J. Kerner, F.U. Hartl, and M. Hayer-Hartl. Structural features of the groel-groes nano-cage required for rapid folding of encapsulated protein. *Cell*, 125(5):903–914, 2006. JUN 2.
- [168] R.H.H. van den Heuvel and A.J.R. Heck. Native protein mass spectrometry: from intact oligomers to functional machineries. *Current Opinion in Chemical Biology*, 8(5):519–526, 2004. OCT.
- [169] A. Richardson and C. Georgopoulos. Genetic analysis of the bacteriophage t4-encoded cochaperonin gp31. *Genetics*, 152(4):1449–1457, 1999. AUG.
- [170] E. Quate-Randall and A. Joachimiak. Purification of groel from an overproducing e. coli strain. *Methods in Molecular Biology: Chaperonin Protocols*, 140:29–39, 2000.
- [171] P.A. Voziyan and M.T. Fisher. Chaperonin-assisted folding of glutamine synthetase under nonpermissive conditions: Off-pathway aggregation propensity does not determine the co-chaperonin requirement. *Protein Science*, 9(12):2405–2412, 2000. DEC.
- [172] I.V. Chernushevich and B.A. Thomson. Collisional cooling of large ions in electrospray mass spectrometry. *Analytical Chemistry*, 76(6):1754–1760, 2004. MAR 15.
- [173] A.J.R. Heck and P.J. Derrick. Selective fragmentation of single isotopic ions of proteins up to 17 kda using 9.4 tesla fourier transform ion cyclotron resonance. *European Mass Spectrometry*, 4(3):181–188, 1998.

-
- [174] R.H.H. van den Heuvel, E. van Duijn, H. Mazon, S.A. Synowsky, K. Lorenzen, C. Versluis, S.J.J. Brouns, D. Langridge, J. Van Der Oost, J. Hoyes, and A.J.R. Heck. Improving the performance of a quadrupole time-of-flight instrument for macromolecular mass spectrometry. *Analytical Chemistry*, 78:7473–7483, 2006.
- [175] J. Zondlo, K.E. Fisher, Z.L. Lin, K.R. Ducote, and E. Eisenstein. Monomer-heptamer equilibrium of the escherichia-coli chaperonin groes. *Biochemistry*, 34(33):10334–10339, 1995. AUG 22.
- [176] F. Sobott and C.V. Robinson. Characterising electrosprayed biomolecules using tandem-ms - the noncovalent groel chaperonin assembly. *International Journal of Mass Spectrometry*, 236(1-3):25–32, 2004. AUG.
- [177] J. C. Jurchen and E. R. Williams. Origin of asymmetric charge partitioning in the dissociation of gas-phase protein homodimers. *Journal of the American Chemical Society*, 125(9):2817–2826, 2003. MAR 5.
- [178] X.H. Guo, M.C. Duursma, P.G. Kistemaker, N.M.M. Nibbering, K. Vekey, L. Drahos, and R.M.A. Heeren. Manipulating internal energy of protonated biomolecules in electrospray ionization fourier transform ion cyclotron resonance mass spectrometry. *Journal of Mass Spectrometry*, 38(6):597–606, 2003.
- [179] R.M.A. Heeren and K. Vekey. A novel method to determine collisional energy transfer efficiency by fourier transform ion cyclotron resonance mass spectrometry. *Rapid Communications in Mass Spectrometry*, 12(17):1175–1181, 1998.
- [180] L. Drahos, R.M.A. Heeren, C. Collette, E. De Pauw, and K. Vekey. Thermal energy distribution observed in electrospray ionization. *Journal of Mass Spectrometry*, 34(12):1373–1379, 1999.
- [181] R.B.J. Geels, S.M. van der Vies, A.J.R. Heck, and R.M.A. Heeren. Electron capture dissociation as structural probe for noncovalent gas-phase protein assemblies. *Analytical Chemistry*, 78(20):7191–7196, 2006.
- [182] Isao Sakane, Kunihiro Hongo, Fumihiro Motojima, Shigeto Murayama, Tomohiro Mizobata, and Yasushi Kawata. Structural stability of covalently linked groes heptamer: advantages in the formation of oligomeric structure. *Journal of Molecular Biology*, 367(4):1171–1185, Apr 2007.

- [183] Neil Bascos, Jesse Guidry, and Pernilla Wittung-Stafshede. Monomer topology defines folding speed of heptamer. *Protein Science*, 13(5):1317–1321, May 2004.
- [184] Jesse J Guidry and Pernilla Wittung-Stafshede. Low stability for monomeric human chaperonin protein 10: interprotein interactions contribute majority of oligomer stability. *Archives of Biochemistry and Biophysics*, 405(2):280–282, Sep 2002.
- [185] Kathryn Luke and Pernilla Wittung-Stafshede. Folding and assembly pathways of co-chaperonin proteins 10: Origin of bacterial thermostability. *Archives of Biochemistry and Biophysics*, 456(1):8–18, Dec 2006.
- [186] Michael Perham, Mingzhi Chen, Jianpeng Ma, and Pernilla Wittung-Stafshede. Unfolding of heptameric co-chaperonin protein follows "fly casting" mechanism: observation of transient nonnative heptamer. *Journal of the American Chemical Society*, 127(47):16402–16403, Nov 2005.
- [187] O. Boudker, M. J. Todd, and E. Freire. The structural stability of the co-chaperonin groes. *Journal of Molecular Biology*, 272(5):770–779, Oct 1997.
- [188] L.J. Donald, D.J. Stokell, N.J. Holliday, W. Ens, K.G. Standing, and H.W. Duckworth. Multiple equilibria of the escherichia coli chaperonin groes revealed by mass spectrometry. *Protein Science*, 14(5):1375–1379, 2005. MAY.
- [189] J. J. Guidry, C. K. Moczygemba, N. K. Steede, S. J. Landry, and P. Wittung-Stafshede. Reversible denaturation of oligomeric human chaperonin 10: denatured state depends on chemical denaturant. *Protein Science*, 9(11):2109–2117, Nov 2000.
- [190] Jesse J Guidry, Frank Shewmaker, Karol Maskos, Samuel Landry, and Pernilla Wittung-Stafshede. Probing the interface in a human co-chaperonin heptamer: residues disrupting oligomeric unfolded state identified. *BMC Biochem*, 4:14, Oct 2003.
- [191] T. Higurashi, K. Nosaka, T. Mizobata, J. Nagai, and Y. Kawata. Unfolding and refolding of escherichia coli chaperonin groes is expressed by a three-state model. *Journal of Molecular Biology*, 291(3):703–713, Aug 1999.
- [192] Takashi Higurashi, Yuzuru Hiragi, Kaoru Ichimura, Yasutaka Seki, Kunitsugu Soda, Tomohiro Mizobata, and Yasushi Kawata. Structural stability and solution structure of chaperonin groes heptamer studied

-
- by synchrotron small-angle x-ray scattering. *Journal of Molecular Biology*, 333(3):605–620, Oct 2003.
- [193] Kathryn Luke, David Apiyo, and Pernilla Wittung-Stafshede. Dissecting homo-heptamer thermodynamics by isothermal titration calorimetry: entropy-driven assembly of co-chaperonin protein 10. *Biophysical Journal*, 89(5):3332–3336, Nov 2005.
- [194] Kathryn Luke, Michael Perham, and Pernilla Wittung-Stafshede. Kinetic folding and assembly mechanisms differ for two homologous heptamers. *Journal of Molecular Biology*, 363(3):729–742, Oct 2006.
- [195] Isao Sakane, Mitsuyoshi Ikeda, Chiduru Matsumoto, Takashi Higurashi, Katsuaki Inoue, Kunihiro Hongo, Tomohiro Mizobata, and Yasushi Kawata. Structural stability of oligomeric chaperonin 10: the role of two beta-strands at the n and c termini in structural stabilization. *Journal of Molecular Biology*, 344(4):1123–1133, Dec 2004.
- [196] R.B.J. Geels, S.M. Van der Vies, A.J.R. Heck, and R.M.A. Heeren. Comparison of solution phase and gas phase dissociation behaviour of large noncovalent complexes. *Poster presented at 53rd ASMS Conference*, San Antonio, TX, 2005.
- [197] S.K. Chowdhury, V. Katta, and B.T. Chait. Probing conformational changes in proteins by mass spectrometry. *Journal of the American Chemical Society*, 112:9012–9013, 1990.
- [198] Ewald T J van den Bremer, Wim Jiskoot, Richard James, Geoffrey R Moore, Colin Kleanthous, Albert J R Heck, and Claudia S Maier. Probing metal ion binding and conformational properties of the colicin e9 endonuclease by electrospray ionization time-of-flight mass spectrometry. *Protein Science*, 11(7):1738–1752, Jul 2002.
- [199] R. Grandori. Electrospray-ionization mass spectrometry for protein conformational studies. *Current Organic Chemistry*, 7:1589–1603, 2003.
- [200] Anthony T Iavarone and Evan R Williams. Mechanism of charging and supercharging molecules in electrospray ionization. *Journal of the American Chemical Society*, 125(8):2319–2327, Feb 2003.
- [201] L. Konermann and D. J. Douglas. Unfolding of proteins monitored by electrospray ionization mass spectrometry: a comparison of positive and negative ion modes. *Journal of the American Society for Mass Spectrometry*, 9(12):1248–1254, Dec 1998.

- [202] I. M. Taban, Y. E. M. van den Burgt, M. Duursma, Z. Takáts, M. Seynen, M. Konijnenburg, A. Vijftigschild, and R. M. A. Attema, I. and Heeren. A novel workflow control system for fticr-ms allows for unique on-the-fly data-dependent decisions. *Rapid Communications in Mass Spectrometry*, submitted, 2008.
- [203] Lars Konermann. A minimalist model for exploring conformational effects on the electrospray charge state distribution of proteins. *Journal of Physical Chemistry B*, 111(23):6534–6543, Jun 2007.

Summary

Interactions in nature are always directed towards minimizing the free energy of a system. The individual (folding) state of a protein molecule is dictated by its associated free energy. After the amino acid chain is synthesized the protein needs to attain its three dimensional lowest free energy structure; a process that is directed by thermodynamics. The obtained lowest free energy conformation will not always correspond to the biologically active conformation of a given protein, i.e. the protein is misfolded in its lowest energy state. Misfolded proteins can be the cause of many known diseases like Alzheimer's Disease, Parkinson's Disease, Creutzfeldt-Jacob syndrome and BSE. These misfolded proteins cannot obtain their biologically active, native state without help from other molecules. These helper molecules influence the folding energy landscape of the protein. The landscape is altered in such a way that the proper native biological state corresponds to the lowest free energy state, or that the probability of the protein eventually ending up in the native state is increased. These helper proteins are called molecular chaperones and comprise a large group of protein families of which the chaperonins and the heat-shock proteins have been extensively studied.

The chaperonins are protein complexes with folding cages, in which the unfolded or partly folded substrate protein is allowed to fold. They avoid interaction of the protein with other protein molecules and actively create an environment that promotes proper folding in an ATP-dependant process. The chaperonin folding cage is formed by a large double ring structured protein and a smaller protein (the co-chaperonin) that forms the lid of the cage. This thesis focusses on two co-chaperonin proteins, GroES and gp31. Both co-chaperonins form noncovalent homoheptamers arranged in a circular fashion, of masses 72kDa and 84kDa respectively. They both work with the same chaperonin protein: GroEL, but gp31 is the bacteriophage T4 analog of GroES. GroEL and GroES are normal *E.coli* proteins. GroES is substituted by gp31 to allow for proper folding of the bacteriophage T4 capsid protein (gp23), during production of progeny bacteriophages in *E.coli*. Investigations have indicated that the size of the folding cavity is larger in the case of the GroEL-gp31 combination, than

for the GroEL-GroES combination. Gp23 is a relatively large substrate molecule that might be too large to fit inside the GroEL-GroES structure. This can explain why gp23 cannot be folded by GroEL-GroES. In this thesis both co-chaperonins were investigated using mass spectrometry with the aim to develop novel strategies for analyzing large noncovalent complexes. The two co-chaperonin proteins make suitable model systems since they have been studied extensively both *in vitro* using biochemical analysis and *in vivo*.

Chapter one starts with an overview of the basics behind protein folding and function and continues to explain the role of chaperonin complexes along the road to proper protein folding. The GroEL-GroES chaperonin system functions as a two-stroke engine, having two folding cavities on either site, alternately inducing folding of the substrates in an ATP-dependent manner. A misfolded substrate is partly unfolded by hydrophobic interactions with the chaperonin-complex. This puts the substrate molecule back on top of its folding energy landscape. From this position the substrate protein can follow along a path down through the folding funnel. The chaperonin complex also actively alters the folding funnel to prevent misfolding.

Chapter two details the mass spectrometry (MS) techniques used in this thesis. To be able to measure large intact protein assemblies in a mass spectrometer, they need to be evaporated and ionized softly. Electrospray ionization is a method that performs this task excellently. The sample protein is dissolved in an ammonium acetate solution of physiological pH (6.8) and subsequently electrosprayed and ionized. Once ionized and in the gas-phase, the mass over charge (m/z) ratio of the ions can be determined via various techniques. Techniques used in this thesis are Time-of-Flight (ToF-MS) m/z determination and Fourier Transformation (FT-ICR-MS) based m/z determination. Mass analysis of the ions using the ToF-MS is relatively quick and easy. Besides direct mass analysis of the sample, it is also possible to perform an activation/dissociation step of the ions before mass analysis, with a small extension of this instrument. The activation/dissociation of the ions is based on collisions meaning that the (m/z selected) ion cloud can be accelerated and collided with Argon gas to induce dissociation of the parent ions. The fragment ions can then subsequently be mass analyzed.

FT-ICR-MS has the advantage of trapping the ions combined with non-destructive detection. This means it is possible to perform multiple activation/dissociation experiments on the same ions, and mass analysis can be performed after each activation step. With FT-ICR-MS more activation/dissociation techniques of the ions are possible than with the

ToF-MS. It is possible to irradiate the trapped ions with electrons to induce recombination. The liberation of energy into the ion upon recombination also induces fragmentation, but results in different types of fragments. In addition, the ion cloud can also be irradiated with laser light. The photons are absorbed by the ions, heating them up and inducing fragmentation in, again, a different manner. Combining these techniques gives a vast field of possibilities to analyse noncovalent protein complexes in the gas-phase. It is also possible to probe solution-phase manipulation using mass spectrometry. By controlling the temperature of the spray sample at the moment of spraying, thermodynamic equilibria can be altered, changing the composition of the sample. Subsequent analysis by mass spectrometry allows for easy investigation of the resulting species.

In **chapter three** applications of electron irradiation of the trapped ion cloud using FT-ICR-MS are presented. Backbone fragmentation is not expected easily for large protein complexes, since the complexes have a large number of degrees of freedom over which to distribute the released energy. For relatively small proteins Electron Capture Dissociation (ECD) leads to cleavage of covalent backbone bonds. However, for gp31 dissociation of a noncovalent bond, for a specific charge state is observed. ECD has not been reported to lead to dissociation of noncovalent bonds before. Other, lower, charge states of gp31 ions only exhibit charge reduction without fragmentation. We show that ECD leads exclusively to fission of the noncovalent bonds and not to backbone cleavages whereby the fragment products may still be bound to the protein. The selectivity of fragmentation for a specific charge state is explained by assuming a different gas-phase conformation for that specific charge state as compared to the other charge states. This conformational difference is attributed to the higher Coulomb repulsion within the parent ion for that charge state that induces a conformational change. The structural differences result in different reaction pathways when using ECD.

In **chapter four** different Collision Activated Dissociation (CAD) techniques are used on GroES and gp31. By comparing the techniques we have gained insight into the dissociation mechanisms of the two co-chaperonin proteins. The following techniques were used: in-source collisional activation (nozzle-skimmer dissociation, NS-CAD), on-resonance collisional activation in the ICR-cell (on res. CAD) and sustained off-resonance collisional activation in the ICR-cell (SORI-CAD). The activation techniques can be ordered on the basis of their speed: from fast activation/collisions (NS-CAD) to increasingly slower activation (SORI-CAD). For all activation techniques used the gas-phase stabilities are comparable and the major dissociation pathway for both GroES and gp31 is the ejection of an unfolded

monomer from the complex. The extend of unfolding (as determined by the charge uptake of the ejected monomer) increases for increasingly slower activation techniques, demonstration that the different activation techniques yield complementary data. Two factors govern the dissociation: 1) the internal energy built-up via the collisions and 2) the Coulomb repulsion (and corresponding redistribution of charges) within the ion. The first factor has the upper hand when fast activation is used. The second factor has the upper hand when slower activation is used. The redistribution of the charges directs the dissociation in the second case, leading to a higher average charge on the monomer. The effective separation of the monomer from the complex occurs before complete redistribution of charges to the monomer has occurred for the faster activation techniques. This shows the correlation between the time frame of activation and the degree of unfolding of the ejected monomer. A difference in the behavior of GroES and gp31 is observed when the slower activation techniques are used. This different behavior of the two protein complexes is rationalized to be dependent on the gas-phase structures of gp31, GroES and their dissociation products.

Chapter five shows an application of probing thermal equilibria *in vitro* using mass spectrometry. A temperature controlled electrospray setup is described that allows for accurate temperature control of the spray sample up to the moment of spraying. With such a setup it is possible to probe the prevailing equilibrium configurations of proteins complexes in the sample. The study of stoichiometries of protein assemblies in a given sample can give new insights into the temperature-dependent intermediate conformations. For GroES and gp31 we report that temperature-dependent equilibria exists for all possible lower oligomers (i.e. hexamers, pentamers, tetramers, trimers and dimers; these stoichiometries are not biologically functional) and that the thermal unfolding/disassembly transition cannot be viewed as a two-state transition from heptamer to monomer. The solution-phase temperature-dependency determined by MS agrees rather well with fluorescence data. This shows mass spectrometry can provide useful extra information about the stoichiometry of protein complexes during thermal denaturation measurements *in vitro*.

Comparing the solution-phase activation to gas-phase activation gives insight into the role of the solvent on stabilizing the different conformations in solution. Gas-phase activation via Infrared MultiPhoton Dissociation (IRMPD) leads to a breakdown pathway that is different from the breakdown pathway in the solution-phase. In the gas-phase the lower oligomers, except for hexamers and some pentamers (for gp31) are not seen, clearly demonstrating that conformational changes of GroES and gp31 due to heating in solution are significantly influenced by the presence of solvent molecules.

Samenvatting

De wetten van de thermodynamica vertellen dat interacties in de natuur altijd gericht zijn op het verlagen van de vrije-energie in een systeem. Zo ook de specifieke vorm en vouwing, behorende bij een bepaalde toestand van een eiwit. Na de synthese van de aminozuurketen moet een eiwit zijn drie-dimensionale structuur met de laagste vrije-energie zien te bereiken. Het kan echter zijn dat de laagste vrije-energie structuur niet overeenkomt met de biologisch actieve vorm (i.e. vouwingstoestand) van het eiwit, resulterend in een misvouwen eiwit. Ook kan een eiwit misvouwen zijn als het in een lokaal vrije-energie minimum terecht komt in plaats van in het globale minimum. Misvouwen eiwitten kunnen de oorzaak zijn van vele bekende ziekten, zoals Alzheimer, Parkinson, Creutzfeldt-Jacob en BSE (gekkekoeienziekte). Sommige verkeerd gevouwen eiwitten kunnen hun biologisch actieve vouwingstoestand niet meer bereiken zonder de hulp van andere eiwitten. De hulp-eiwitten veranderen het energielandschap van het vouwingsproces. Deze verandering zorgt ervoor dat de laagste vrije-energie toestand overeenkomt met de biologisch actieve toestand, of dat de kans wordt vergroot, dat het eiwit uiteindelijk in de biologisch actieve toestand zal belanden. Een veel bestudeerde familie van deze hulp-eiwitten is de familie van de chaperonne eiwitten.

De chaperonne eiwitten vormen structuren met een semi-doorlaatbare holte (kooi), waarbinnen het ongevouwen of gedeeltelijk gevouwen eiwit kan worden opgesloten. Een opgesloten eiwit wordt op die manier beschermd tegen interacties met andere moleculen in de cel. Het chaperonne eiwit helpt het andere eiwit met vouwen. De kooi van de chaperonne wordt gevormd door een groot, hol eiwit, waarop een kleiner eiwit, de co-chaperonne, als deksel past. Dit proefschrift beschrijft een onderzoek aan twee van deze co-chaperonnes: GroES en gp31. Beide co-chaperonnes zijn zelf eiwitcomplexen die bestaan uit zeven identieke niet-covalent gebonden eiwitten (zgn. heptameren) georganiseerd als een ring en wegen respectievelijk 72kDa en 84kDa. De beide co-chaperonnes kunnen met dezelfde chaperonne (GroEL) de vouwingsholte vormen. GroEL is zelf ook een eiwitcomplex en bestaat uit een dubbele ring van zeven identieke niet-covalent gebonden eiwitten. Binnen in elke ring bevindt zich de holte waarin een substraat eiwit past. De

co-chaperonnes kunnen de holte afdekken en zorgen zo voor een afgesloten geheel. GroES en gp31 zijn elkaars analoog. Echter, GroES komt uit *E.coli*, net zoals GroEL, terwijl gp31 van bacteriofaag T4 afkomstig is en alleen tijdens infectie in de *E.coli* bacterie wordt gemaakt. Bacteriofaag T4 neemt het chaperonne systeem van de gastheer over wanneer hij *E.coli* infecteert. Dat is nodig om het belangrijkste eiwit dat de mantel van de bacteriofaag vormt, genaamd gp23, te kunnen vouwen. Gp23 kan niet worden gevouwen door het GroEL-GroES complex, maar wel als GroES wordt vervangen door gp31. Het GroEL-gp31 chaperonne complex heeft namelijk een grotere vouwingsholte, waar het relatief grote eiwit gp23 net in past. De holte in het GroEL-GroES chaperonne complex is te klein voor gp23. In dit proefschrift wordt beschreven op welke manier de beide co-chaperonnes kunnen worden bestudeerd met behulp van massaspectrometrie. Het nut van nieuwe technieken voor eiwit analyse met behulp van massaspectrometrie voor de analyse van zulke grote niet-covalent gebonden eiwitcomplexen zal worden bestudeerd. Dit zal mede gebeuren in het licht van het biologisch functionele verschil tussen de twee eiwitten.

Hoofdstuk één beschrijft het basis concept van de eiwitvouwing en de relatie ervan met de biologische functionaliteit van een eiwit. Vervolgens wordt ingegaan op de rol van chaperonne eiwitten bij het bereiken van de biologisch actieve vouwingstoestand van een eiwit, met name de GroEL-GroES chaperonne. Dit grote eiwitcomplex werkt als een twee-takt motor. Het chaperonne complex heeft twee vouwingsholtes die aan elkaar zijn gespiegeld. Er kan afwisselend een eiwit worden gevouwen in de holte aan de ene kant en in de holte aan de andere kant. Aan het oppervlak van een eiwit bevinden zich hydrofobe gedeelten wanneer een eiwit ongevouwen of slechts gedeeltelijk gevouwen is. Deze oppervlakken hebben een grote affiniteit voor de binnenkant van de holte in het chaperonne complex. Het wordt voor een deel ontvouwen door de binding aan de chaperonne en op die manier teruggezet op een hoger gedeelte van zijn energielandschap voor vouwing. Vanaf dit punt kan het eiwit zijn pad weer opnieuw vervolgen over het energielandschap. Dit energielandschap kan door de opsluiting van het eiwit veranderd zijn, zodat de laagste energietoestand met grotere waarschijnlijkheid wordt bereikt. ATP hydrolyse is nodig om de energie vrij te maken, die nodig is voor de conformatieveranderingen van de chaperonne en de dissociatie van het GroES of gp31 eiwit, zodat het eiwit de holte kan verlaten wanneer het goed gevouwen is. Is het eiwit echter nog niet voldoende gevouwen, dan kan het opnieuw aan de chaperonne binden om vervolgens in een tweede cyclus verder te vouwen.

Hoofdstuk twee behandelt de massaspectrometrische technieken die worden gebruikt in dit proefschrift. Om niet-covalent gebonden eiwitcomplexen

intact te kunnen meten in de gas-fase, moeten deze voorzichtig worden verdampt en geïoniseerd. Electrospray ionisatie is een techniek die dat mogelijk maakt. Een waterige ammonium acetaat oplossing (met pH 6.8) met daarin het opgelost eiwit wordt verstoven, waarna het eiwit kan worden geanalyseerd. Als het eiwit eenmaal in de gas-fase is en het is geïoniseerd, dan kan met behulp van verschillende technieken de ratio van de massa ten opzichte van de elektrische lading worden bepaald (de m/z ratio). In dit proefschrift worden de volgende technieken gebruikt: vluchttijd massaspectrometrie (Eng.: *Time-of-Flight*, ToF-MS) en massaspectrometrie gebaseerd op de frequentie van ionen cyclotron resonantie bepaald via een Fourier transformatie (FT-ICR-MS).

FT-ICR-MS heeft als voordeel boven ToF-MS, dat de ionen gevangen blijven en de detectie van de ionen op een niet-destructieve manier plaatsvindt. Daardoor is het mogelijk om dezelfde ionen meerdere malen te meten en de ionen tussen de metingen door te onderwerpen aan verschillende soorten activerings- en dissociatie technieken. Eiwitten analyseren met behulp van de ToF-MS is eenvoudiger en sneller, maar het is slechts mogelijk de ionen eenmalig te meten. Ook met de ToF-MS is het mogelijk om de gas-fase ionen te dissociëren voor de meting, echter veel minder uitgebreid dan bij FT-ICR-MS. Onder dissociatie van de ionen bij ToF-MS wordt verstaan, dat de ionen versneld worden en vervolgens botsen met argon gas. De botsingen, indien hevig genoeg, leiden tot fragmentatie van de ionen, waarbij de amidebinding, een covalente binding tussen twee aminozuren, wordt verbroken. Dit is dissociatie van een covalente binding. Hierna kunnen de fragmenten worden gemeten. Er zijn bij FT-ICR-MS naast botsingsactivering nog vele andere mogelijkheden om de ionen te dissociëren. De ionen kunnen worden blootgesteld aan een elektronenbundel. De negatieve elektronen kunnen worden ingevangen door de positief geladen eiwit-ionen, waarbij er recombinatie energie vrijkomt, leidend tot dissociatie van het ion. Hierbij ontstaan andere fragmenten dan via botsingsactivering. Daarnaast kunnen die ionen ook worden bestraald met laserlicht. De fotonen worden dan geabsorbeerd door de eiwit-ionen, waarbij deze opwarmen en uiteindelijk ook zullen dissociëren. Hierbij ontstaan weer andere fragmenten dan bij de eerder genoemde technieken. Deze technieken leveren gezamenlijk vele mogelijkheden om de ionen in de gas-fase te activeren en hun gedrag te bestuderen.

Het is ook mogelijk om activering van eiwitten in de vloeistof-fase te bestuderen met behulp van massaspectrometrie. Thermodynamische en chemische evenwichten kunnen worden beïnvloed door de temperatuur van het eiwit in de vloeistof-fase te variëren. Hierdoor wordt de samenstelling van het monster beïnvloed. Deze samenstelling kan weer worden gemeten met behulp van massaspectrometrie.

In **hoofdstuk drie** worden de effecten van blootstelling aan een elektronbundel voor GroES en gp31 bestudeerd. De vrijgekomen recombinatie energie wordt bij deze grote complexen verdeeld over een groot aantal vrijheidsgraden. Het ligt daarom niet voor de hand dat deze grote complexen makkelijk zullen fragmenteren. Er moet dan veel energie worden toegevoegd, voordat er bij een bepaalde covalente binding genoeg energie is om deze te breken. Voor kleinere eiwitten leidt invangst van een elektron wel tot fragmentatie van een covalente binding. Elektron invangst bij gp31 leidt voor een specifieke ladingstoestand tot dissociatie van niet-covalente bindingen. Hierbij valt één van de zeven (sub-)eiwitten uit het chaperonne complex. Elektron invangst leidend tot dissociatie van niet-covalente bindingen, is voorheen nog nooit waargenomen. De overige, lagere ladingstoestanden van gp31 vertonen alleen ladingsreductie en geen dissociatie bij elektron invangst. Voor de ladingstoestand van gp31 die wel dissocieert, wordt aangetoond dat elektron invangst dissociatie exclusief leidt tot dissociatie van de niet-covalente bindingen. Er is geen sprake van dissociatie van covalente bindingen, waarbij de fragmenten gebonden blijven aan het ion via niet-covalente interacties. De selectiviteit van de dissociatie voor één specifieke ladingstoestand wordt verklaard door aan te nemen, dat de gasfase vorm van die ladingstoestand beduidend anders is, dan voor de lagere ladingstoestanden. De verandering in de gas-fase vorm van het eiwit wordt toegekend aan de aanwezigheid van hogere Coulomb afstoting tussen de ladingen op het hooggeladen eiwit. Deze afstoting induceert de vormverandering. De vormverschillen leiden tot verschillende fragmentatiepaden bij gebruik van elektron invangst dissociatie.

In **hoofdstuk vier** worden verschillende botsingsactiveringstechnieken toegepast op GroES en gp31 om de verschillen tussen de technieken en tussen de eiwitten te onderzoeken. De vergelijking van de technieken toont aan hoe de fragmentatie paden van de eiwitten bij de gebruikte technieken verschillen. De gebruikte technieken zijn: botsingsactivering in de bron van de massa spectrometer (snelste activering), resonante excitatie in combinatie met botsingsactivering (minder snelle activering) en niet-resonante excitatie in combinatie met botsingsactivering (nog minder snelle manier van activeren). De gas-fase stabiliteiten van de eiwitten zijn vergelijkbaar voor alle gebruikte technieken. De drie activeringstechnieken leiden alle tot uitstoting van een eiwitmolecuul (monomeer) uit het complex, i.e. dissociatie van niet-covalente bindingen. Het uitgestoten eiwitmolecuul heeft grotendeels zijn originele vorm verloren en is zogenaamd ontvouwen. De mate van ontvouwing wordt gemeten aan de hand van het aantal ladingen, dat het uitgestoten monomeer meeneemt van het originele complex. Het uitgestoten monomeer is steeds verder ontvouwen, naarmate de activering minder snel is. Er zijn twee factoren van invloed op de dissociatie: 1) de

opbouw van interne energie via de botsingen en 2) de Coulomb afstoting binnen het ion (met bijbehorende herverdeling van lading over het ion). Bij snelle activering zal de eerste factor de overhand hebben en bij langzame activering zal de tweede factor de overhand hebben. Langzame activering leidt relatief tot een hoge lading op het uitgestoten monomeer. Bij de snellere activeringstechniek zal het monomeer van het complex dissociëren voordat er voldoende tijd is geweest om alle ladingen te herdistribueren naar het monomeer. Er wordt zodoende een correlatie gelegd tussen de tijdsschaal van activering en de mate waarin het monomeer is ontvouwen. Er wordt ook een verschil in het gedrag tussen GroES en gp31 waargenomen naarmate de activering langzamer is. Dit verschil in gedrag wordt verklaard op basis van de gas-fase structuur van gp31, GroES en hun dissociatieproducten.

Hoofdstuk vijf laat een toepassing zien van de meting van thermische evenwichten *in vitro* met behulp van massaspectrometrie. Hierbij wordt een electrospray opstelling gebruikt, waarmee de temperatuur van het te verstuiwen monster nauwkeurig kan worden ingesteld tot op het moment van verstuiwing. Met deze techniek kan bij elke temperatuur de eiwitsamenstelling van het monster worden bepaald. De opbouw van eiwitcomplexen kan zodoende worden bestudeerd als functie van de temperatuur. Alle tussenvormen van het complex kunnen worden gemeten naarmate de temperatuur wordt verhoogd en het biologisch werkzame complex van zeven eiwitten uit elkaar valt. Het blijkt dat zowel voor GroES als voor gp31 alle aantallen eiwitten in een complex voorkomen, afhankelijk van de temperatuur. Dit betekent dat er naast een complex van zeven, ook complexen van zes, vijf, vier, drie en twee eiwitten worden waargenomen en er uiteindelijk, bij hoge temperatuur, alleen losse eiwitten over blijven. De overgang van een compleet werkzaam complex naar een verzameling ontvouwen monomeren kan dus niet worden gezien als een overgang bestaande uit één stap. De gemeten temperatuursafhankelijkheid van de GroES en gp31 eiwitten met behulp van massaspectrometrie komen redelijk overeen met fluorescentie metingen. Dit onderzoek toont aan dat massaspectrometrie goed kan worden gebruikt om aanvullende informatie te verkrijgen over de samenstelling van eiwitcomplexen bij thermische denaturatie metingen *in vitro*.

Het vergelijken van het gedrag van de complexen in de vloeistof-fase en in de gas-fase geeft inzicht in de rol van het oplosmiddel (met name water) bij de stabilisatie van de verschillende (tussen-)vormen van de eiwitcomplexen in de vloeistof. Gas-fase activering van de eiwitten met behulp van laserlicht resulteert in een fragmentatie pad dat afwijkt van het fragmentatie pad in de vloeistof-fase. De tussenvormen van het eiwit zoals waargenomen bij vloeistof-fase dissociatie, worden niet waargenomen bij gas-fase dissociatie, afgezien van het hexameer (zes eiwitten in het complex) en in veel mindere

mate het pentameer (vijf eiwitten in het complex, bij gp31). Dit geeft duidelijk aan dat de veranderingen van de conformatie ten gevolge van het verwarmen in de vloeistof-fase significant worden beïnvloed door de aanwezigheid van het oplosmiddel.

Nawoord

Wat heb ik een leuke tijd gehad op Amolf. Dat had ik van tevoren nooit kunnen bedenken. Wie verwacht er nou veel lol op een instituut vol fysicasters (mij inclusief). Al snel bleek Amolf een zeer vriendelijke en gezellige omgeving. Ik ben echter wel voorgelogen bij het nemen van de aanstelling. Ik ging er namelijk vanuit dat Amolf een fysica instituut is (Atoom en MOLEcuul **Fysica**, toch?). Ik werd echter omgeven door collega's die rare onderwerpen zoals scheikunde en biologie hadden gestudeerd..... What happened? Vervolgens kwam ik er na enige tijd achter dat zelfs mijn baas een aanstelling kreeg aan de Universiteit Utrecht bij de faculteit **Scheikunde** en ik dus uiteindelijk in de scheikunde bleek te gaan promoveren, again: What happened? Verloochen ik nou mijn afkomst, of is dit een welkome aanvulling op mijn oude, vertrouwde fysica omgeving? Het bleek dat laatste te zijn, want er zit zeer veel moois in de combinatie van natuurkunde, scheikunde en biologie.

Het was voor mij wel even wennen in het begin. Opeens stond ik halve dagen in een chemisch lab waar ik voordien nog nooit een voet binnen de deur had gezet. Dat moet een leuk gezicht zijn geweest, zo'n SA-loze jongen te zien ronddwalen in het chemisch lab (SA-loos is *situational awareness*-loos, met andere woorden, hij heeft geen idee wat hij aan het doen is; Vincent, bedankt voor de uitdrukking). Daarnaast moest ik tussen neus en lippen door ook nog maar even de hele biochemie opleiding doen (dit is schromelijk overdreven, want het kwam namelijk neer op enkele hoofdstukken uit het bekende boek van Stryer). Dit was overigens wel heel leerzaam en het bleek, dat ik nog best wat van de lessen van dhr. Westra (mijn middelbare schoolleraar biologie) had onthouden. Langzaam maar zeker maakten vreemde begrippen als: *chemotrypsin*, *dephosphorylation* en *post-translational modification*, zich van mij meester (let wel: niet andersom!)

Ik heb mij nooit voor de volle 100% ingezet. 80% om precies te zijn. In eerste instantie had ik die deeltijdaanstelling gekregen om mijn hobby, freestyle buckelpiste skiën, op wedstrijdniveau te kunnen voortzetten. Ik ben mijn promotie dan ook begonnen met een hele maand trainen in de sneeuw. Volgens mij kan je het bij geen enkele andere baas voor elkaar

krijgen dat je met een maand "vakantie" mag beginnen.... Geweldig. Helaas liep mijn skicarrière snel achteruit vanwege hoge kosten en blessures. Maar die 80% aanstelling die bleef! Het is erg lekker geweest om 20% van de tijd mezelf ook op andere vlakken te kunnen ontplooiën: huis verbouwen (had ik niet zonder de uitvoerige hulp van mijn ouders gekund), website bouwen, relaxen.... Amolf bedankt. Wouter, ik heb je veel extra werk bezorgd door deze constructie, bedankt daarvoor.

Allereerst wil ik graag iets over mijn begeleiders vertellen. Het gevleugelde enthousiasme waarmee Ron met nieuwe ideeën komt is fantastisch. Hierdoor wil je alle ideeën onmiddellijk uitproberen. Wist je het niet voor elkaar te krijgen om een goed signaal uit het apparaat te krijgen, dan kwam Ron even langs en regelde het voor je. Echter ook andersom. Had je een lekker signaal uit het apparaat, dan kwam Ron even langs om dat signaal naar de Filistijnen te helpen. We hebben op conferenties menig biertje gedronken en veel lol gehad. Een prima baas. De combinatie met mijn andere promotoren maakte mijn onderzoek compleet. Ik heb genoten van discussies met Albert en Saskia over de toepassingen en biologische kant van het geheel. Jullie boden een mooie tegenhanger voor mijn eigen, met name methodologische, insteek. Ik vond het heel fijn en leerzaam om met zulke vooraanstaande wetenschappers te mogen samenwerken.

De groep van Macromolecular Ion Physics op Amolf, onze groep, heeft mijn tijd op Amolf uitermate vriendelijk, leuk en inspirerend gemaakt. Zo heb ik lang op een kamer gezeten met Maarten. Volgens mij had ik geen beter kamergenoot kunnen treffen. Ik heb veel met je opgetrokken op en buiten het werk. Zo'n beetje alles wat ter sprake kwam, werd door ons lekker de grond in geboord, heerlijk. Met Marc heb ik vele uurtjes bij de FT-MS doorgebracht, waarbij ik met zijn hip-hop achtergrond kennis heb kunnen maken. Marc, bedankt voor al je hulp bij het meten met en tunen van de FT-MS. Başak, Lennaert, Romulus, Luke, Ioana, Martin, Gert, Jonathan, Erika, Andriy, Piet, Jaap en ook oud-collega's Xinghua, Andreas, Anne, Todd, Liam, Yuri, Sander, Stefan (ooit win je nog wel eens met kolonisten), Aleksey, bedankt voor de leuke samenwerking op en buiten het werk. Ook Oscar, een net-niet oud collega, was goed voor veel lol en gezelligheid.

Ook aan de hulp vanuit Utrecht heb ik veel gehad. Esther, jij hebt mij de beginselen van het monster hanteren en naaldjes trekken bijgebracht. Je was nooit te beroerd om mij te komen helpen met experimenteren en jouw eigenhandig opgezuiverde eiwitten aan mij beschikbaar te stellen. Helemaal top. Ook met Robert heb ik leuk samengewerkt en gediscussieerd. Cees en Arjan, ook bedankt voor jullie vele bijspringen en meedenken bij het uitvoeren van experimenten in Utrecht.

De samenwerking met Laura om de tubuline te zien te krijgen in de massaspectrometer was erg gezellig. Helaas wel vruchteloos, maar dat maakt niet uit. Ook heb ik fijn samengewerkt met Stephane op de VU tijdens de fluorescentie metingen; bedankt en geweldig dat je de controlemeting ook nog uit wilde voeren.

De deelname aan de 'maaiveld'-wedstrijd met een groep Amolfers was zeer geslaagd. We hadden mooie discussies over hoe we dit kikkerlandje concurrerend kunnen maken in de kenniseconomie. Uiteraard hadden wij het beste idee om dit te bewerkstelligen, maar misschien, heel misschien, niet het meest praktisch haalbare idee. Ik blijf erbij dat een continu lopende schoolklassen-innovatie-wedstrijd in de vorm van een sportcompetitie de beste lange termijn oplossing is voor Nederland! Mede-maaivaarders: Eva, Siebe, Maarten, Gerbrand, Annemieke en Adriaan, bedankt voor de gezelligheid.

Ik heb ruim een jaar mee mogen helpen in de personeelsvereniging van Amolf, waarbij ik vruchtbaar heb samengewerkt met vele leuke mensen en waarbij de gezelligheid altijd troef was. Yves, Annemieke, Katrien, Willem, Janne, Simon, Marijn, Grace en Arjan, het was erg leuk.

De ondersteunende afdelingen van Amolf hebben mij veel geholpen. Bijvoorbeeld bij het maken van de ThermoProbe, het verlagen van het ruisniveau van de FT-MS en vele andere aanpassingen. Dirk-Jan en Iliya, Idsart, Duncan, Hans, Ton, Ronald, Macro S. en Marco K. Jan, wat heb je vaak aan de capillairtjes gepriegeld voor me. Ook de jongens van IT-beheer stonden altijd voor me klaar, Rutger, Richard, Jan en Lars. Zou Dalton ooit nog meer gaan doen dan alleen maar kabaal maken? Ivo, wat hebben we een lol gehad met de promotie van Maarten. Grace en Silvia zijn twee van de liefste vrouwen die ik ken. Zij zijn de uitvinders van klantvriendelijkheid. En Marvin, tja, jammer dat je altijd zo treurig was!

Het leuke is dat de collega's van Amolf niet alleen met werk voor je klaar staan, maar er ook zijn voor de nodige privé zaken. Frans heeft menigmaal voor me in de hulpwerkplaats één en ander afgedraaid (al dan niet werkgerelateerd) en hij is tevens een zeer behoorlijke gipsplaatschroever! Hincó, ik geniet nog elke dag van mijn keukenkastgrepen, prachtig zijn ze. Zijn we nou ook nog een keer bijna door mijn fiets heen gezakt..? Dat herinner ik me niet goed meer, het was een beetje wazig die avond. Willem en André, ik heb veel aan jullie gevraagd over bouwtechnische problemen en via jullie de juiste mannetjes weten te bereiken. Ik heb het zelfs niet nagelaten om de Amolf schoonmaakploeg bij mij thuis aan het werk te zetten, Tineke en Eugenie. Ook heeft mijn motor volledige zomers in de stalling op Amolf mogen staan, heel fijn.

Een mooi fenomeen op Amolf is ook de lunchclub. Tijdens de lunch is onze groep verdeeld in twee kampen. Het ene kamp, de rijken, gaan elke

dag naar de kantine om zich te laten verwennen door warme kroketten en andere geneugten, terwijl het andere kamp, waaronder ik, op Amolf blijft om te genieten van de culinaire hoogstandjes van de Deen, Appie en de Deka. Wat zijn we een stelletjes ongelooflijke foodcritici bij elkaar. Maar weinig producten kwamen goed uit onze tests. Jerre, Frank, Gert, Katrien, Maarten en Sander, ik heb veel gelachen en ook het gevecht om de kaasschaaf met de andere groep heeft tot veel vermaak geleid.

Ik herinner me nog de talloze malen dat ik mijn ouders heb proberen uit te leggen wat ik eigenlijk doe... nou, laat maar. We praten wel weer over golfen. Nee hoor, grapje, jullie waren zeer geïnteresseerd en dat heb ik altijd heel fijn gevonden.

Corinne, nu ik kennis heb gemaakt met biochemie krijg ik steeds meer waardering voor jouw farmaceutische kennis. Je hebt zelfs mijn anti-pillen houding aan het wankelen weten te brengen.

Fenna, jij legt tegenwoordig beter uit wat ik doe dan ikzelf. Verder geen woorden aan vuil maken, dit is al g nant genoeg.



Rimco Geels, 7 februari 2008

Curriculum Vitae

Rimco Geels werd geboren op 31 juli 1977 te Alphen aan den Rijn. Hij heeft een VWO opleiding genoten op het Petrus Canisius College te Alkmaar, waarna hij aan de Rijksuniversiteit Groningen vanaf 1995 technische natuurkunde is gaan studeren. In het jaar daarna heeft hij economie opgepakt als tweede studie. Hij heeft een bedrijfsstage voor natuurkunde gedaan bij Philips Image Sensors op het NatLab te Eindhoven, waar hij onderzoek verrichte naar mogelijke verbeteringen voor CCD-sensoren. Tijdens zijn afstudeerproject bij het Kernfysisch Versneller Instituut te Groningen heeft hij onderzoek verricht naar de interactie van hooggeladen ionen met metallische oppervlakken. Ten behoeve van de studie economie heeft hij twee afstudeeronderzoeken gedaan. Eén op de economie faculteit van de Rijksuniversiteit Groningen voor de studierichting management en organisatie, waarbij hij onderzocht hoe bepaalde bedrijfscharacteristieken correleerden met de remuneratie van top bestuurders. Het tweede afstudeeronderzoek voor de studierichting financiering en belegging heeft hij volbracht bij ING Investment Management te Den Haag, waarbij hij de mogelijkheden van risicobudgettering ten behoeve van beleggingsportfolio's heeft onderzocht.

Begin 2003 is hij een promotietraject gestart bij het FOM-instituut AMOLF te Amsterdam onder leiding van prof. dr. Ron M.A. Heeren, prof. dr. Saskia M. van der Vies en prof. dr. Albert J.R. Heck. Het onderwerp van de promotie was: het exploreren van de thermodynamica van eiwitvouwing in de gas-fase met behulp van massa spectrometrie, waarbij met name de co-chaperonnes GroES en gp31 werden bestudeerd. De onderzoeksresultaten zijn onder meer gepresenteerd tijdens lezingen op de 'European FT-MS Conference' in Konstanz (Duitsland, 2004) en op de 'International Mass Spectrometry Conference' in Praag (Tsjechië, 2006).

List of Publications

Rimco B.J. Geels, Saskia M. van der Vies, Albert J.R. Heck, and Ron M.A. Heeren. Electron Capture Dissociation as Structural Probe for Noncovalent Gas-Phase Protein Assemblies, *Analytical Chemistry*, 2006, 78(20), 7191-7196.

Rimco B.J. Geels, Saskia M. van der Vies, Albert J.R. Heck, and Ron M.A. Heeren. Comparative Gas-Phase Activation of Two Similar Noncovalent Heptameric Protein Complexes: gp31 and GroES, *International Journal of Mass Spectrometry*, 2007, 265(2-3), 159-168.

Rimco B.J. Geels, Stephane Calmat, Albert J.R. Heck, Saskia M. van der Vies, and Ron M.A. Heeren. Solution-Phase and Gas-Phase Thermal Activation of the Co-Chaperonins GroES and gp31 Probed by Mass Spectrometry, *Analytical Chemistry*, in preparation.